PCP-driven Cardiac Remodeling Couples Changes in Actomyosin Tension with Myocyte Differentiation

DISSERTATION
zur Erlangung des Akademischen Grades
doctor rerum naturalium (Dr. rer. nat.)
im Fach Biologie
eingereicht an der

Lebenswissenschaftlichen Fakultät
der Humboldt-Universität zu Berlin

angefertigt von M.Sc. Marie Swinarski

Präsidentin der Humboldt-Universität zu Berlin
Prof. Dr.-Ing. habil. Dr. Sabine Kunst

Dekan der Lebenswissenschaftlichen Fakultät
Prof. Dr. Bernhard Grimm

Gutachter:

Prof. Dr. Holger Gerhardt
Prof. Dr. Christian Mosimann
Prof. Dr. Thomas Sommer

Tag der mündlichen Prüfung: 5. April 2017

I completed my doctorate studies from September 2011 to November 2015 under the supervision of Dr. D. Panáková at the Max Delbrück Center for Molecular Medicine, Berlin-Buch.

I herewith declare that I have produced this paper without the prohibited assistance of third parties and without making use of aids other than those specified; notions taken over directly or indirectly from other sources have been identified as such. This paper has not previously been presented in identical or similar form to any other German or foreign examination board.

Berlin, 30.10.2016

M. Swinarski

For my Loved Ones.

Contents

Abstract

Formation of a complex multiple-chambered heart from the simple linear heart tube does not only require orchestrated morphogenesis of the myocardium, but also cardiac muscle differentiation and changes in intercellular electrical coupling. To date, the processes that lead to the formation of a functional syncytium are incompletely understood. One of the major pathways controlling multiple aspects of organogenesis and tissue morphogenesis is the planar cell polarity (PCP) pathway. Changes in tissue architecture are controlled by cell intercalation and collective cell migration. It is widely accepted that Wnt/PCP signaling plays a crucial role in guiding these cellular processes. This study provides evidence that morphogenesis of the heart is controlled by the non-canonical ligands Wnt11 and Wnt5b and the PCP core components Fzd7, Vangl2, Dvl2, and Pk1 through regulation of cell rearrangements during embryonic cardiac remodeling. Downstream effectors of the PCP pathway target adhesion processes, cytoskeleton, and migration. Here, it is revealed that PCP signaling in the heart affects cardiomyocyte morphology and actomyosin organization. Specifically, changes in the subcellular localization of the phosphorylated non-muscle myosin II regulatory light chain (pMRLC) at LHT stage are targeted by the PCP pathway core components. Furthermore, actomyosin relocalization concurs with changes in nuclear tension and SRF signal transduction within the myocardium. This study unravels a novel function of the PCP core component Pk1 in regulation of SRF translocation and target gene expression that is critical to cardiac maturation. Taken together, this study provides evidence that the PCP pathway is a major regulator of cardiac remodeling and organ maturation by modulating mechanosensitive SRF signal transduction involved in muscle differentiation.

Zusammenfassung

Im Zuge der frühen embryonalen Herzentwicklung entstehen ausgehend von einem einfachen Herzschlauch zwei deutlich voneinander getrennte Herzkammern. Die Kardiomyozyten des Atriums und Ventrikels weisen jeweils spezifische Eigenschaften auf, die sich morphologisch wie auch funktionell auf das Herz auswirken. Der Prozess dieser Spezifizierung ist jedoch bis dato nur partiell verstanden. Veränderungen in der Gewebsarchitektur werden hauptsächlich durch Zellinterkalation und kollektive Zellmigration erreicht. Viele Studien zeigen, dass der Wnt/PCP-Signalweg eine essentielle Rolle in der Regulation dieser Bewegungen einnimmt. Die Daten dieser Studie belegen, dass die nicht-kanonischen Liganden Wnt11 und Wnt5b sowie die Kernkomponenten des PCP Signalweges Fzd7, Vangl2, Dvl2 und Pk1 an der Steuerung der Reorganisation der Kardiomyozyten während der Kammerbildung beteiligt sind, was Einfluss auf die Architektur des frühen Myokardiums nimmt. Effektoren des PCP Signalweges umfassen das Zytoskelett sowie Adhäsions- und Migrationsprozesse. In dieser Studie wird gezeigt, dass die Komponenten dieses Signalweges im Myokardium hauptsächlich Prozesse der Actomyosin Modulation regulieren und damit unter anderem die Morphologie der Kardiomyozyten beeinflussen. Zusätzlich ist die frühe Kardiogenese durch eine Relokalisierung der phosphorylierten Form der Myosin Regulatory Light Chain (MRLC) vom Kern zur Membran gekennzeichnet. Hier wird gezeigt, dass die Phosphorylierung von MRLC sowie die Relokalisation von den Kernkomponenten des PCP Signalweges kontrolliert werden. Die vorliegende Studie legt weiterhin Indizien vor, dass es im Verlauf der frühen Herzentwicklung unter anderem durch die Relokalisierung von pMRLC zu Änderungen in der Gewebespannung kommt, welche sich auf die nukleäre Spannung auswirken und damit Veränderungen in der Genregulation hervorrufen. Diese Veränderungen werden hauptsächlich durch Effekte auf die Lokalisation und Aktivität des Serum Response Factors (SRF) vermittelt, welche in diesem Kontext durch die PCP Kernkomponente Pk1 reguliert sind. Zusammenfassend zeigen die hier vorgelegten Untersuchungen, dass der PCP Signalweg essentiell für die durch SRF gesteuerte Muskeldifferenzierung und die damit einhergehende Reifung des Herzens ist.

1 Introduction

Congenital heart defects (CHD) refer to anomalies in the structure of the heart or great vessels that are present at birth. In Europe, CHD account for nearly one-third of newborns with major congenital anomalies diagnosed prenatally or in infancy (EUROCAT Access Prevalence Tables). Despite recent advances in prenatal diagnosis and treatment, CHD remain the leading cause of infant mortality with an average total prevalence of 0.8% of births in Europe (Dolk et al., 2011). Although there have been many advances in the understanding of CHD and several associated genes have been identified, the fundamental mechanisms involved in the emergence of these birth defects remain incompletely understood. Elucidating these mechanisms is therefore pivotal for improving treatment of both congenital and acquired heart disease.

1.1 Early Cardiogenesis in Zebrafish

Zebrafish are the ideal model organism to study early embryogenesis, because of their rapid external development, transparency of embryos and large amounts of offspring. In particular the fact that they develop for up to five days post fertilization (dpf) on diffused oxygen, allows studying the function of genes involved in cardiovascular development, which loss-of-function usually causes lethality in other models (Burggren and Pinder, 1991; Chen and Fishman, 1996; Reiter et al., 1999; Yelon et al., 2000).

Directly after fertilization, non-yolk cytoplasm streams towards the animal pole forming a single cell that is clearly separated from the granule-rich cytoplasm of the yolk. The following two to three hours post fertilization (hpf) are marked by cell divisions that lead to formation of the 128-cell Blastula stage. It is at this time that a membrane-enclosed group of nuclei on top of the yolk – the yolk syncytial layer (YSL) that serves as a boundary between yolk and blastoderm – is formed. After four hours of development, epiboly is initiated with the yolk bulging toward the animal pole and migration of blastomeres from the animal to the vegetal pole. After five hpf half of the yolk is covered by blastoderm (50%-epiboly) and a thickened marginal region – the germ ring – appears, marking the beginning of gastrulation. Convergence movements lead to local accumulation of cells at one position along the germ ring forming the embryonic shield. By the end of gastrulation, at around ten hpf the three primary germ layers – ectoderm, endoderm, and mesoderm – have been formed by involution that folds the blastoderm layer back upon itself, and the dorsoventral and anteroposterior body axis is established. Subsequently, segmentation is initiated by furrowing of the first somite at around 10.5 hpf (Kimmel et al., 2005).

Cardiac development is initiated by specification of myocardial and endocardial progenitor cells within the mesodermal germ layer at 5 hpf (Figure 1 A) (de Pater et al., 2009; Hami et al., 2011; Keegan, 2004). Before the start of gastrulation, two pools of myocardial progenitor cell types: atrial and ventricular precursors, are specified in two groups in the marginal zone at either side of the embryo with ventricular progenitors closer to the margin (Figure 1 B) (Buckingham et al., 2005; Stainier et al., 1993). At the same time endocardial progenitors locate to similar regions of the margin (Lee et al., 1994). During gastrulation and early somite stages, the cardiac progenitor cells migrate to the posterior half of the anterior lateral plate mesoderm (ALPM). The myocardial progenitors then migrate over the midline to form a disc-shaped epithelium that fuses to develop the heart cone (Figure 1 C, D). Both, the endoderm and YSL were shown to control the migration of progenitors to the ventral midline (Glickman and Yelon, 2002; Kikuchi et al., 2000; Reiter et al., 1999; Sakaguchi, 2006). After the onset of somitogenesis, cardiac progenitors can be visualized by either their common expression of the transcription factor gene *nkx2.5* and the cardiac myosin regulatory light chain gene *myl7* or by atrial / ventricular precursor specific expression of ventricular myosin heavy chain (*vmhc*) or atrial myosin heavy chain (*amhc/myh6*) (Glickman and Yelon, 2002; Yelon et al., 1999). During migration of myocardial precursors to the midline, endocardial progenitors proceed to coat the interior of the heart cone (Bussmann et al., 2007). At approximately 22 hpf, further migration of both, endocardial and myocardial precursors, leads to formation of the linear heart tube (LHT) a transient structure composed of an inner endothelial tube surrounded by an immature myocardial single-cell layer (Figure 1 E).

At 24 hpf left-right asymmetry of the developing heart is achieved through laterality cues that initiate cardiac jogging and looping. First, leftward jogging displaces the LHT relative to the dorsal midline (Figure 1 F). Subsequent cardiac looping creates distinct asymmetry of the heart at 36 hpf (Figure 1 G) (Ahmad, 2004). Ciliary function within the laterality organ known as Kuppfer's vesicle has been shown to be crucial for the direction of cardiac jogging and looping (Ferrante et al., 2008; Spéder et al., 2007).

The vertebrate heart is specified and formed by two heart fields: first heart field (FHF) and second heart field (SHF). In mouse, cardiomyocytes of the FHF form the left ventricle (LV) and large portions of the atria, while the SHF builds most of the right ventricle (RV) and the outflow tract (OFT) (Buckingham et al., 2005; Hamblet, 2002; Henderson et al., 2006). In zebrafish, the LHT is formed by the FHF cardiomyocytes (Mosimann et al., 2015). As cardiogenesis proceeds, cardiomyocytes of the SHF are added to the arterial and venous pole of the heart tube (de Pater et al., 2009; Gessert and Kühl, 2010; Hami et al., 2011; Mosimann et al., 2015; Rohr et al., 2008; Zhou et al., 2011).

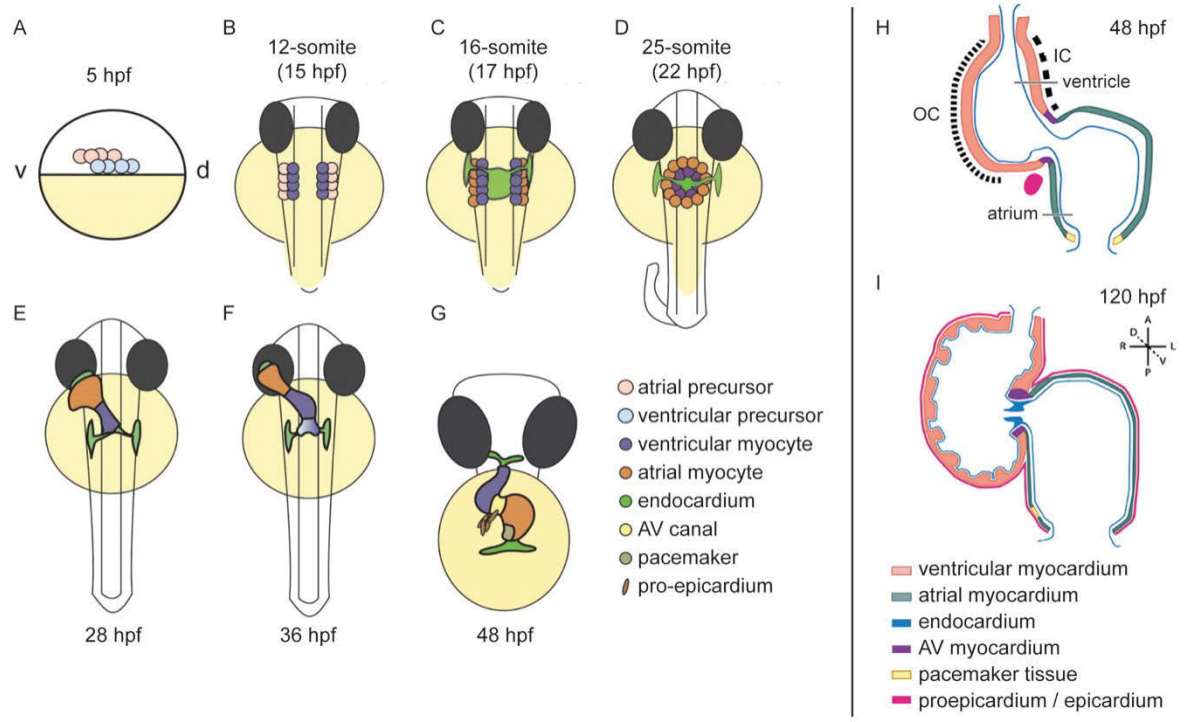

Figure 1: Early cardiac development in zebrafish. (A) Cardiac progenitor cells are specified within the mesodermal germ layer. (B) Atrial and ventricular precursors are specified in two groups in the marginal zone of the pharyngeal mesoderm. (C) Endocardial progenitors lie anterior in the anterior lateral plate mesoderm (ALPM). Precursors migrate to the ventral midline and (D) bilateral heart fields fuse to form a heart cone with endocardial cells in the center. (E) Formation of the primitive linear heart tube (LHT) with the endocardium as an inner lining. The venous pole of the LHT is located at the anterior left and the arterial pole stays fixed at the midline. (F) Cardiac looping establishes left-right asymmetry and (G) AV canal formation separates atrium from ventricle while the heart assumes a characteristic S-formed shape. (H, I) Transversal view of chambered heart. (H) Ventricular morphology establishes characteristic OC and IC regions (I) Ventricular trabeculation has started and the AV valve has formed. (A) lateral view, (B-F) dorsal view, (G) ventral view. IC = inner curvature, OC = outer curvature, hpf = hours post fertilization, AV = atrioventricular. (modified from: Bakkers, 2011; Staudt & Stainier, 2012).

The accrual of SHF and bulging of cardiomyocytes off the heart tube contributes to the formation and the expansion of the cardiac chambers (Figure 1 G, H) (Christoffels et al., 2000). In zebrafish ventricle, cardiomyocytes of the SHF are incorporated mainly to the inner curvature (IC), while the outer curvature (OC) mostly consists of cells of the FHF (de Pater et al., 2009; Mosimann et al., 2015). After cardiac looping and formation of the two-chambered heart clear differences in size and shape between OC and IC cardiomyocytes emerge (Figure 1 H) (Auman et al., 2007).

At LHT stage and during cardiac looping only two cellular layers form the primitive heart: the endocardium surrounded by the myocardium. At 48 hpf another extracardiac layer, the pro-epicardium, can be distinguished close to the ventral wall of the looped heart (Figure 1 H). The pro-epicardium consists of a group of spherical cells that attach to the

myocardium and start to spread over the myocardial surface to form the epicardium at 72 hpf (Figure 1 I) (Liu and Stainier, 2010; Peralta et al., 2013; Serluca, 2008).

In the course of cardiac looping two pronounced areas of constriction appear: the atrioventricular (AV) canal between atrium and ventricle, and the OFT between ventricle and great arteries (Hinton and Yutzey, 2011; Hu et al., 2000). Subsequently, cardiac cushion tissue in these regions is formed predominantly by endocardial epithelial-mesenchymal transition (EMT) (Markwald et al., 1977; Markwald et al., 1975). The AV and OFT cushion tissues ensure further development of valve primordia to maintain unidirectional blood flow. Here, the cushion tissue of the OFT gives rise to semilunar valve, whereas AV valve originates from that of the AV region (Figure 1 I) (Person et al., 2005). While cardiac growth at LHT stage is mainly achieved through addition of SHF cardiomyocytes, proliferation within the myocardium increases progressively after 48 hpf (Liu et al., 2010). Around 72 hpf at the end of cardiac looping cardiac trabeculation is initiated. This process describes the formation of a meshwork of highly organized sheet-like muscular structures within the ventricular cavities (Ben-Shachar et al., 1985). These trabeculae form through extrusion and expansion of differentiated cardiomyocytes and therefore consist of myocardial cells that are mantled by the endocardial layer. The purpose of these trabeculae is to increase cardiac output and maximize nutrition and oxygen uptake in the embryonic myocardium before the development of coronary arteries (Liu et al., 2010; Rychter and Ostádal, 1971; Sedmera et al., 1997). For subsequent cardiac chamber maturation, remodeling of trabeculae is essential and requires myocardial proliferation, development of the coronary vasculature and maturation of the conduction system (Weiford et al., 2004). At around 120 hpf the AV valves are fully formed preventing retrograde flow between the chambers and the epicardium covers the entire surface of the myocardium (Figure 1 I).

During embryonic development, the heart is the first organ to form and function. Thus, cardiogenesis comprises not only morphological, but also functional changes within the myocardium. Importantly, the heart maintains its physiologic pumping function during remodeling from LHT stage to its chambered form. This requires synchronization of cardiac remodeling and electrical coupling between cardiomyocytes. Blood flow, established as the blood is pumped from the venous to the arterial pole, is crucial to ensuing cardiogenesis, together with other embryogenic processes that respond to hemodynamic signals (Dietrich et al., 2014; Moorman, 2003; North et al., 2009; Reckova, 2003). Although still controversial, at the early stages the linear hear tube contracts either as a peristaltic or as an impedance pump (Forouhar, 2006; Männer et al., 2010). Cardiomyocytes of the linear heart tube are characterized by its slow proliferation rate, slow conduction velocity, and poor contractility (Panáková et al., 2010; Rana et al., 2013; Soufan et al., 2006). As the formation of the two

cardiac chambers proceeds, cardiomyocytes of the OFT, IC, AV canal, and sinus venosus (SV) preserve this primary phenotype and give rise to the, zones of slow conduction (Christoffels et al., 2010; Mosimann et al., 2015; Panáková et al., 2010). Whereas atrial and ventricular cardiomyocytes acquire different characteristics that are associated with fast conduction velocity and increased contractility (Christoffels et al., 2010).

1.1.1 Gene Regulatory Networks in Cardiac Development

During early heart development cardiomyocyte differentiation is controlled by interactions between various cardiac-restricted evolutionary conserved transcription factors that direct cardiac cell fates, myocyte differentiation, and cardiac morphogenesis (Moorman, 2003; Olson, 2006; Staudt and Stainier, 2012).

Specification of cardiac precursors is regulated by a variety of signaling pathways, including retinoic acid (RA) (Keegan, 2005), Wnt (Ueno et al., 2007), Hedgehog (Hh) (Voss et al., 2009), fibroblast growth factor (Fgf) (Marques et al., 2008), bone morphogenic protein (Bmp) (Dietrich et al., 2014; Marques and Yelon, 2009; North et al., 2009; Reckova, 2003; Reiter et al., 2001), and Nodal (Keegan, 2004; Reiter et al., 2001; Stainier et al., 1993). Induction of heart lineages requires inhibition of Wnt signaling in lateral margins of the head precursor zone, where BMP signaling is maintained (Marvin, 2001). Here, both BMPs, Wnts and Wnt antagonists likely act in a concentration-dependent manner to ensure cardiac cell specification (Alsan and Schultheiss, 2002; Schneider, 2001). However, how the multitude of pathways interacts with each other to control the cell fate of myocardial progenitors remains mostly elusive.

The first wave of cardiac progenitor migration from mesendodermal structures is governed by Fgf8 and the basic helix-loop-helix transcription factors Mesoderm posterior 1 and 2 (Mesp 1 and 2) (Kitajima et al., 2000; Sun et al., 1999). Subsequent cardiac gene expression is regulated by a kernel of transcription factors that is expressed in cardiomyocytes and indispensable for initiation and maintenance of cardiac gene expression: NK2 transcription factor related, locus 2 (Nkx2.5), GATA-binding protein 4 (Gata4), T-box 5 and 20 (Tbx5 and Tbx20), heart and neural crest derivatives expressed transcript 1 or 2 (Hand1/Hand2), the MADS domain TF serum response factor (SRF) and myocyte-enhancer factor 2A (Mef2a) (Cripps and Olson, 2002; Harvey et al., 2002; He et al., 2011). Notably, not only Gata4, but also other members of the GATA transcription factor family - Gata5 and Gata6 - control several aspects of heart formation from specification to migration (Holtzinger and Evans, 2007; Hu et al., 2000; Peterkin et al., 2007). Another transcription factor, Myocardin, was shown to be co-expressed with Nkx2.5. Myocardin belongs to a family of chromatin-remodeling proteins and forms a ternary complex with SRF. Binding of Myocardin to SRF

binding sites was shown to result in efficacious activation of cardiac gene expression (Wang et al., 2001).

The transcription factor Hand2 functions to increase the amount of ventricular progenitors and is necessary for the maintenance of the expression of *tbx5* (T-box transcription factor 5), that has been shown to be crucial for heart development (Garrity et al., 2002; Le A Trinh et al., 2005). Further migration of cardiac progenitor cells to the ALPM requires *nkx2.5*, *gata5*, and *hand2* activity as well as G-protein receptors (Chen and Fishman, 1996; Hsu et al., 1998; Reiter et al., 1999; Scott et al., 2007; Yelon et al., 2000). Cardiac cell differentiation within the ALPM is controlled by neighboring vascular and hematopoietic precursors that affect *hand2* expression and control atrial cell number (Schoenebeck et al., 2007).

Jogging of the LHT and cardiac looping require cues of the left-right asymmetry signaling pathways that comprise the nodal-related gene southpaw (spaw) and its downstream effector pitx2, lefty1, and lefty2 (Ahmad, 2004). Pitx2 is furthermore crucial for the patterning of the aortic arches, the OFT, and the AV valves and cushions (Liu et al., 2002). Restricted expression of *bmp4*, *versican* and *notch1b* was observed within zones of constriction in the AV canal and OFT region (Beis, 2005; Timmerman et al., 2003; Walsh and Stainier, 2001). Several other signaling pathways were implicated in AV canal development, such as Calcineurin, Wnt, TGF-β, Prostaglandin and ErbB/Neureguling signaling cascades (Chang et al., 2004; Hurlstone et al., 2003; Scherz et al., 2008).

The factors that control FHF and SHF specification are still poorly understood. However, Islet1 (Isl1), a LIM homeodomain transcription factor, has been described as a marker of the SHF, while Tbx5 marks progenitors of the FHF (Cai et al., 2003; Gessert and Kühl, 2009). Furthermore, it has been documented that proliferation and patterning of the SHF require Nkx2.5, Mef2c, Hand2, Pitx2, Foxh1 (Buckingham et al., 2005). Additionally, regulation of FGF ligand expression by Wnt/β-catenin and Notch signaling is crucial for proper SHF cell specification, while BMP and non-canonical Wnt signaling are essential for cardiomyocyte differentiation (Cohen et al., 2012; High et al., 2009; Hutson et al., 2010; Klaus et al., 2012; Park et al., 2008; Watanabe et al., 2010).

Atrial and ventricular chamber formation is accompanied by morphological and functional changes within the myocardium. Several regulatory pathways regulate the processes that guide the development of the early single layered myocardium. A diverse set of transcription factors regulates cardiac chamber morphogenesis; most notably the T-box transcription factors Tbx2, Tbx3, Tbx5, and Tbx20, as well as Gata4, Nkx2.5, Nkx2.7, and Hand1. While Tbx5 and Tbx20 promote differentiation of atrial and ventricular cardiomyocytes by interaction with Nkx2.5 and Gata4, interaction of Tbx2 and Tbx3 with these transcription factors represses such specification. Here, both Nkx2.5 and Gata4 are highly expressed

throughout the primitive heart tube, whereas the different isoforms of T-box transcription factors show distinct expression patterns within the myocardium (Hoogaars et al., 2007). Furthermore, cardiac chamber size likely is regulated by both Nkx2.5 and Nkx2.7 (Targoff et al., 2013; Tu et al., 2009).

1.2 Wnt Signaling in Cardiogenesis

Wnt proteins are evolutionary conserved secreted cysteine-rich glycoproteins that regulate crucial aspects of embryonic development including proliferation, migration, cell-fate specification, adhesion and regeneration processes as well as ion homeostasis (De, 2011; Lim and Nusse, 2013; Willert and Nusse, 2012). Dysregulation of Wnt signaling is implicated in a variety of diseases such as cancer, bone malformations, obesity, diabetes, and neurodegenerative defects (Christodoulides, 2006; De Ferrari and Moon, 2006; Faienza et al., 2014; Giles et al., 2003; Grant et al., 2006; Nusse, 2005). The first member of the Wnt family, Wnt1, was discovered in mice during the 1980s as a proto-oncogene named int-1 acting in oncovirus-induced breast cancer (Nusse and Varmus, 1982). Later it was revealed that int-1 is a sequence homologue to the gene wingless in *Drosophila melanogaster* that functions as a segment polarity gene and a combination of both gene names led to its description as Wnt (Nüsslein-Volhard and Wieschaus, 1980; Rijsewijk et al., 1987). To date, nineteen Wnt genes have been identified in mammals that fall into 12 conserved Wnt subfamilies. Here, different Wnt ligands activate either the canonical or the non-canonical cascade: (1) Canonical: Wnt1, Wnt2, Wnt3, Wnt8a, Wnt8b, Wnt10a, and Wnt10b, (2) Non-canonical: Wnt4, Wnt5a, Wnt5b, Wnt6, Wnt7a, Wnt7b, and Wnt11), and (3) indeterminate groups: Wnt2b and Wnt9b (Wnt Website: www.stanford.edu/ ~rnusse/wntwindow.html).

The classical characterization of Wnt signaling distinguishes between the canonical and non-canonical pathway. Briefly, the highly evolutionary conserved canonical Wnt transduction pathway acts through the stabilization of β-catenin regulating the expression of TCF/LEF target genes. In cells with little to no active Wnt signaling cytosolic β-Catenin is frequently N-terminally phosphorylated, ubiquitinated and targeted for proteolysis by the E3-ubiquitin ligase in the so-called β-Catenin destruction complex comprising Axin, the Adenomatous polyposis coli (APC) protein and the Glycogen synthase kinase 3 (GSK3β) (Aberle et al., 1997; Ikeda, 1998; Kitagawa et al., 1999).

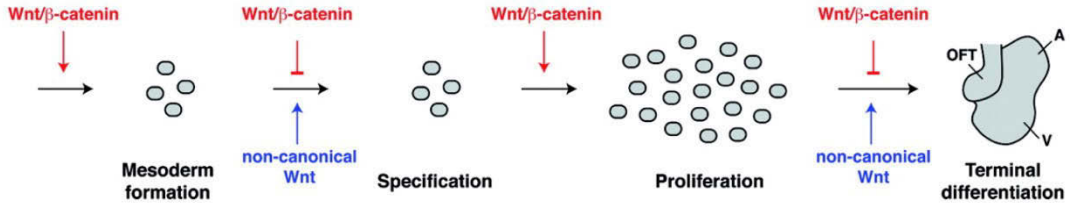

Figure 2: Canonical Wnt / β-Catenin pathway activity is temporally regulated to ensure proper heart development. Mesoderm formation and proliferation of cardiomyocytes requires activation of canonical Wnt signaling. In contrast, specification of cardiac progenitors and terminal differentiation require attenuation of the canonical branch, while non-canonical Wnt signaling promotes these processes (modified from: Gessert & Kühl, 2010).

Activation of the Wnt signaling cascade leads to stabilization and accumulation of β-Catenin within the cytoplasm (Kimelman and Xu, 2006). Cytosolic β-Catenin translocates to the nucleus, where it regulates downstream gene expression by binding to Tcf/LEF family members (Behrens et al., 1996; Hsu et al., 1998; Keller et al., 1985). Tight temporal control of canonical Wnt/β-catenin signaling activity is absolutely crucial during early cardiogenesis where it is indispensable for early cardiac specification, but must be attenuated for the development of cardiomyocytes (Tzahor, 2007). Specifically, Wnt/β-catenin signaling acts upstream of processes that induce mesoderm formation and control Mesp1 activity that was described as the earliest marker of cardiovascular lineage (Behringer et al., 1999; Lindsley, 2006; Saga, 2000). Later in development, however, canonical Wnt signal transduction is attenuated through Notch activity to allow cardiomyocyte differentiation, which additionally requires activation of the Wnt non-canonical pathway (Kwon et al., 2009; Pandur et al., 2002; Yamashita et al., 2005). Proliferation of cardiomyocytes is regulated by activation of Wnt/β-Catenin signaling (Norden and Kispert, 2012; Norden et al., 2011). Finally, inhibition of Wnt/β-Catenin signaling is required to ensure terminal differentiation of cardiomyocytes (Naito et al., 2006; Qyang et al., 2007; Ueno et al., 2007; Zhu et al., 2008). At the same time, Wnt non-canonical signaling is activated to initiate terminal differentiation of cardiomyocyte (Figure 2) (Garriock et al., 2005; Gessert et al., 2008; Ueno et al., 2007). Several Wnt ligands are expressed during early cardiogenesis, including Wnt8, Wnt2a and b, Wnt5a and Wnt11 (Cohen et al., 2008).

Studies in *Drosophila*, *Xenopus* and zebrafish revealed β-Catenin-independent non-canonical Wnt transduction pathways that comprise Wnt/Ca^{2+} signaling and the planar cell polarity (PCP) pathway (Figure 3) (Gessert and Kühl, 2010; Phillips, 2005; Yates et al., 2010a; Yates et al., 2010b; Ybot-Gonzalez et al., 2007). In zebrafish, injection of Fzd2 and Wnt5a mRNA led to increased intracellular Ca^{2+} levels during gastrulation (Moon et al., 1997). Heterotrimeric G-proteins activate Phosphoinositide-3-kinase (PI3K) and

Phospholipase C (PLC) leading to the synthesis of Inositol-1,4-5-triphosphate (IP_3) and Diacylglycerol that triggers release of intracellular Ca^{2+} from the endoplasmic reticulum (Cantley, 2002; Moon et al., 1997; Sheldahl et al., 2003). Released Ca^{2+} ions activate the Protein kinase C (PKC), Calcineurin (CaCN) and the Ca^{2+}/Calmodulin-dependent protein kinase II (CamKII) (Figure 3) (Kühl et al., 2000; Saneyoshi et al., 2002). Moreover, non-canonical signaling mediated by Wnt11 was shown to attenuate transmembrane Ca^{2+} influx through down-regulation of L-type calcium channel (LTCC) conductance (Figure 3) (Panáková et al., 2010).

The second classical branch of non-canonical Wnt signaling is the PCP pathway, which is the focus of this study and described in detail in the following section.

1.2.1 Planar Cell Polarity Pathway

PCP signaling refers to mechanisms responsible for the alignment of cells in a cooperative manner with a specific orientation that is orthogonal to the apicobasal axis within epithelial sheets. The non-canonical Wnt/PCP pathway was initially discovered in *Drosophila melanogaster* where it controls the alignment of actin hairs (trichomes) of the wing disc epithelium and the rotation of ommatidia in the eye (Adler et al., 1997; Gubb and García-Bellido, 1982; Strutt et al., 1997; Wong and Adler, 1993).

Although it is widely accepted that PCP needs to be established and maintained throughout the life-cycle of an organism, early studies in zebrafish and *Xenopus* mainly focused on its function in guiding convergent extension movements of mesenchymal cells during vertebrate gastrulation (Heisenberg et al., 2000; Tada and Smith, 2000; Wallingford et al., 2000). However, PCP signaling is indispensable for several morphogenetic processes also during organ development, in neural tube closure, ear patterning and hearing as well as lung and kidney branching (Phillips, 2005; Yates et al., 2010b; Yates et al., 2010a; Ybot-Gonzalez et al., 2007). Hence, it is not surprising that also proper cardiac development is dependent on planar cell polarity (PCP) signaling. It has been shown that defective regulation of the PCP pathway does generally result in CHD (Hamblet, 2002; Henderson et al., 2006; Marlow et al., 2002; Unterseher et al., 2004). Although the underlying mechanisms remain unresolved, it was shown that one of the major ligands of Wnt non-canonical signaling in the heart is Wnt11 that is crucial to normal heart development and cardiac gene expression. Furthermore, its overexpression was sufficient to induce contractile tissue formation (Afouda et al., 2008; Pandur et al., 2002).

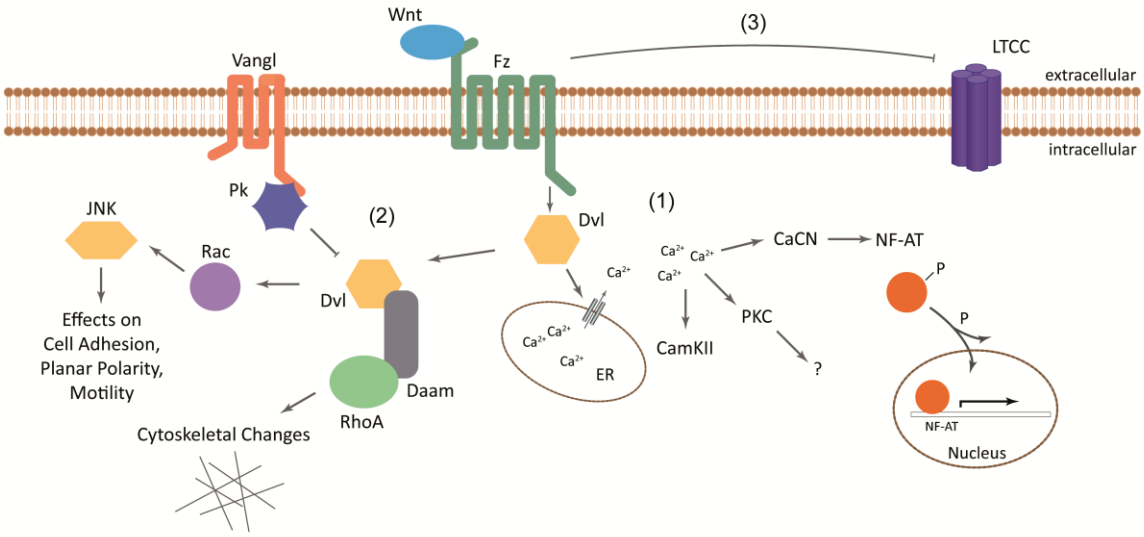

Figure 3: Non-canonical Wnt signaling comprises the PCP pathway and Ca^{2+} signaling. Binding of non-canonical Wnt ligands to the transmembrane receptor Fzd initiates PCP and/or Ca^{2+} signaling. The signal is relayed through the cytosolic protein Dvl that either (1) ensures Ca^{2+} release from the endoplasmic reticulum to activate the Calmodulin Kinase II (CamKII), the Protein kinase C (PKC), and Calcineurin (CaCN) that initiates NF-AT regulated gene expression or (2) forms a complex with Daam and RhoA to act on actomyosin and JNK to regulate effects on cell adhesion, planar polarity, and motility. (3) Wnt11 attenuation of LTCC function limits transmembrane Ca^{2+} influx.

The PCP pathway core components Frizzled (Fzd), Van Gogh-like (Vangl), Dishevelled (Dvl), and Prickle (Pk) are transmembrane or membrane-associated proteins. Common for both canonical and non-canonical Wnt pathways is the initiation of signal transduction by binding of Wnt ligands to the seven-pass transmembrane receptor Fzd. The signal is then relayed through the cytosolic protein Dvl, which serves as a hub able to distinguish between signal transmission to either the canonical or to non-canonical branches of Wnt signaling. This is achieved through binding of interaction partners to its either N-terminal DIX (Dishevelled, Axin), central PDZ (Post-synaptic density 95, Discs-large, Zonula occludens-1) or C-terminal DEP domain (Dishevelled, Egl-10, Plekstrin) (Gao and Chen, 2010). The DIX domain is essential for the canonical Wnt pathway, the DEP domain mediates non-canonical PCP and Ca^{2+} signaling, while the PDZ domain is required for both non-canonical and canonical Wnt signaling (Axelrod et al., 1998; Boutros et al., 1998; Wallingford and Habas, 2005).

Core components that are unique to Wnt/PCP signaling include the four-pass transmembrane protein Vangl, the cytoplasmic LIM- and PET-domain containing protein Pk, the atypical protocadherin Flamingo (Fmi), and the Ankyrin-repeat protein Diego (Dgo) (Chae et al., 1999; Feiguin et al., 2001; Gubb et al., 1999; Usui et al., 1999; Wolff and Rubin, 1998). Fzd, Dvl and Dgo are described as positive regulators of PCP signaling, while Pk and Vangl function as antagonists of the system (Ciruna et al., 2006). While Fmi can recruit either Fzd

or Vangl, both Dvl and Pk can be solely recruited by Vangl (Zallen, 2007). Furthermore, Dvl interacts competitively with either Pk or Dgo leading to either inhibition or activation of signal transduction (Jenny et al., 2005). In the Drosophila wing disc, PCP core components assume an asymmetric distribution with accumulation of Vangl and Pk at the proximal and Fzd, Dvl, and Dgo at the distal apical cortex of the membrane (Gray et al., 2011). Intercellular interaction of the core components establishes overall tissue polarity (Carvajal-Gonzalez et al., 2014). Finally, transmission of the signal to the effector proteins RhoA, Rac, and JNK results in changes of the cytoskeleton, planar polarity, cell adhesion, and cellular motility (Figure 3) (Marlow et al., 2002; Unterseher et al., 2004). Several studies show that the function of the PCP core components is highly dependent on proper expression of each of the aforementioned components (Keegan, 2004; Klein and Mlodzik, 2005; Krasnow et al., 1995).

1.3 PCP in Development and Disease

Generally, genetic disruptions in PCP signaling cause severe developmental abnormalities like failure of neural tube closure or left/right patterning defects. Both the ligands and core-components of Wnt non-canonical PCP signaling are crucial for various aspects of development from gastrulation movements to the morphogenesis of various organs. The necessity of tightly regulated non-canonical Wnt signaling during cardiogenesis was proven in several studies that implicate PCP signaling in the specification of cardiac progenitor cells, linear heart tube formation, cardiac looping and OFT development, and wound healing after myocardial infarction (MI) (Brade et al., 2006). A variety of Wnt ligands is upregulated in MI models and involved in subsequent development of hypertrophic phenotypes and cardiac wound healing (Aisagbonhi et al., 2011; Oerlemans et al., 2010). Furthermore, PCP signaling is pivotal to establishment of left-right asymmetry as both loss of Pk1a and Wnt11 leads to inverted heart looping (Oteiza et al., 2010).

Notably, loss or overexpression of either core component of the PCP signaling pathway results in severe cardiomyopathies. Cardiac-specific Dvl upregulation in mice results in myocardial hypertrophy (Malekar et al., 2010). *Looptail* (Lp) mutant mice, which carry a missense mutation in Vangl2, display neural tube defects like spina bifida or craniorachischisis as well as heart looping defects during early cardiogenesis and the outflow tract abnormality double-outlet right ventricle (DORV) (Henderson et al., 2001; McGreevy et al., 2015). In humans, homozygous mutations in Pk1 result in progressive myoclonus epilepsy that is characterized by general neurological decline resulting in seizures, ataxia, and dementia and in neural tube closure defects (Bassuk et al., 2008; Bosoi et al., 2011). Furthermore, it was shown in mice that Pk1 is highly expressed in developing digit rays and

required for limb growth (Yang et al., 2013). In zebrafish, overexpression of a dominant-negative mutant of Dvl2 missing the DEP domain induced cardiac bifida phenotypes (Matsui, 2005).

Although dysregulation of Wnt signaling cascades mainly results in heart defects, few studies show beneficial outcomes after suppression of the Wnt signaling cascade. Here, expression of secreted frizzled related proteins (SFRPs) that compete for Wnt binding to Fzd was shown to have positive effects on cardiac remodeling after injury (He et al., 2010; Mirotsou et al., 2007).

1.4 Tissue Morphogenesis During Organogenesis

Morphogenesis refers to the processes during embryonic development where tissues undergo bending, narrowing, lengthening, branching, and folding to acquire distinct shapes necessary to form functional organs. During morphogenesis, proper organ shape is acquired by tight regulation of the interplay between changes in cell shape, cell organization, and mechanical forces that affect the tissue architecture (Papusheva and Heisenberg, 2010).

1.4.1 Collective Cell Behaviors

Firstly, the importance of changes in cell shape and organization was studied extensively for convergent extension (CE) movements during *Xenopus* gastrulation. Here, convergence movements narrow embryonic tissues over the mediolateral axis, whereas extension movements elongate them along the perpendicular axis from head to tail (Wallingford et al., 2002). These movements are mostly guided by mediolateral intercalation and directed migration of cells (Figure 4 A) (Solnica-Krezel, 2005). During mediolateral narrowing, cells become elongated to facilitate intercalation movements and simultaneous rostrocaudal elongation of the body axis (Keller and Shih, 1992). Directed migration of cells, on the other hand, is guided by medial and lateral formation of lamellipodia that attach to neighboring cells thereby promoting intercalation movements (Elul and Keller, 2000). Additionally, cell behaviors such as polarized cell division and apical-basal elongation of cells contribute to CE (Gong et al., 2004). It is well known that non-canonical Wnt signaling is required for mediolateral cell polarization that underlies CE movements; e.g. vangl2- deficient embryos show severe defects in body axis elongation (Heisenberg et al., 2000; Sepich et al., 2000; Tada and Smith, 2000). Moreover, downstream effectors of PCP signaling that comprise RhoA, Rac, and Cdc42 were shown to mediate migrative behavior of cells (Choi and Han, 2002; Tahinci and Symes, 2003).

In general, asymmetric and polarized cell morphology is the basis for organization and maintenance of the function of several organs and tissues. This becomes apparent in the structure of nerve cells that are clearly polarized with dendrites on the one and axons on the other side of the cell body. However, also cells within a tissue plane often have to assume distinct polarization patterns, which is especially true for epithelia (Martin-Belmonte and Perez-Moreno, 2011). Importantly, the myocardium of the developing heart displays clear epithelial tissue characteristics such as apicobasal polarity at least until 96 hpf (Vanderploeg et al., 2012).

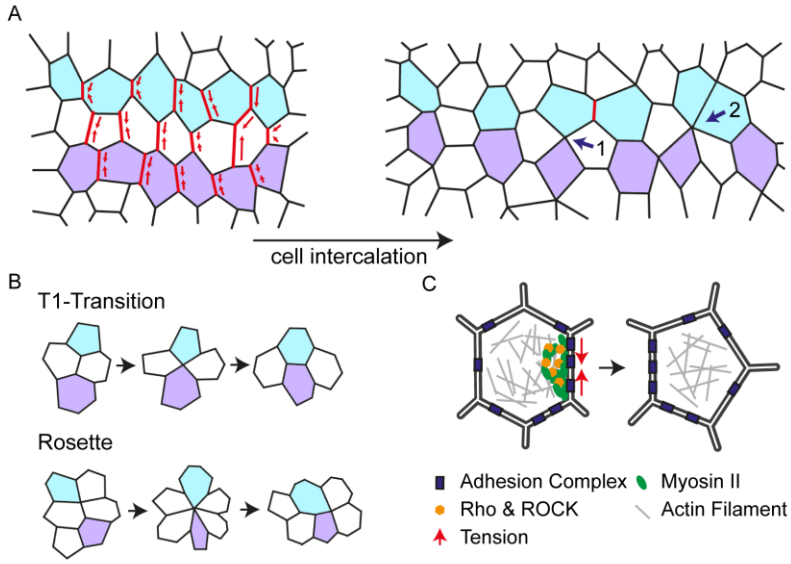

Figure 4: Tissue morphogenesis is driven by diverse mechanisms of collective cell behaviors. (A) Mediolateral cell intercalation drives convergent extension (CE) during zebrafish gastrulation by spatial regulation of NMII. Shrinkage of 'vertical' junctions through anisotropic tension exerted by medial-apical actomyosin and polarized NMII (in red) and extension of 'horizontal' ones drives tissue elongation along the anteroposterior axis. Within epithelial tissues, clusters of (1) four or (2) more cells form during these movements. (B) Epithelial remodeling is characterized by these T1 transitions and formation of rosettes. T1 transitions mediate cell rearrangements in clusters consisting of four cells. Collectives containing five or more cells remodel via formation of multicellular rosettes that are resolved in direction of tissue extension. (C) Transmission of tension requires changes in adhesion by E-cadherin re-localization to junctions and spatial regulation of myosin phosphorylation through kinases such as Rho and ROCK (modified from: Tada and Heisenberg, 2012; Lecuit, 2015).

Whereas mesenchymal tissue morphogenesis is mostly driven by cell intercalation and directed cell migration, rearrangements in apicobasally polarized epithelia are often regulated by additional mechanisms that have been characterized and defined as epithelial remodeling. In detail, epithelial remodeling describes the establishment of unique migratory patterns of apicobasally polarized cells that influence their position within planar polarized tissues guiding morphogenesis of many organs including lung, kidney, and the eye (Lienkamp et al., 2012; Rackley and Stripp, 2012; Zallen and Blankenship, 2008). Epithelial remodeling can be classified in two general modes that are directed by non-muscle myosin II (NMII)-conducted tensional changes of apical junctions. First, in a cluster of four cells shortening of the junction between two cells over the perpendicular axis of tissue extension leads to so called T1 transition that is completed by formation of a new junction along the axis of tissue elongation (Figure 4 B). Second, in groups of five to twelve cells the same mechanism leads to formation of flower-shaped multi-cellular rosettes (Figure 4 B) (Bertet et al., 2004; Blankenship et al., 2006).

Shortening of apical junctions is mediated by actomyosin contraction that leads to further recruitment of myosin II to these junctions (Fernandez-Gonzalez et al., 2009). Additionally, E-cadherin endocytosis at apical junctions is required for NMII-mediated junctional shrinkage (Levayer et al., 2011). Thus, coordinated action of actomyosin and adhesion underlies tissue morphogenesis regulated by epithelial remodeling (Figure 4 C).

1.4.2 Mechanical Forces During Tissue Morphogenesis

Mechanical forces direct various cellular processes: epithelial sheets undergo dramatic changes during embryonic development, muscle contraction underlies the remodeling of connective tissue, and vasculogenesis is dependent on changes in blood pressure (Ateshian and Humphrey, 2012; Fournier et al., 2010; Halcox and Deanfield, 2007). The first mechanical model for epithelial morphogenesis emerged in 1980 when Odell and colleagues discussed efficient mechanisms of epithelial cell shape changes through force generation by apical subcortical bands of microfilaments (Odell et al., 1980). It is known that mechanical forces, which drive tissue morphogenesis, are typically generated by molecular motors and transmitted via cytoskeletal components and adhesion molecules within and between cells (Heisenberg and Bellaïche, 2013).

One of the major requirements for force transmission is intercellular attachment generated through the formation of junctional complexes such as adherens and tight junctions. Adherens junctions (AJ) connect neighboring cell membrane and their actin cytoskeletons. This form of cell-cell adhesion is mainly dependent on members of the cadherin family that include classical cadherins (e.g. N-, E- and VE-Cadherin), protocadherins, and atypical

cadherins (e.g. Fat, Dachsous, Fmi). Homo- and heterophilic interactions between these transmembrane proteins of neighboring cells are mediated by their extracellular domains containing characteristic extracellular cadherin repeats (Yap et al., 1997). However, cadherins are not only required for adhesion between cells, but also for several aspects of tissue morphogenesis such as cell sorting, boundary formation, coordinated cell movements as well as the regulation of cell and tissue polarity (Halbleib and Nelson, 2006). These additional functions mainly rely on the interaction of the intracellular domain of cadherin with intracellular binding partners like the membrane associated components α- and β-catenin that transduce cadherin activity to the cytoskeleton to adjust actomyosin contractility (Harris and Tepass, 2010; Weis and Nelson, 2006). Here, tensile force was shown to strengthen the bond between cadherin, α- and β-catenin and actin filaments (Buckley et al., 2014). Both catenins were shown to be substantial for epithelial cohesiveness and transmission of tension within the epithelial sheet (Bazellières et al., 2015).

Another crucial regulator of mechanical force transduction and intra- as well as intercellular tension is actomyosin. Actomyosin was first discovered during the 1940s in muscle, when it was observed that actin and myosin form highly organized bundles of filaments that constitute more than half of the total protein (Straub, 1942). Many years later, both proteins were detected in other cell types showing that actomyosin in muscle tissue was a specialized form of a common system. Actomyosin contractility is a key regulator of cell morphology and tissue morphogenesis (Lecuit et al., 2011). First, stability and changes of cell shapes are generated through a cortex of F-actin meshwork located beneath the plasma membrane that resists and generates force (Bovellan et al., 2014). Second, active contractile tension is generated by ATP hydrolysis within myosin to move along these F-actin filaments (Howard and Clark, 2002). Junction shrinkage during epithelial remodeling is dependent on both actomyosin contractility and decreased adhesion. However, constriction of intercellular myosin cables seems to be crucial, since mutations in NMII perturb rosette formation during Drosophila axis elongation (Simoes et al., 2010).

NMII is a major regulator of the actomyosin tension that assumes several functions, including generation of cortical tension, mediating cytokinesis, and the regulation of cell shape changes during development, and needs to be therefore tightly controlled to maintain tensional homeostasis (Krendel, 2005; Vicente-Manzanares et al., 2009). The NMII hexameric molecule is formed by one pair of homodimerized heavy chains, two regulatory light chains (MRLC), and two essential light chains. Actomyosin contractility is regulated by dynamic phosphorylation of MRLC at the highly conserved amino acid residues T18 and S19 in vertebrates. This is achieved through several signaling pathways including those downstream of the Rho-associated protein kinase (ROCK), the Myotonic dystrophy kinase-

related Cdc42-binding kinase (MRCK, activated by Cdc42) and Myosin light chain kinase (MLCK, activated by Ca^{2+}) (Matsumura, 2005). Moreover, activation of MRLC through phosphorylation is controlled via inhibition of Myosin phosphatase target subunit 1 (MYPT1) activity that is mediated by its phosphorylation through ROCK (Kimura et al., 1996). Mechanisms upstream of this complex network of kinases and phosphatases comprise the induction of small GTPases by Rho GEFs leading to enhanced ROCK function and activation of Formin and Formin-related proteins such as Daam (Nishimura et al., 2012).

Cells need to sense physical constraints and exert mechanical forces to achieve organ-specific shape, cell-fate and differentiation. The forces generated by above-mentioned mechanisms result in strain of proteins and membranes. This leads to transduction into biochemical signals mostly through tension-dependent removal of an auto-inhibitory domain, which induces conformational changes in binding pockets of protein-protein interactions that are under tension (Yusko and Asbury, 2014). Likely candidates that are currently discussed as sensors of mechanical force and tension include stretch activated ion channels, the cytoskeleton, cell adhesion sites including cell adhesion molecules (CAMs) such as cadherins and integrins, cytoskeleton-linking proteins such as vinculin and talin and signaling proteins such as focal adhesion kinase (FAK) (Franze et al., 2009; Moore et al., 2012; Renaudin et al., 2000). Furthermore, the nucleus itself was discussed previously to respond to changes in intracellular tension. Here, mechanoregulation at integrins within the cell membrane was described to direct forces through the cytoplasmic cytoskeleton to the nuclear cortex resulting in changes in gene transcription (Swift et al., 2013).

Several studies explore mechanisms involved in force-dependent tissue morphogenesis. For instance, during vasculogenesis shear force exerted on endothelial cells generated by fluid flow ensures proper vessel formation (Freund et al., 2012). The significance of proper tensional homeostasis to achieve cell fate specification and differentiation was elucidated by the imitation of stem cell niches utilizing physiologically specific biomaterials and microfluidics. However, the understanding of the specific roles of mechanical forces in tissue morphogenesis, cell fate specification and differentiation remains incomplete.

1.5 Mechanosensitive SRF Signal Transduction

The serum response factor (SRF) was named after its function as a transcriptional regulator during the initiation of mitogenesis in response to serum-stimulation of various cultured mammalian cells (Norman et al., 1988; Treisman, 1986). Later, SRF was implicated in controlling morphogenetic movements and migration during embryonic development (Arsenian et al., 1998). This founding member of the MADS-domain containing family is highly conserved from fly to human and encoded by a single gene (Mueller and Nordheim,

1991; Shore and Sharrocks, 1995). Target genes of SRF share the presence of single or multiple copies of a CArG box – the consensus element CC[A/T]$_2$A[A/T]$_3$GG that binds SRF homodimers (Niu et al., 2007; Selvaraj et al., 2004; Sun et al., 2006; Zhang et al., 2005). In silico approaches have determined that the CArGome comprises more than 8000 evolutionary conserved CArG elements (Benson et al., 2011).

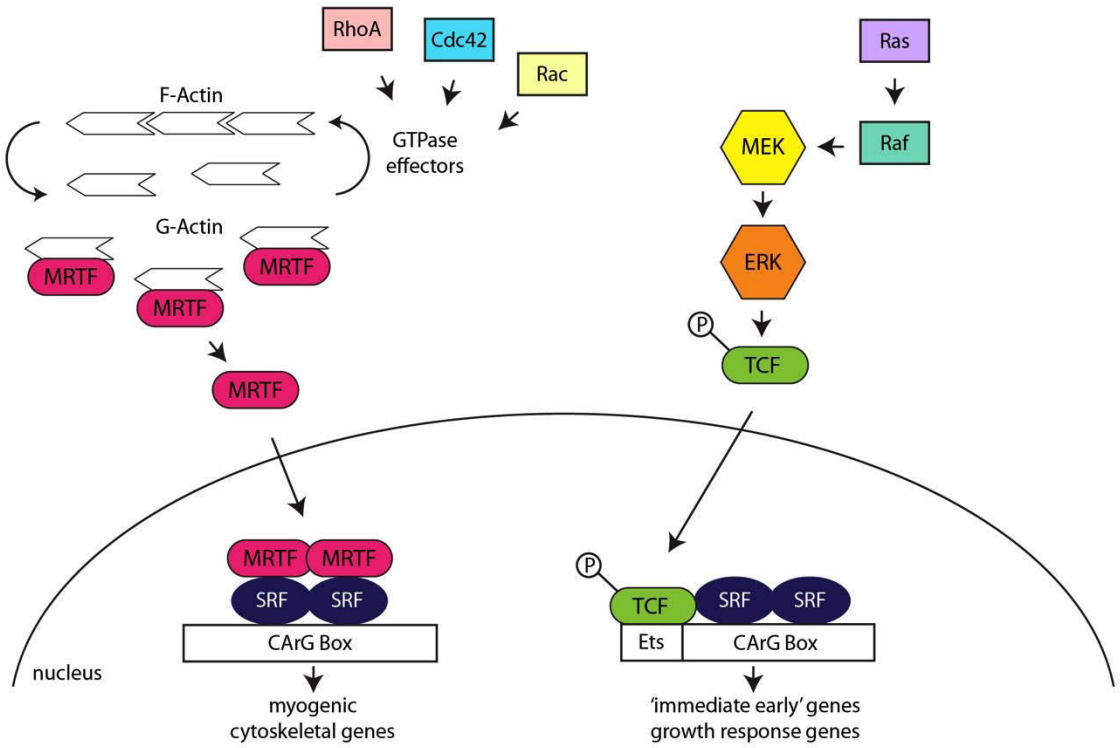

Figure 5: Two general SRF transduction cascades activate myogenic or growth response gene expression. (Left) SRF signaling responsible for myogenic and cytoskeletal gene expression is initiated by activation of Rho family GTPases that increase actin polymerization from monomeric G-Actin. Subsequent separation of G-Actin / MRTF complexes allows translocation of the MRTF cofactor into the nucleus where it binds and activates SRF. (Right) Activation of the MAP kinase pathway through Ras, Raf, MEK, and ERK phosphorylates the transcription factor TCF which leads to its translocation to the nucleus and binding to its own Ets DNA recognition site and SRF. This activates expression of 'immediate early' and growth response genes.

SRF signal transduction acts on two distinct classes of target genes: (1) mitogen-responsive "immediate-early" and growth-related genes encoding signaling molecules, cytoskeletal components, and transcription factors, and (2) muscle specific genes expressed in cardiac, smooth and skeletal muscle (Figure 5) (Pipes, 2006; Sun et al., 2006). The interaction of

SRF with two families of signal-regulated and tissue-specific cofactors determines unique target gene expression.

Firstly, members of the ternary complex factor (TCF) family of Ets domain proteins (e.g. Elk1) are activated by mitogen activated protein kinase (MAPK) phosphorylation that initiates rapid but transient expression of immediate-early genes like c-fos or by the Ras-Raf-MEK-ERK pathway that activates growth response genes (Treisman, 1994). Secondly, a signal-regulated SRF cofactor family, the myocardin-related transcription factors (MRTFs and MALs), ensures transcription of many genes encoding actin isoforms or actin binding proteins (ABP) such as vinculin or myosin (Olson and Nordheim, 2010).

Apart from the aforementioned two major cofactor families, other transcription factors have been implicated in SRF regulation. Positive regulation of SRF signal transduction is attained by members of the GATA family of zinc finger transcription factors as well as the Nkx2.5 family of homeodomain proteins (Belaguli et al., 2000; Chen and Schwartz, 1996).

Negatively acting SRF cofactors comprise the LIM-only protein FHL2, that antagonizes MAL-SRF dependent transcription, and the cardiac-enriched homeodomain-only cofactor HOP (Chen et al., 2002; Philippar et al., 2004; Shin et al., 2002).

SRF activation via the MRTF pathway is indispensible for cardiac muscle differentiation and the activation of smooth muscle contractile genes (Du et al., 2003; Wang et al., 2001). In mouse, SRF expression within the cardiac crescent is first observed when cardiac progenitor cells migrate to the midline to form a linear heart tube (Barron et al., 2005; Olson and Srivastava, 1996). During cardiogenesis the SRF target genes α-skeletal (*acta1*), α-cardiac (*actc1*) and α-smooth-muscle actin (*acta2*) are co-expressed in healthy myocardium and their abundance is dependent on the species, developmental stage, and pathological state (Boheler et al., 1991; Carrier et al., 1992). Here, the onset of cardiomyocyte differentiation is marked by *acta2* expression, which is subsequently followed by *acta1* and *actc1* expression as development proceeds (Ruzicka, 1988).

Cardiac development is marked by persistent and acute changes in myocardial tension throughout the formation and maturation of the heart. Previous studies showed that changes in tension mediate myogenic cofactor activity, providing a feedback mechanism for enhancing cytoskeletal strength (Somogyi and Rørth, 2004). Moreover, recent evidence emerged, that the SRF transduction pathway is regulated by actin dynamics and requires tensional homeostasis within tissues (McGee et al., 2011; Miano et al., 2006).

Several studies suggest that SRF expression needs to be tightly controlled during cardiac development. Spatially restricted deletion of SRF in the embryonic heart results in thinning of the myocardial wall, severely disrupted sarcomeric structure and results in death of mice embryos at E11.5 (Niu et al., 2008; Parlakian et al., 2004). In gain-of-function studies cardiac-

specific overexpression of wild-type or dominant-negative SRF resulted in heart failure due to severe changes in actomyosin composition (Zhang et al., 2001).

1.6 Aim of the Study

Establishing a functional cardiac syncytium requires coordinated tissue morphogenesis and formation of proper intercellular electrical coupling. The role of Wnt signaling during the morphogenesis of various organs (e.g. kidney and eye) has been studied extensively. Although several CHDs have been linked to deficiencies in Wnt signaling, its function during early cardiogenesis remains unclear.

The aim of this study is to shed light on our understanding of mechanisms mediated by Wnt/PCP signaling that underlie the development of the chambered heart from the linear heart tube using the zebrafish animal model. In loss-of-function studies, it will address potential regulatory pathways that target the remodeling of early myocardium. Thus, the study aims at elucidating cellular processes required for establishing cardiac architecture, and effects of Wnt non-canonical PCP signaling on mechanisms guiding the morphogenesis of the early myocardium. Furthermore, it will address if and how the PCP pathway is involved in cardiomyocyte differentiation and cardiac maturation.

2 Results

2.1 Ventricular Cardiomyocytes Acquire Regionally Specific Morphology During Cardiac Chamber Formation

Proper morphogenesis of the two cardiac chambers from the primitive heart tube is crucial for the function of the zebrafish heart. At linear heart tube (LHT) stage the entire myocardium consists of a homogeneous cell population of small and circular cells. By the time the two cardiac chambers form, the atrial and ventricular cardiomyocytes acquire distinct characteristics; atrial cells become larger and form a squamous epithelium, while ventricular cells are much smaller and cuboidal. At the same time morphological and physiological differences between the outer (OC) and inner (IC) curvatures of the ventricle are established (Figure 6 A, OC – green, IC – red) that are important for proper cardiac function e.g. asymmetries in action potential propagation (Panáková et al., 2010). As the name suggests, OC and IC cardiomyocytes display different morphological characteristics depending on their position within the zebrafish ventricular chamber when measured at the cross-section at the level of the apical tight junctions (Auman et al., 2007; Scherz et al., 2008).

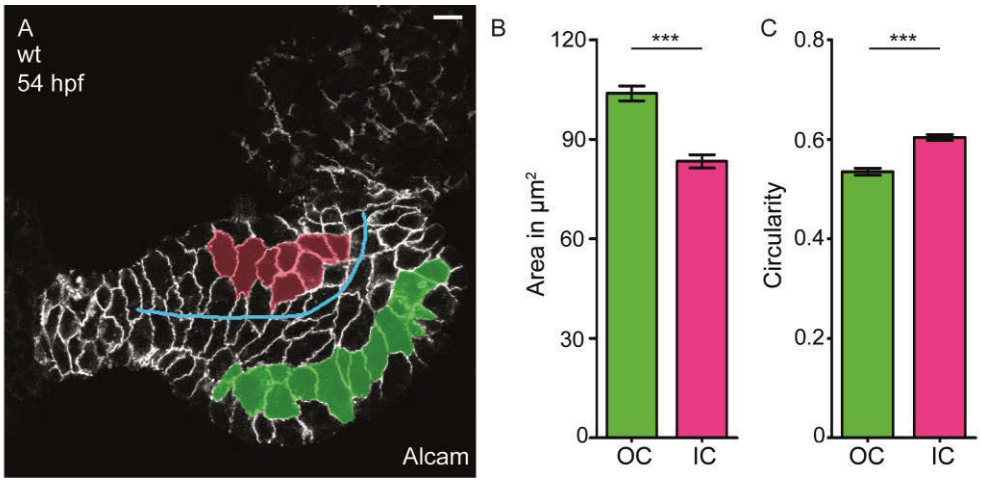

Figure 6: Chamber formation induces regionally restricted cell shape changes. (A) Confocal images of two-chambered hearts at 54 hpf stained for Alcam as a membrane marker were analyzed with Packing Analyzer software (Aigouy et al., 2010) for size and circularity of OC (green) and IC (red) cardiomyocytes. (B, C) Cells of the outer curvature become larger and elongated (n=239, area = 104 µm², circularity = 0.53), while cells of the inner curvature remain relatively small and rounded (n=210, area = 83 µm², circularity = 0.6). OC = outer curvature, IC = inner curvature. Scale bar = 10 µm. *** = P<0.001; t-test.

To corroborate the region-specific characteristics of these cells, a number of parameters such as circularity, size and cell orientation were measured by using open-source Packing Analyzer software that determines cellular outlines by utilizing the watershed algorithm (Aigouy et al., 2010). Here, in line with previous reports, cells of the OC are larger and less cuboidal compared to IC cardiomyocytes with an average area of 104 μm² and circularity value of 0.53, while the latter are 83 μm² in size and have a circularity value of 0.6 (Figure 6 B, C). These data confirm that regionally specific changes in cardiomyocyte cell shape within the ventricle accompany cardiac chamber formation in zebrafish.

2.2 Mechanisms of Epithelial Remodeling Underlie Cardiac Chamber Formation

Formation of the two cardiac chambers from the primitive heart tube requires integration of cells that are added from the second pool of cardiac progenitors as well as expansion of the atrium and ventricle; an uncharacterized molecular and cellular process that to date is termed “cardiac ballooning” (Christoffels et al., 2000; Risebro and Riley, 2006; van den Berg and Moorman, 2009). It has been proposed that cell neighbor exchange through epithelial remodeling provides an efficient mechanism for the rearrangement of cells within a single layered epithelium during organ formation (Blankenship et al., 2006; Farhadifar et al., 2007; Villasenor et al., 2010). This process is marked by transitory states in which four (T1 transition) or more cells (rosette) converge into a single vertex and subsequently resolve in the opposite direction, thus reshaping the tissue (Bertet et al., 2004; Fletcher et al., 2014; Tada and Heisenberg, 2012; Yu and Fernandez-Gonzalez, 2016).

To determine whether mechanisms of epithelial remodeling underlie cardiac chamber formation, whole embryo time-lapse imaging of non-contractile hearts of *tnnt2* morphant zebrafish embryos was performed during LHT transition to two-chambered state in a transgenic line *Tg(myl7:lck-eGFP)* that expresses membrane-tethered eGFP within cardiomyocytes. Snapshots of a movie depicted in Figure 7 follow over time one rosette within the ventricular myocardium that at t = 0 h (26 hpf) consisted of five cells that shared a central vertex. Within the next 5 h (31 hpf) this rosette resolves fully as new cell junctions are formed and cells change their position in respect to each other within the myocardium suggesting that cardiac ballooning is guided by cell rearrangements regulated through mechanisms of epithelial remodeling (Figure 7).

As aforementioned, myocardial architecture differs significantly between LHT stage and after formation of the atrium and ventricle. Moreover, addition of cardiomyocytes from the SHF requires substantial incorporation of cells into the cardiac tube.

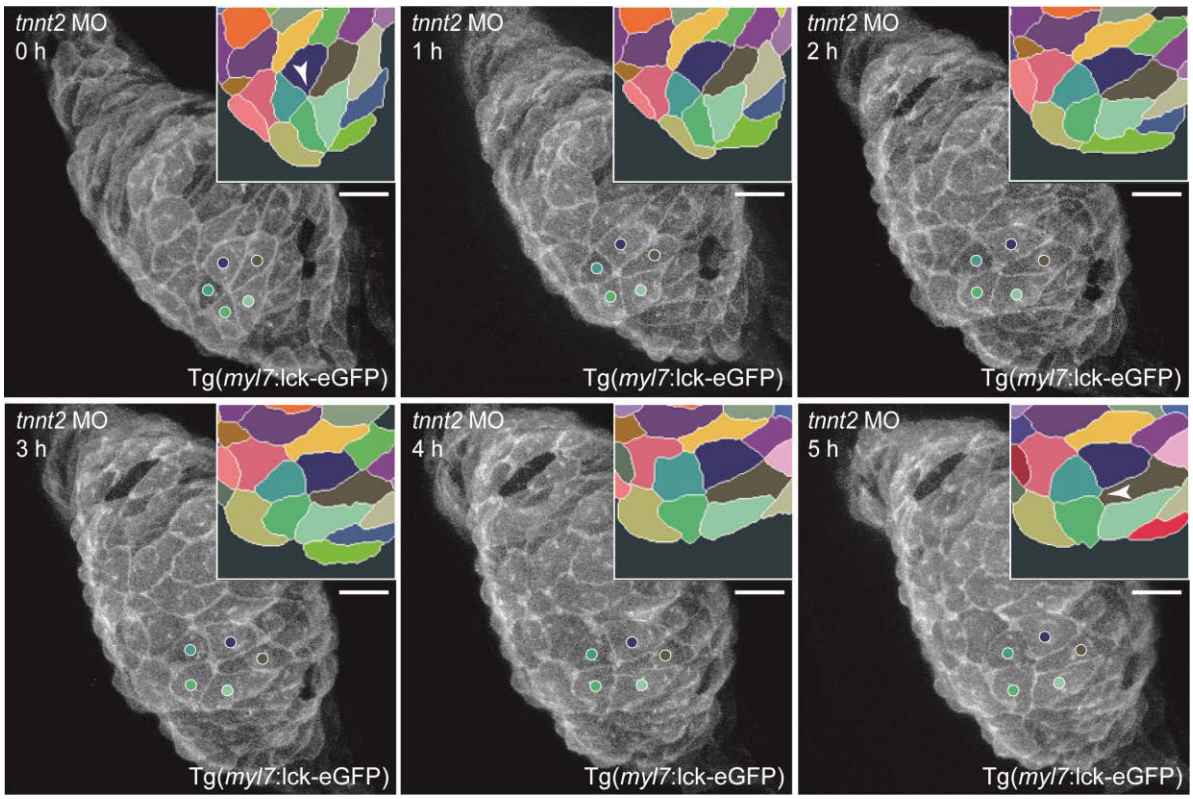

Figure 7: Whole embryo time-lapse imaging of resolving rosette in non-contractile *tnnt2*-deficient heart. At t = 0 the LHT (26 hpf) features a rosette consisting of five cells that share a common vertex (arrowhead). During the following 5 h this rosette resolves fully and new cell junctions are formed (arrowhead). Scale bar = 10 µm.

Live imaging showed that cardiac chamber formation is at least in part driven by epithelial remodeling. To quantify cell rearrangements within the zebrafish myocardium during chamber formation, transitory states where four (T1 transition) or more cells (rosette) converge into a central vertex were counted at distinct stages of cardiac development. To that end, hearts were fixed and stained for the transmembrane glycoprotein Alcam that served as a membrane marker at 26, 54, and 72 hpf (Figure 8 A-C). Quantification of transitory states was performed using the Packing Analyzer software (Aigouy et al., 2010). At 26 hpf transitory states are highly abundant within the myocardium of the LHT (n=11; 9.1 transitions per 100 cells) (Figure 8 A, D). The number of transitory states is decreased significantly by 40% at 54 hpf after the two chambers have formed with 5.2 transitions per 100 cells (n=10; P<0.01) (Figure 8 B, D). The presence of transitory states does not change significantly in the following 18 h (n=6; 4.5 transitions per 100 cells) (Figure 8 C, D). The data show that the number of transitory states is indicative of the state of myocardial remodeling. Moreover, the data suggests that mechanisms of epithelial remodeling drive cardiac chamber formation of the vertebrate heart within the first 54 h of development.

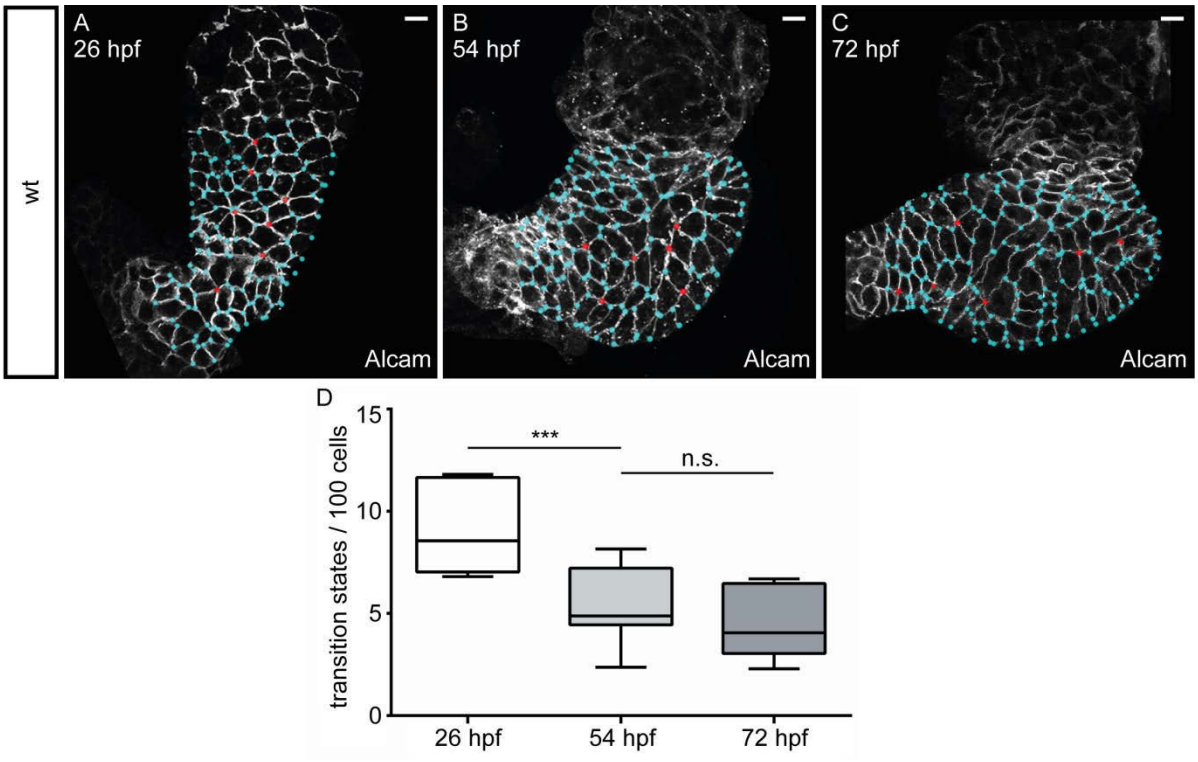

Figure 8: Epithelial remodeling guides cardiac chamber formation. (A-C) Confocal images of wild-type hearts at 26 hpf, 54hpf and 72 hpf stained for Alcam as a membrane marker with transitory states highlighted in red. (A, D) At LHT stage the myocardium features 9.1 transitory states per 100 cells (n=11). (B, D) After formation of the cardiac chambers the number of transitory states is decreased to 5.2 per 100 cells (n=10). (C, D) Hearts at 72 hpf display on average 4.5 transitory states per 100 cells (n=6). Scale bar = 10 µm. *** = P<0.01; one-way ANOVA.

2.3 PCP Guides Cardiac Chamber Formation by Targeting Mechanisms of Epithelial Remodeling

2.3.1 Wnt11 and Wnt5b Control Cell Rearrangements

Non-canonical Wnt signaling through both Wnt5 and Wnt11 was shown to be essential for proper cardiac development (Cohen et al., 2012; Pandur et al., 2002). In mice, both coordinate proper right ventricular OFT morphogenesis by targeting cytoskeletal organization (Zhou et al., 2007). Moreover, both were shown to be essential regulators of epithelial remodeling (Cervantes et al., 2009; Heisenberg et al., 2000).

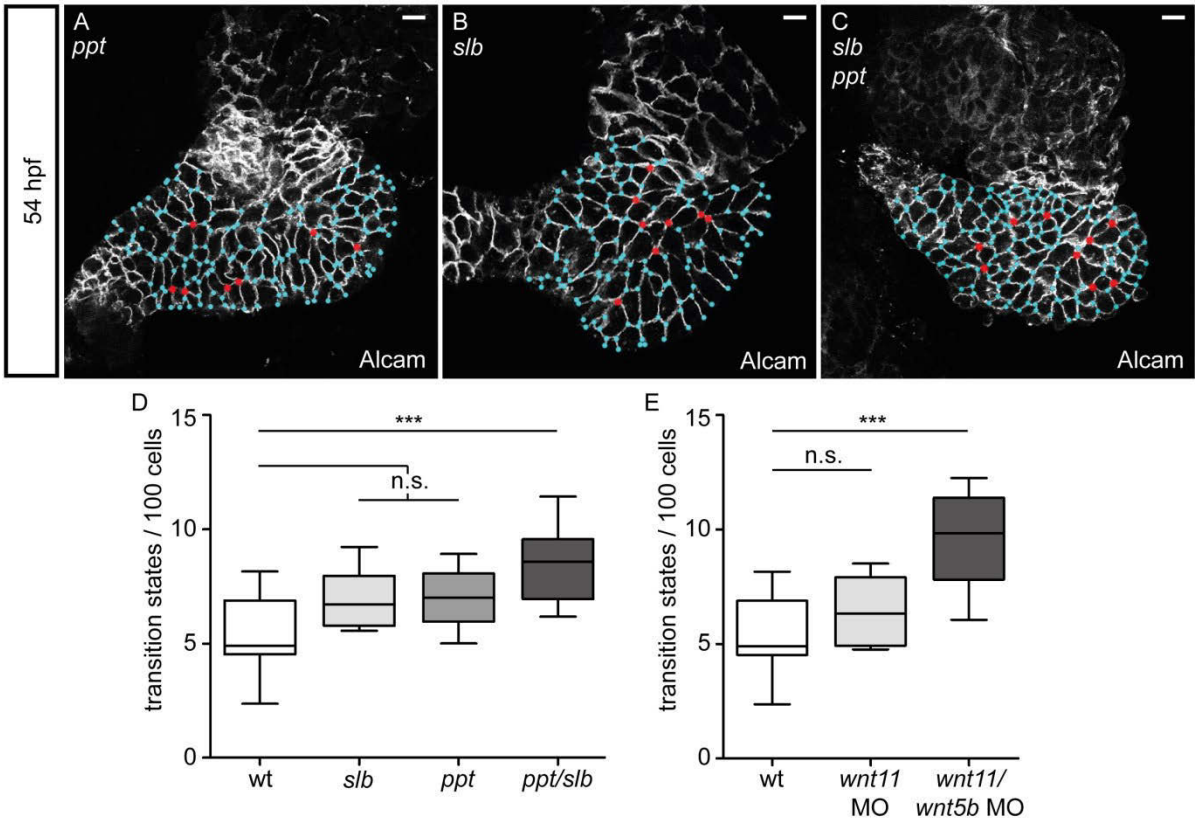

Figure 9: Non-canonical ligands Wnt11 and Wnt5b govern epithelial remodeling during chamber formation. (A-C) Confocal images of hearts at 54 hpf stained for Alcam showing transitory states in red. (A) Hearts of *wnt5b* (n=6) and (B) *wnt11* (n=5) deficient zebrafish show slight increase in transitory states. (C) Loss of both Wnt11 and Wnt5b significantly increases the number of transitory states (n=6). (D) Quantification of transitory states in *slb*, *ppt*, and *slb/ppt* double mutant. (E) Quantification of T1 transitions and rosettes in hearts with decreased levels of Wnt11 alone and both Wnt11 and Wnt5b. Scale bar = 10 µm. *** = P<0.001, one-way ANOVA.

I have shown that changes in morphogenesis of the embryonic myocardium are reflected in the number of T1 transitions and rosettes seen early after cardiac chamber formation. To assess the function of Wnt ligands during embryonic cardiac remodeling the number of transitory states at 54 hpf was determined in the hearts of Wnt5b mutant *pipetail (ppt)* (Figure 9 A), and the Wnt11 mutant *silberblick (slb)* (Figure 9 B). The data were corroborated by injection of morpholino oligonucleotides targeting transcription start sites (ATG sites) of both ligands. All data were compared to the number of transitory states in the hearts of wild type controls at 54 hpf. There was a mild increase in the number of T1 transitions and rosettes in *slb* (6.8 per 100 cells; n=5; n.s.) (Figure 9 B, D), *ppt* mutants (7 per 100 cells; n=6; n.s.) (Figure 9 A, D) and in *wnt11* morphant hearts (6.4 per 100 cells; n=5; n.s.) (Figure 9 E). To investigate whether Wnt5b and Wnt11 can compensate for loss of function of the other and act redundantly, the number of transition states in hearts of *slb/ppt* double mutants was determined (Figure 9 C). Here, simultaneous loss of both Wnt11 and Wnt5b increased the

number of transitory states by approx. 25% to 8.5 per 100 cells (n=6; P<0.01) (Figure 9 C, D). The effect on cell rearrangements was confirmed in hearts where levels of both Wnt11 and Wnt5b were reduced using subthreshold concentrations of morpholino (9.6 per 100 cells; n=6; P<0.01) (Figure 9 E). In summary, these findings suggest that non-canonical Wnt11 and Wnt5b are either redundant or act synergistically to guide chamber formation through regulation of cell rearrangement process within the single-cell layered myocardium.

2.3.2 PCP Pathway Core Components Regulate Cardiac Remodeling

PCP proteins have been described in guiding cell intercalation movements and rearrangements in many instances (Roszko et al., 2009). The core PCP pathway components that are expressed in the heart comprise the transmembrane proteins Fzd7 and Vangl2 and the cytoplasmic proteins Dvl2 and Pk1 (Hamblet, 2002; Henderson et al., 2006; Katoh and Katoh, 2003; Yu et al., 2012). All core proteins have been implicated in epithelial remodeling during morphogenesis of several organs like lung and kidney, the ear, or during neural tube development (Sienknecht, 2015; Sokol, 2015). Loss of function studies in both mutants and by using morpholino knockdown of the aforementioned PCP core proteins showed differences in the presence of transitory states within the ventricular myocardium at 54 hpf (Figure 10 A-D). The number of transitory states was increased in hearts of *fzd7a*^{e3} mutant (8.6 per 100 cells; n=7; P<0.001) (Figure 10 A, E), *pk1a*^{c4} transheterozygous mutant (7.2 per 100 cells; n=5; P<0.05) (Figure 10 D, E) and *dvl2* morphant (8.5 per 100 cells; n=7; P<0.01) (Figure 10 B, F), but not of *vangl2*^{m209} mutant (5.9 per 100 cells; n=6; n.s.) (Figure 10 C, E) as compared to wild type (5.2 per 100 cells) (Figure 8 B, D). Importantly, quantification of transitory states in the hearts of putative null mutants of the core PCP components or in the hearts with their decreased levels using morpholino knockdown technology produced similar results (compare Figure 10 E and F). Here, *fzd7a*-morphant hearts showed highly increased amount of T1-transitions and rosettes with 10.6 transitory states per 100 cells (n=9; P<0.001) (Figure 10 F). Reduction in *pk1a*-levels led to mild increase in T1-transitions and rosettes (7.3 per 100 cells; n=6; n.s.) (Figure 10 F). In *vangl2*-deficient hearts the number of transitory states was mildly reduced to 3.8 per 100 cells (n=9; n.s.) (Figure 10 F). This supports the idea that both methods can be used interchangeably in this context. Taken together, these results strongly indicate that PCP signaling regulates cardiomyocyte rearrangements by targeting mechanisms of epithelial remodeling during early stages of cardiac development.

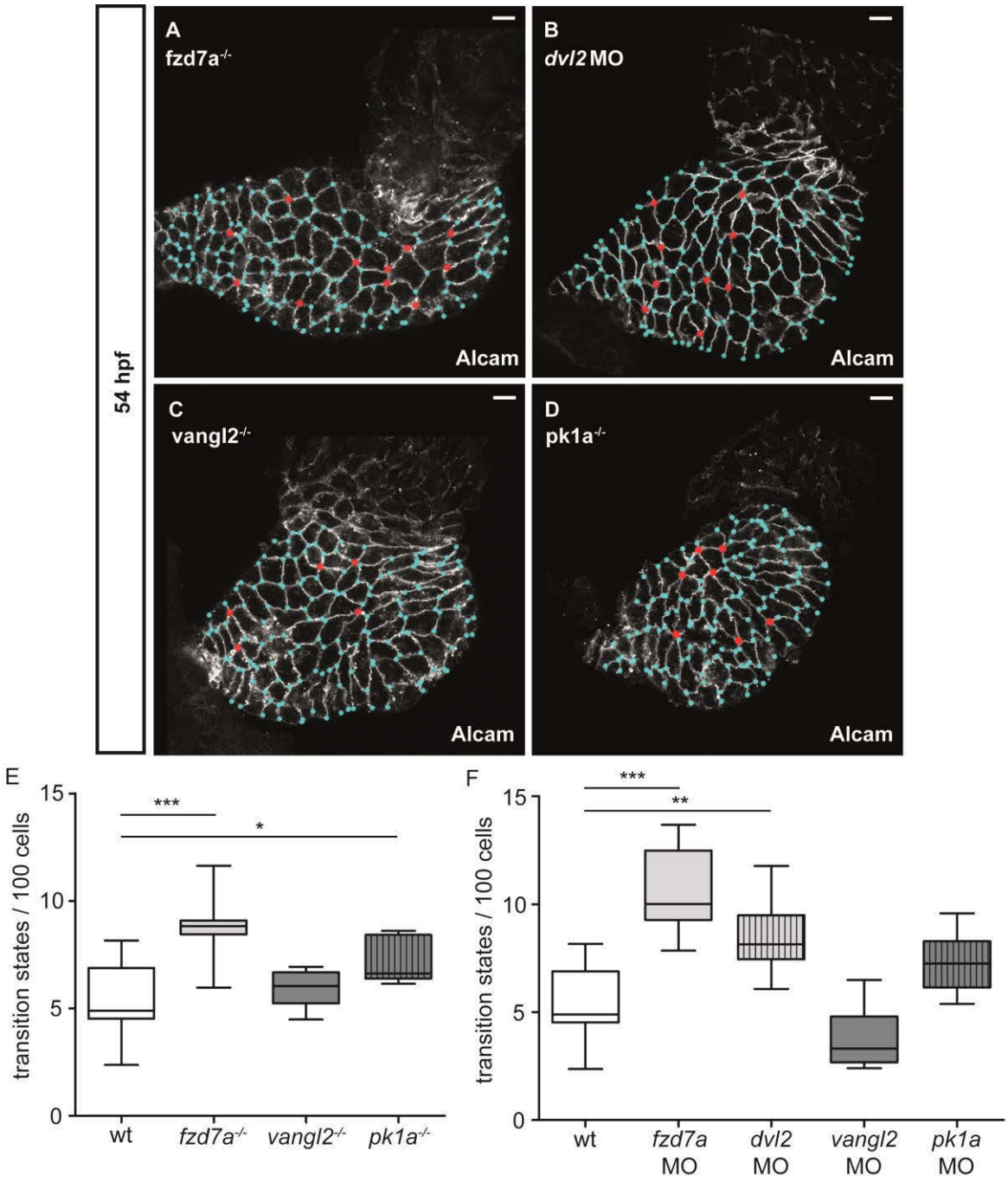

Figure 10: Number of transitory states (red) is altered in PCP deficient hearts. (A-D) Confocal images of PCP-deficient hearts at 54 hpf stained for Alcam showing transitory states in red. (E) In *fzd7a* mutant hearts the number of transitory states is increased by approx. 2-fold. Loss of *pk1a* also increases amount of T1 transitions and rosettes. In *vangl2*-deficient hearts the number of transitory states is slightly decreased (NS). (F) Quantification of transitory states in PCP morphants corroborates data acquired using genetic mutant approach. Scale bar = 10 µm. ** = P < 0.01, *** = P < 0.001; one-way ANOVA.

The increased presence of transitory states at 54 hpf in the absence of Fzd7a, Dvl2 and Pk1a can be explained by either their increased formation frequency or by the reduced ability of the cells to form new cell boundaries. To get more insight, the quantification of transitory states was performed at 26 hpf, assuming that an increase in T1 transitions and rosettes already at this early stage hints at increased frequency of rosette formation. Indeed, in hearts with decreased levels of Fzd7a, the number of transitory states is already slightly increased at LHT stage (Figure 11 B, D). In contrast, reduction in Vangl2 led to mildly decreased number of T1 transitions and rosettes (Figure 11 C, D). Changes in the effectiveness of cell rearrangements during early cardiogenesis seem to correlate at least partially with the overall shape of the chambered heart. While *fzd7a* mutant hearts that show more transitory states are elongated, *vangl2* mutant hearts fail to elongate and form more rounded chambers (Figure 11 A, C). However, both mutants show defects in cardiac looping suggesting that cardiac chamber formation is regulated by additional mechanisms.

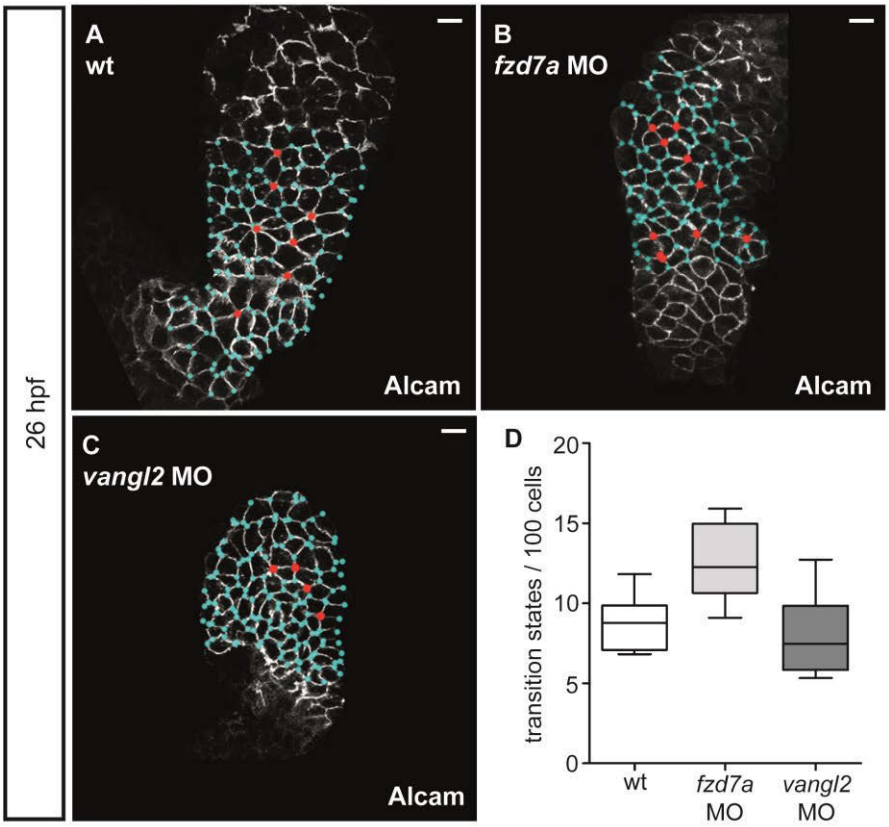

Figure 11: Reduction in Fzd7a results in increased number of transitory states already at LHT stage. (A-C) Confocal images of hearts at LHT stage (26 hpf) stained for Alcam showing transitory states in red. (D) Quantification shows a slight increase of transitory states in *fzd7a* morphant (n=5; n.s.) compared to wild-type hearts (n=11), while reduction in *vangl2* levels led to a mild reduction (n=6; n.s.). Scale bar = 10 µm; one-way ANOVA.

2.4 The PCP Pathway Controls FHF / SHF Contribution

Ventricles of *fzd7a* deficient hearts were overall smaller and consisted of less cardiomyocytes. Measurements of cardiomyocyte size and circularity within OC and IC regions revealed that in *fzd7a* morphant hearts distinct regional differences between cells of these ventricular areas are not established (Figure 12 A, B). Cardiomyocytes with decreased levels of Fzd7a are overall smaller compared to *vangl2* deficient or wild type cells with an average cell area of approximately 60 µm² (Figure 12 A). Furthermore, all ventricular cells in hearts with reduced levels of *fzd7a* are more rounded with circularity values comparable to those of wild-type IC cells (OC = 0.61, IC = 0.58; compare Figure 6 C with Figure 12 B). Loss of Vangl2 did not affect the establishment of ventricular OC and IC cardiomyocyte region-specific morphologies (Figure 12 A, B). These data show that cardiomyocytes in hearts with reduced levels of Fzd7a retain the more rounded and smaller morphology of cells at LHT stage. Their failure to develop regional specification proposes a role for PCP signaling in differentiation processes during early cardiogenesis.

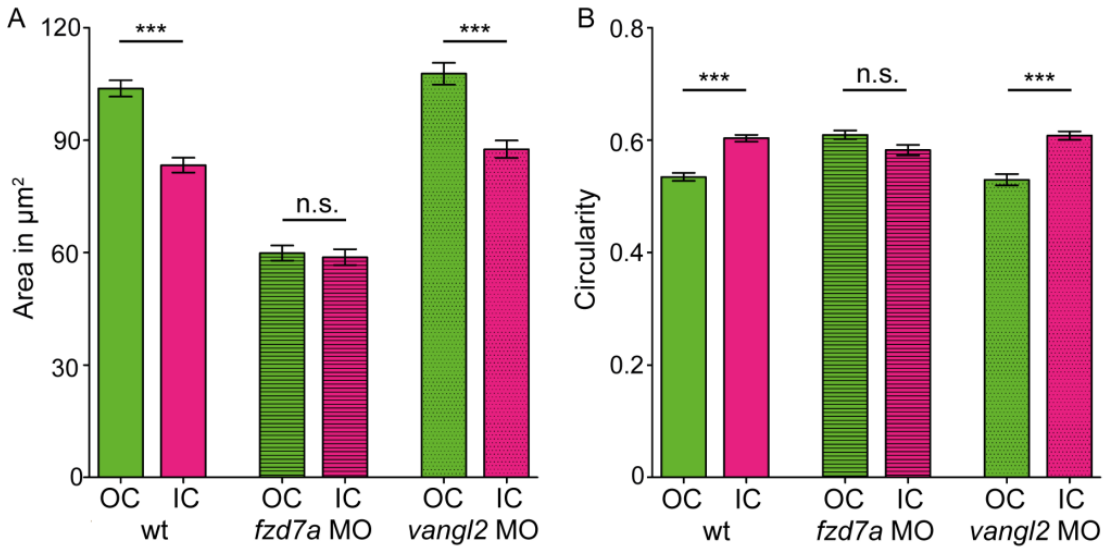

Figure 12: Loss of Fzd7a results in failure to establish region-specific IC and OC cardiomyocyte morphologies. (A, B) Measurements of OC and IC cardiomyocyte size and circularity in wild type hearts (OC: n=241; IC: n=212), in Fzd7a-deficient hearts (OC: n=154; IC: n=145), or those with reduction in Vangl2 (OC: n=167; IC: n=171). (A) Significant differences in size between IC and OC cardiomyocytes as observed in wild type and *vangl2*-deficient hearts were lost in *fzd7a*-morphant hearts. Cardiomyocytes of the *fzd7a*-morphant ventricle are overall significally reduced in size (OC: 60 µm²; IC: 59 µm²) compared to wild type (OC: 103 µm²; IC: 83 µm²) and *vangl2*-deficient hearts (OC: 108 µm²; IC: 88 µm²). (B) Analysis of circularity in OC and IC regions of the ventricles reveals defects in OC cardiomyocyte elongation in *fzd7a* morphant hearts as cells are overall more circular and fail to establish regionally restricted differences in size and circularity. *** = P<0.001; t-test.

Studies in chicken and zebrafish revealed that the proliferation rate of cardiomyocytes of the LHT is minimal and that overall organ growth is achieved by addition of a second pool of differentiating cardiomyocytes from the SHF that ensures cardiac chamber formation (de Pater et al., 2009; Kelly, 2012; Mosimann et al., 2015; van den Berg and Moorman, 2009). In zebrafish these cells are integrated into the heart tube from both cardiac poles, which in ventricle comprises IC and OFT region in particular (de Pater et al., 2009; Mosimann et al., 2015). Hearts with reduction or complete loss of *fzd7a* show decreased organ size and defects in regional specification of cardiomyocytes. To assess whether changes in SHF accrual in *fzd7a* morphant hearts contributed to the observed phenotypes a transgenic line was used that expresses GFP in a FHF specific manner under the *draculin* (*drl*) promoter [*Tg(drl:eGFP)*] (Mosimann et al., 2015).

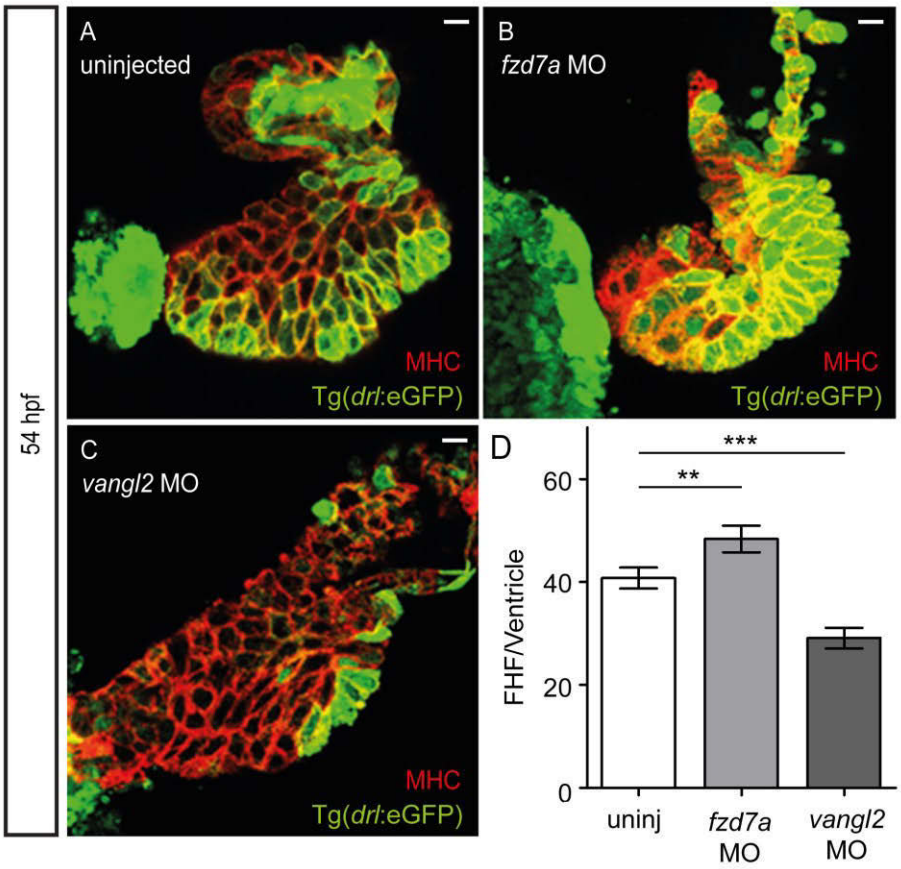

Figure 13: Dysregulation of the PCP pathway affects FHF / SHF ratio in 54 hpf hearts. (A-C) Confocal images of hearts at 54 hpf stained for myosin heavy chain (MHC) and expressing GFP under the *draculin* (*drl*) promoter that marks FHF specifically (A, D) In the uninjected control FHF portion makes up 40% of the ventricle. (B, D) FHF / ventricle ratio is increased to 48 % in *fzd7a*-deficient hearts. (C, D) In hearts with reduced levels of *vangl2*, the FHF composes 29% of the ventricle. Scale bar = 10 µm. ** = P<0.01, *** = P < 0.001 one-way ANOVA.

In hearts with reduced levels of either *fzd7a* or *vangl2* the area of GFP-positive cells was measured in relation to the entire ventricular area (Figure 13 B, C, D). In wild-type hearts, the FHF accounts for 40 % of the ventricular chamber (Figure 13 A, D). Analysis of the FHF / ventricle ratio showed that loss of Fzd7a increases FHF amount within the ventricular myocardium (48 %) (Figure 13 B, D), while loss of Vangl2 decreases the FHF contribution to the heart to 29 % (Figure 13 C, D). These results indicate that PCP mediates FHF / SHF specification or SHF cardiomyocytes accrual to the LHT.

2.5 PCP Regulates Ventricular Tissue Architecture

During chamber formation, ventricular cardiomyocytes not only acquire region-specific morphologies, but also assume distinct orientations within OC, IC, the OFT and the AV-junction of the zebrafish myocardium. Using a customized version of the Packing Analyzer software, cell orientation within the ventricle was investigated to describe myocardial architecture in more detail. The program analyzes cardiomyocytes orientation within the aforementioned regions by placing a tangent on the respective cell in regard to the overall outline of the ventricle. It then relates the elongation tensor of the cardiomyocyte to the 90-degree angle placed on this tangent. In wild type hearts, cells of the OC and IC assume a 0-degree orientation, those at the AV-junction and within the OFT region are oriented in a 90-degree angle (Figure 14).

As aforementioned, the overall ventricular morphology of *fzd7a* and *vangl2* mutant hearts is defective with more elongated or more rounded chambers, respectively. To investigate the involvement of Wnt non-canonical signaling in establishing proper ventricular form, analysis of cardiomyocytes orientation in loss-of-function studies targeting the core PCP proteins Fzd7a, Dvl2, Vangl2, and Pk1a was performed. Here, loss of Fzd7a resulted in severe disruption of cardiomyocytes orientation, especially in regions close to the OFT (Figure 14). Decreased levels of Dvl2, Pk1a and Vangl2 resulted mainly in increased variability of cell orientation within the OFT region (Figure 14). For statistical analysis of angle distribution in the OFT region Rayleigh's test was performed to assess significance of the mean direction by using a concentration parameter of a circular distribution. Here, low values of Rayleigh's R represent highly concentrated values with little distribution. The mean angle of OFT cardiomyocyte orientation in wild type hearts is 92,27 degrees with low distribution (Rayleigh's R = 9.25×10^{-9}). In contrast, morpholino knockdown of *fzd7a* results in a shift of the mean angle to 96,01 degrees with higher variance (Rayleigh's R = 6.5×10^{-2}). In hearts with complete loss of Fzd7a the mean angle of cardiomyocyte orientation in the OFT region is even more shifted to 118.42 degrees (Rayleigh's R = 1.69×10^{-1}).

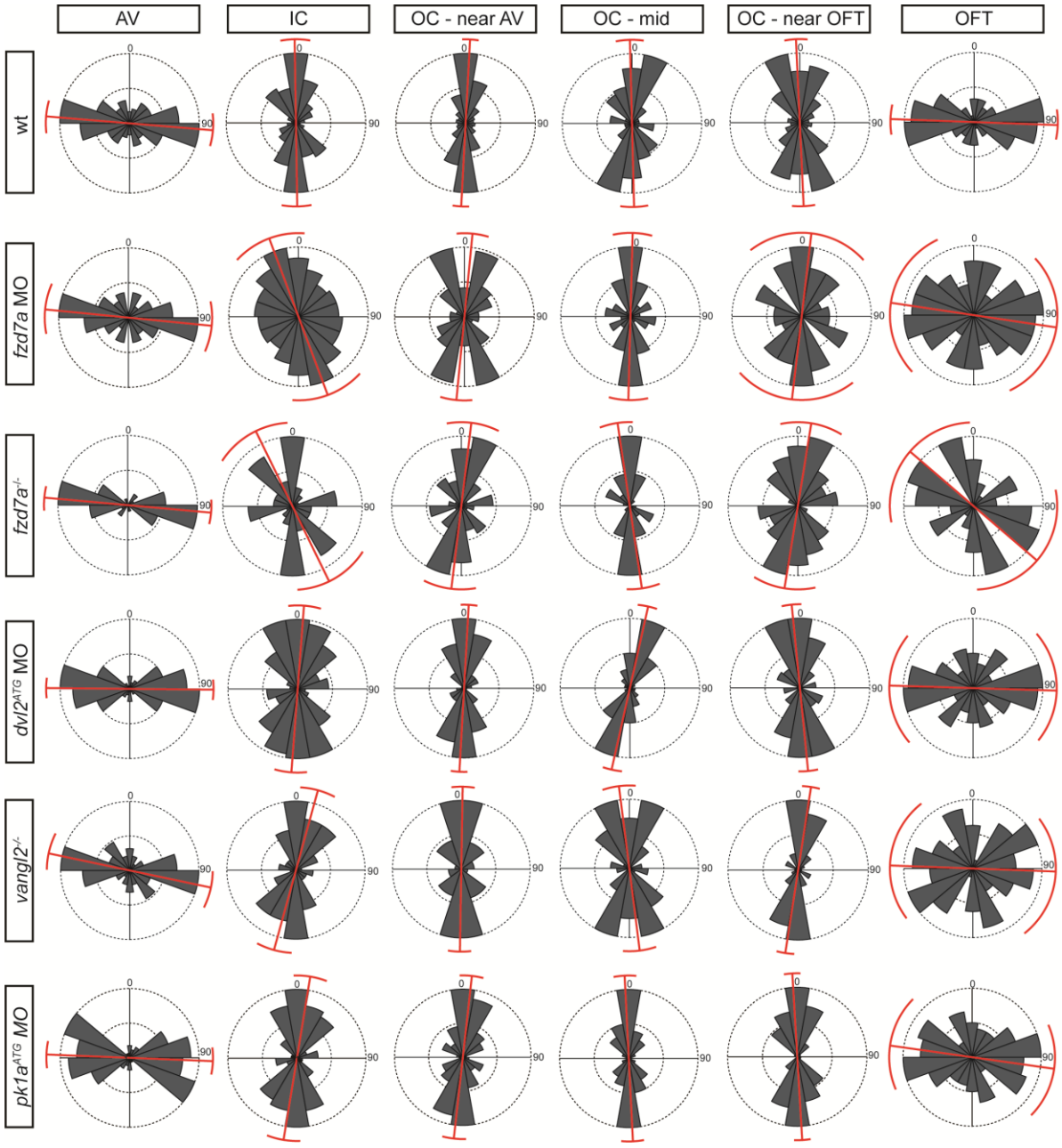

Figure 14: Loss of PCP core components results in OFT defects. Cardiomyocytes assume distinct orientations within the ventricular chamber. Angles are defined relative to a 90-degree angle above a tangent placed on the outline of the ventricle. Wild type cardiomyocytes of the AV (n = 92) and OFT region (n = 86) are positioned in a 90-degree angle, while cells of the IC (n = 57) and OC (n = 295) assume a 0-degree angle. Loss of Fzd7a leads to severe defects in cardiomyocyte orientation within the OFT (n = 89), the OC region close to the OFT (n = 84) and the IC (n = 162). Similarly, defects in OFT cardiomyocyte arrangement are entailed by decreased levels in Dvl2 (n = 72), Vangl2 (n = 47), and Pk1a (n = 66).

While the mean angle of OFT cardiomyocytes is not altered in *vangl2* mutant hearts, the variability of angles is very high (90.04 degrees; Rayleigh's R = 2.34 x 10^{-1}). Similar effects are observed in *dvl2* morphant (89,52 degrees; Rayleigh's R = 7.82 x 10^{-3}) and *pk1a* morphant hearts (93.45 degrees; Rayleigh's R = 1.36 x 10^{-2}). Taken together, data show that changes in ventricular cell shape that are accompanied by changes in cardiomyocyte orientation, and are mediated by cell rearrangements correlate with the characteristic bean-like shape of the ventricle. Moreover, these data underline the importance of functional PCP signal transduction for proper myocardial morphogenesis of the vertebrate heart.

2.6 PCP Controls Cellular Rearrangements by Affecting Cytoskeleton

2.6.1 PCP Does Not Affect N-Cadherin Localization

Junctional remodeling during morphogenesis is guided by complex mechanisms involving actomyosin modulation as well as changes in adhesion mediated through cadherin localization, turnover and endocytosis (Nishimura and Takeichi, 2009). Several studies suggest that PCP signaling is targeting cell-cell adhesion and cytoskeletal rearrangements in various developmental contexts (Babayeva et al., 2011; Classen et al., 2005; Nagaoka et al., 2014; Ulrich et al., 2005; Zallen, 2007). For instance, during the formation of the zebrafish ciliated laterality organ inhibition of both Wnt11 and Pk1a reduced intercellular adhesion leading to defective Kupffer's vesicle lumen expansion (Oteiza et al., 2010). The remodeling of junctions is at least in part dependent on conformational changes of cadherin (Hong et al., 2011). In the myocardium of the developing heart the only classical Cadherin expressed is N-Cadherin (Linask, 1992). Loss of N-Cadherin is embryonic lethal and misexpression of Cadherins during embryonic development leads to severe cardiomyopathy (Ferreira-Cornwell et al., 2002; Luo et al., 2001).

Quantification of T1 transitions and rosettes in hearts with defective PCP signaling revealed that epithelial remodeling underlies myocardial morphogenesis and cardiac chamber formation. However, it was still unclear whether PCP mediates these processes by changes in adhesion or tension through actomyosin modulation. To assess whether changes in cellular rearrangements are due to differences in adhesion processes, localization and abundance of N-Cadherin was determined in hearts with defective PCP signaling (Figure 15 A-C).

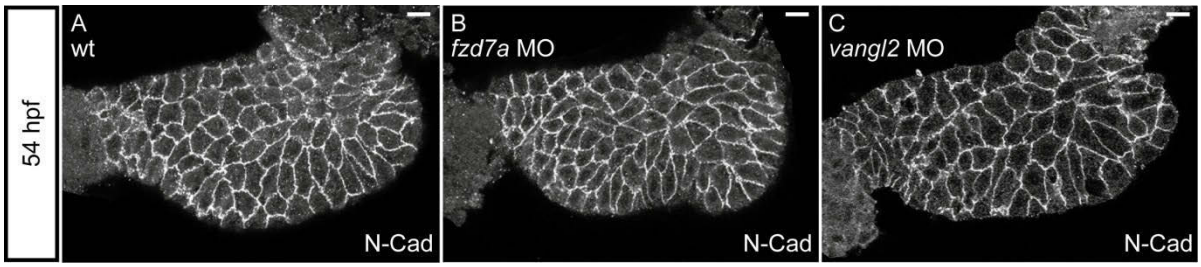

Figure 15: Localization and abundance of N-Cadherin is not changed in PCP-deficient hearts. (A-C) Confocal images of hearts at 54 hpf stained for N-Cadherin (N-Cad). (A) In wild-type hearts N-Cad localizes uniformly to basolateral cell membranes. (B, C) In both *fzd7a*- and *vangl2*-deficient hearts N-Cad localization and abundance were unchanged compared to wild-type hearts. Scale bar = 10 µm.

At 54 hpf N-Cadherin localized uniformly to the basolateral membrane both in wild type hearts (Figure 15 A) and hearts with decreased levels of Fzd7a (Figure 15 B) or Vangl2 (Figure 15 C). Furthermore, no apparent change in N-Cadherin amount was detected within the ventricular myocardium between wild type and Fzd7a- and Vangl2-deficient hearts. Thus, these data show that adhesion processes targeted by PCP signaling are most likely not driving cardiac remodeling suggesting that PCP signaling rather acts on actomyosin structures.

2.6.2 PCP effects on actomyosin

Many cytoskeletal components including microtubules and actomyosin filaments are involved in the generation of cell shape, and thus affect tissue mechanics (Booth et al., 2014; Huber et al., 2015). Hence, changes in cell shape reflect differences in actomyosin organization and can be deployed to describe effects on these structures. To address whether PCP targets cytoskeletal organization during cardiac chamber formation, single cardiomyocyte morphology within the ventricular chamber at 54 hpf was visualized. To that end, cardiomyocyte specific membrane-tethered eGFP (myl7:*lck*-eGFP) was transiently expressed in wild type hearts (Figure 16 A) or in hearts with reduced levels of *fzd7a* (Figure 16 B) or *vangl2* (Figure 16 C). Reduction in Fzd7a increased basal protrusion formation and showed rounded apical morphology of cardiomyocytes indicating that these cells are apically constricted within the myocardium (Figure 16 B). Vangl2 knockdown did not affect cardiomyocyte morphology as severely. However, cells appear to display an overall smoother cell surface compared to wild-type cardiomyocytes and expand to a greater extent over the apicobasal axis (Figure 16 C).

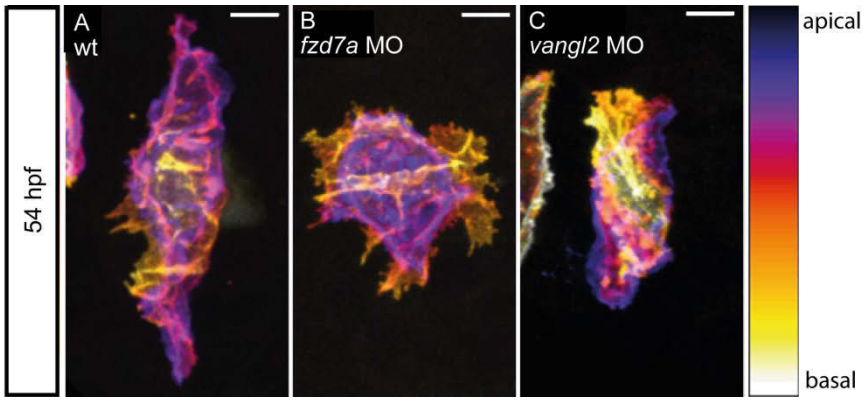

Figure 16: Cellular morphology is altered upon Fzd7a and Vangl2 knockdown. (A-C) Maximal confocal depth projections of single cells expressing membrane-associated eGFP (transient expression of *myl7*:lck-eGFP) depicting basal parts of cardiomyocytes in white/yellow and apical parts in blue/magenta. (A) Wild type OC cardiomyocytes show elongated morphology with few cell protrusions. (B) Cardiomyocytes of *fzd7a* morphant hearts form numerous pronounced basal protrusions and are rounded apically. (C) Reduced levels of Vangl2 mildly affect cardiomyocyte shape with overall slightly smoother surfaces and increased expansion over the apicobasal axis. Scale bar = 5µm.

Effectors of the PCP pathway were shown to spatially organize epithelial actin-based protrusions (Georgiou and Baum, 2010). Increased formation of basal protrusions in hearts with decreased levels of Fzd7a hints at local changes in actin branching morphology. Through transient expression of actin-bound RFP effects of defective PCP signaling on actin structures were investigated.

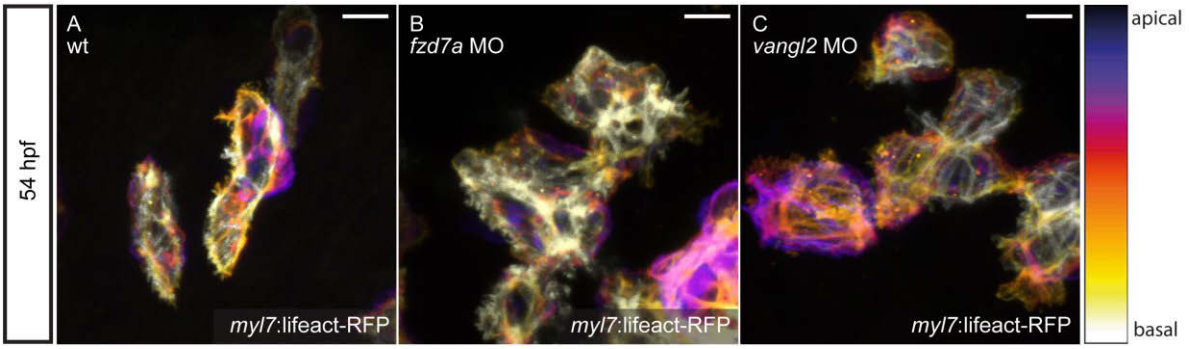

Figure 17: F-Actin is affected in *fzd7a* and *vangl2* morphant hearts. (A-C) Maximal confocal depth projections of sparsely-labeled cardiomyocytes at 54 hpf expressing actin-bound RFP (transient expression of *myl7:lifeact-RFP*) depicting basal parts of cardiomyocytes in white/yellow and apical parts in blue/magenta. (A) F-Actin is organized in structured fibers within wild-type cardiomyocytes, and is visible in cell protrusions and along cell cortex. (B) F-Actin in *fzd7a*-deficient hearts is disorganized forming increased number of basolateral protrusions within individual cardiomyocytes. (C) In hearts with decreased levels of Vangl2, F-Actin fibers are highly organized within the cardiomyocyte cytoplasm, and the cortical F-Actin seems to be less prominent.

Here, wild type OC cardiomyocytes (Figure 17 A) were compared to those with loss of Fzd7a (Figure 17 B) or Vangl2 (Figure 17 C). In wild type cardiomyocytes filamentous actin (F-actin) is visible to be organized in fibers along cell cortex and in cellular protrusions. The absence of Fzd7a resulted in disorganized of actin-based structures, and showed that basal protrusions are predominantly formed by F-actin (Figure 17 B). Conversely, loss of Vangl2 resulted in increased organization of F-actin with actin filaments aligning across cells, while cortical F-actin seems to be reduced (Figure 17 C).

Cells in culture that have no or little contact to neighboring cells behave differently to cells organized within tissues, although several cell types such as MDCK cells display clear characteristics of polarity. In cultured breast cancer cells PCP core proteins were shown to assume distinct compartmentalized distribution at the plasma membrane (Luga et al., 2012). Here, as well as in several other cancer cell lines PCP core proteins control protrusive activity (Asem et al., 2016). To investigate the effects of defective PCP signaling in cardiac cells that are not organized into tissues, H9c2 rat myoblasts were treated with siRNA against *fzd7a* (Figure 18). This cell line expresses all core components of Wnt non-canonical PCP signaling (Rharass T., unpublished). While the untreated H9c2 cells display highly organized F-actin fibers (Figure 18 A), reduction in *fzd7a* levels by siRNA led to formation of long protrusions and disruption of F-actin (Figure 18 B) structures showing that effects on cytoskeletal components are not specific to zebrafish cardiomyocytes.

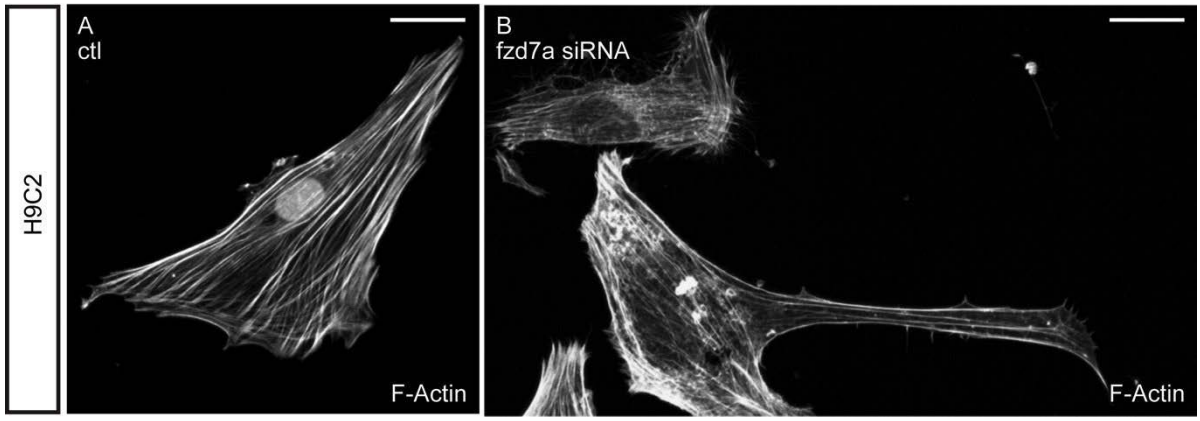

Figure 18: Loss of Fzd7a results in formation of long protrusions in H9c2 rat cardiomyoblasts. (A) Untreated control cell show highly organized F-Actin structures. (B) Knockdown of *fzd7a* induces formation of long protrusions and disorganization of F-Actin fibers. Scale bar = 20µm.

The data shown in the previous sections clearly suggest that PCP targets actin organization to affect cell shape. Epithelial remodeling is characterized by junctional enrichment of both, actin and myosin (Bertet et al., 2004). Specifically, phosphorylation and proper localization of the regulatory light chain of NMII (MRLC) guides constriction of intercellular myosin cables that facilitate rosette formation (Simoes et al., 2014). To that end, the importance of pMRLC during early cardiac remodeling was investigated by determining its localization within the early myocardium at 54 hpf. While in wild-type embryos pMRLC localizes laterally to cell-cell junctions (Figure 19 A), it is mislocalized to the basal side of cardiomyocytes in both *fzd7a* and *wnt11/wnt5b* deficient hearts (Figure 19 B, C). This further corroborates that the PCP pathway regulates proper localization of actomyosin, which is pivotal to cardiac remodeling.

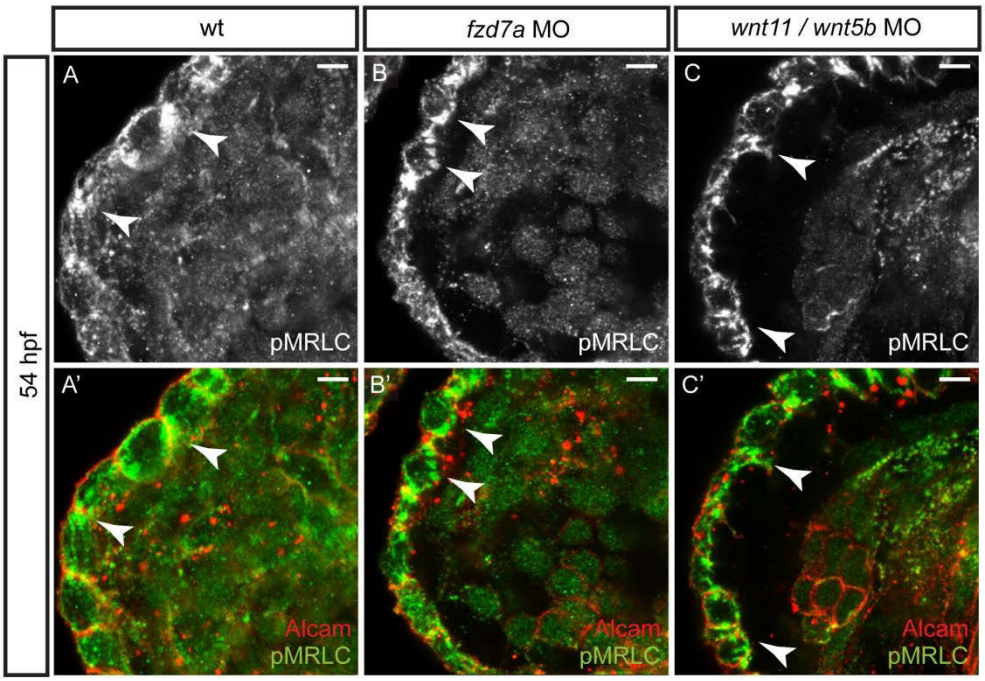

Figure 19: Reduction of Fzd7a and non-canonical Wnt ligands affects pMRLC localization. (A-C, A'-C') Confocal images of OC regions of hearts at 54 hpf stained for Alcam (red) and pMRLC (green). (A, A') In wild-type hearts pMRLC localizes laterally to junctions. (B, B') In hearts with reduced levels of *fzd7a* pMRLC is mislocalized to basal structures of cardiomyocytes (arrowheads). (C, C') Similarly, reduction in Wnt11/Wnt5b leads to basal pMRLC mislocalization (arrowheads). Scale bar = 10 µm.

2.7 The PCP Pathway Regulates Localized Tension

2.7.1 pMRLC and G-Actin Translocate from Nucleus to Membrane During Early Cardiogenesis

In epithelial tissues cells locally produce the required energy to remodel cell contacts by forming actomyosin cables that span two or more cell-cell boundaries (Fernandez-Gonzalez et al., 2009). This active process involves a minimum of four cells, and can include up to twelve cells, connected by supracellular contractile cables (Röper, 2014).

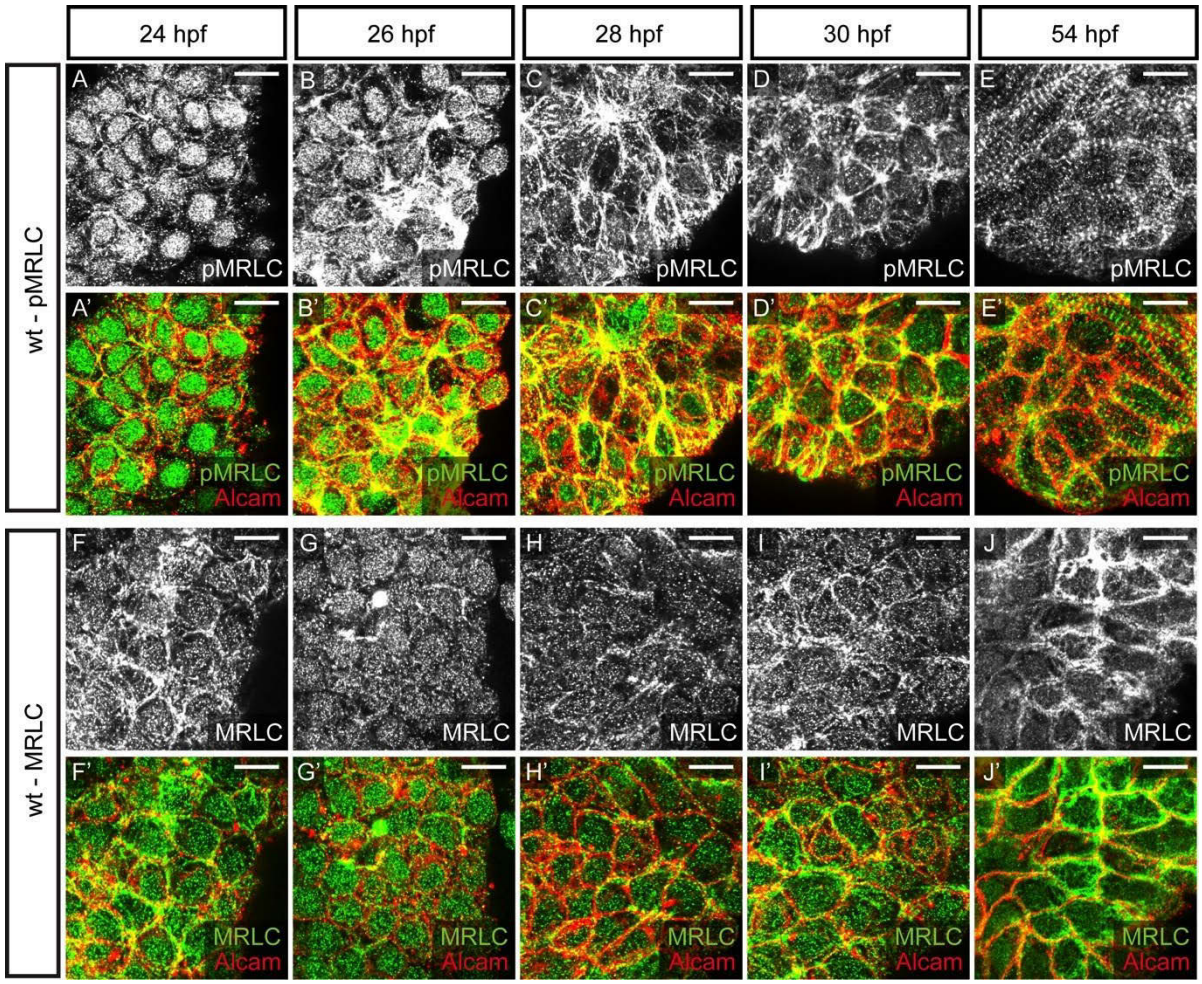

Figure 20: During cardiac remodeling pMRLC localization within the ventricle changes from nuclear compartment to cell junctions. pMRLC translocates from nucleus to membrane between 26 and 28 hpf and accumulates at the junctions, while its unphosphorylated form is mainly localized at the plasma membrane. (A-E) Wild-type hearts stained with phospho-specific (Ser20) antibody against pMRLC and (F-J) its unphosphorylated form at early stages of heart tube remodeling. At 54 hpf both localize to the sarcomeres (E, J). (A'-J') Corresponding merged images of pMRLC (A'-E') or MRLC (F'-J') in green and plasma membrane stained for Alcam in red. Scale bar = 10 µm.

Hearts at LHT stage were stained for pMRLC to investigate its localization and amount during cardiac remodeling and determine if localized tension is underlying cardiomyocyte rearrangements. Changes in pMRLC localization from the nuclear compartment to junctions were observed. In detail, at LHT stage pMRLC is predominantly localized within the nucleus at 24 hpf and translocates to cell junctions of T1 transitions and rosettes before 30 hpf (Figure 20 A-D, A'-D'), thus at the time of cardiac remodeling. This translocation is highly specific to pMRLC, as we never observed its non-phosphorylated form in the nucleus (Figure 20 F-J, F'-I'). At 54 hpf both MRLC and pMRLC accumulate to sarcomeric structures to take part in sarcomerogenesis (Figure 20 E, E', J, J') (Kamm and Stull, 2001). These and all other subsequent data of pMRLC could be reproduced only with the antibody batch Abcam ab2480 (GR-143423-3), and further experiments are required to corroborate these findings.

Actin and myosin are predominantly known for their function as major components of the cytoskeleton that take over structural and regulatory functions in the cytoplasm and at the cell cortex. However, recent studies increasingly focused on their role in the nucleus. Both actin and multiple myosins were already described to be involved in processes within the nuclear compartment. Here, nuclear myosin I (NMI) is the best studied myosin taking part in transcription regulation through interaction with RNA polymerases I and II, and molecular machinery involved in DNA damage repair, and chromosome translocation (Hofmann and de Lanerolle, 2006; Hu et al., 2008; Novak and Titus, 1997; Ye et al., 2008). NMII, and especially nuclear-specific phosphorylation of myosin, was never described or implicated in nuclear mechanisms before. In contrast, recent studies focus extensively on nuclear actin functions. Nuclear actin usually does not form filaments, but instead is almost exclusively found in its globular form or in short oligomers, and is referred to as G-actin (McDonald et al., 2006; Pederson, 2008). Several studies show that G-actin is involved in basically all steps of transcription, especially ensuring transcription through RNA polymerase I and II and mediating mRNA export (Grummt and Pikaard, 2003; Percipalle et al., 2001). Changes in nuclear localization of pMRLC prompted us to explore the localization of G-actin during chamber formation and whether it also undergoes nuclear export during cardiac remodeling. Indeed, staining for G-actin using fluorescently labeled DNaseI that selectively binds to globular actin revealed its predominant localization in the nucleus at 24 hpf and its subsequent translocation to cell cortex within the following 6 h (Figure 21 A-D, A'-D'). Summarizing, at LHT stage both pMRLC and G-actin translocate out of the nucleus to the cell cortex suggesting specific function of actomyosin within the nucleus at different stages during cardiac remodeling.

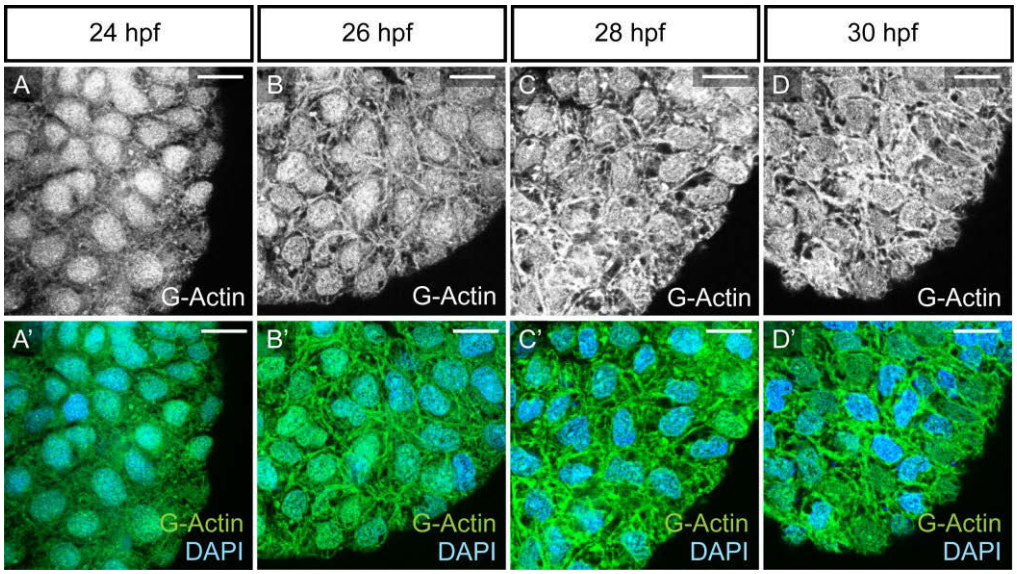

Figure 21: G-Actin localization switches from nuclear to cell cortex between 24 hpf and 30 hpf. (A-D, A'-D') Confocal pictures of hearts during different stages of LHT remodeling stained for G-Actin (green) and the nucleus (DAPI-blue). G-Actin is located within the nuclear compartment at 24 hpf. In the following hours it is translocated to filamentous structures mainly located at the cell periphery (compare A, A' with D, D').

2.7.2 Changes in pMRLC Affect Nuclear Tension and LMNA Localization

Changes in cytoskeletal organization affect tensional homeostasis within the myocardium. Recently, tissue stiffness was shown to strongly correlate to nuclear tension and gene regulation as cells sense, translate, and transmit mechanical cues from the cytosol and the membrane to the nucleus (Buxboim et al., 2014; Swift et al., 2013). Mechanical forces alter the transcription of *Lamin A/C* (LMNA), and the stability of the encoded protein, distorting the nuclear envelope resulting in changes in transcriptional regulation. An increase in *LMNA* activates SRF signal transduction to induce myogenic differentiation (Swift et al., 2013).
It is feasible to assume that nuclear shape can provide insight into the status of nuclear tension in the similar manner as cell shape, and that nuclear localization of pMRLC affects the tension within the nucleus. To that end, solidity of nuclear shapes was determined as a means to measure nuclear tension (Figure 22 A-C). The solidity value describes the actual shape of a 2D object in relation to an ellipse that is fitted to its boundaries (schematic in Figure 22 C).

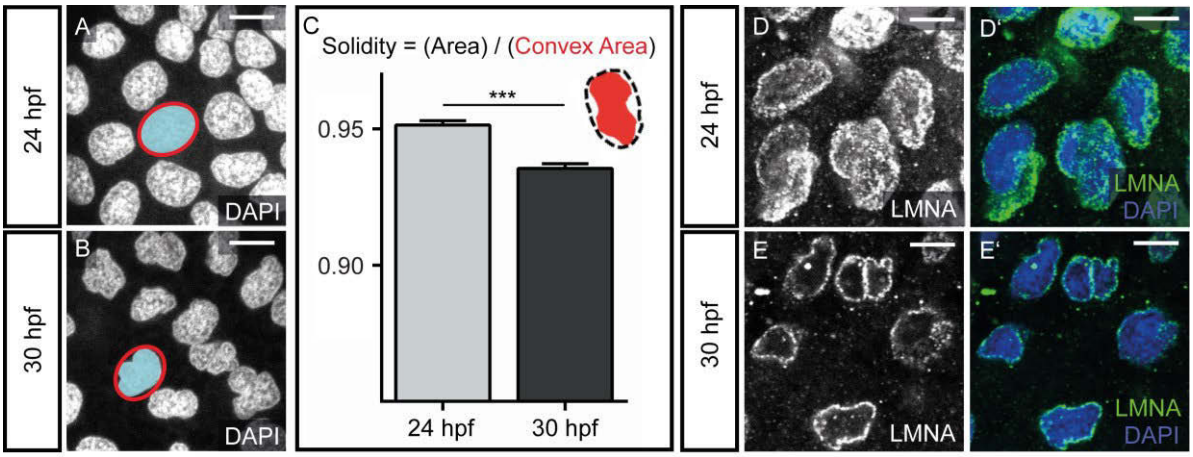

Figure 22: Nuclear shape and LMNA localization within myocardium change during cardiac remodeling. (A, B) Confocal images of myocardial nuclei in hearts at 24 hpf and 30 hpf show differences in nuclear shape. (C) Solidity measures the area of an ellipse fitted to the nuclear outline against the convex area of the nuclear shape. Solidity is increased at 24 hpf reflecting rounder shapes of nuclei. Nuclei at 24 hpf (n=60) are rounder, and more solid than nuclei at 30 hpf (n=104). (D, E; D', E') Confocal images show changes in LMNA distribution within myocardial nuclei during cardiac remodeling. LMNA is highly abundant within the whole nuclear compartment at 24 hpf, but localizes distinctly to the inner nuclear membrane at 30 hpf. Scale bar = 5 µm. *** = $P < 0.001$; t-test.

At 24 hpf high amounts of nuclear pMRLC correlate with rounded shape of nuclei (Figure 22 A, C). With translocation of pMRLC out of the nucleus at 30 hpf, nuclear shape becomes irregular, reflected by a reduction in solidity (Figure 22 B, C). These data suggest that phosphorylation of MRLC within the nucleus or at least its presence in phosphorylated form increases tension within this compartment. Recent studies reveal that changes in nuclear tension are accompanied with altered LMNA abundance and localization at the inner nuclear membrane that correlate strongly to differentiation of specific cell types (Swift et al., 2013). In wild-type hearts LMNA is located diffusely within the nucleus at 24 hpf and distinctly to the inner nuclear membrane at 30 hpf suggesting changes in nuclear stiffness (Figure 22 D, D', E, E').

2.7.3 PCP Pathway Components Regulate pRMLC Localization and Activity

Dynamic interactions between PCP core components and the actomyosin cytoskeleton have been described repeatedly (Wallingford, 2012). Already in 2001 it was shown that PCP alters MRLC contractility through activation of the small GTPase Rho and subsequent ROCK-dependent phosphorylation events (Figure 24) (Winter et al., 2001).

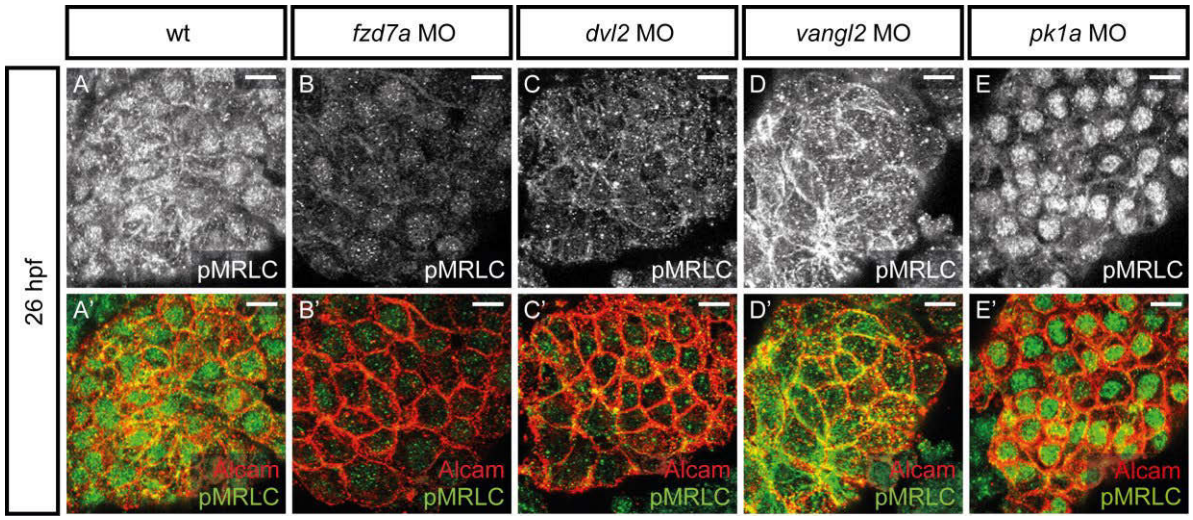

Figure 23: Changes in PCP signal transduction affect pRMLC localization and abundance. (A-E') Confocal images of the myocardium at 26 hpf stained for Alcam (red) and pMRLC (green). pMRLC protein amount is increased in *fzd7a* (B, B') and decreased in *dvl2* (C, C') morphant hearts, while down-regulation of Vangl2 (D, D') and Pk1a (E, E') changes its localization. Scale bar = 10 µm.

To determine effects on pMRLC localization and abundance, PCP-deficient hearts were analyzed at 26 hpf when pMRLC is located both within the nucleus and at the cell membrane. Here, *fzd7a* and *dvl2* morphant hearts show strong reduction in pMRLC amount (Figure 23 B, B', C, C'). In contrast, reduction in Vangl2 or Pk1a levels resulted in changes of pMRLC localization. In *vangl2* morphant hearts pMRLC localizes exclusively to filamentous structures mainly at the cell membrane, while it is almost exclusively located to the nuclear compartment in hearts with reduced levels of Pk1a (Figure 23 D, D', E, E'). This finding indicates that PCP undertakes two distinct roles in pMRLC regulation: (1) While Fzd7 and Dvl2 control the amount of MRLC phosphorylation (2) Vangl2 and Pk1 regulate pMRLC translocation or spatially restricted MRLC phosphorylation.

2.7.4 Nuclear Export of pMRLC Requires Mylk3 Activity

Changes in PCP signaling affect pMRLC abundance as well as localization to either the cell membrane or the nuclear compartment. Changes in pMRLC abundance in PCP-deficient hearts suggest that regulation of upstream kinase activity could be affected. MRLC activity is positively and negatively regulated by various kinases and phosphatases (Figure 24) (Clark et al., 2007). Among these, the Rho-associated protein kinase (ROCK) and the Myosin light-chain kinase (MLCK) have been studied most extensively. While ROCK is known to be regulated by PCP signaling, MLCK acts as a Ca^{2+} dependent kinase activated by binding of Ca^{2+} to calmodulin (Kamm and Stull, 2001; Shimizu et al., 2006).

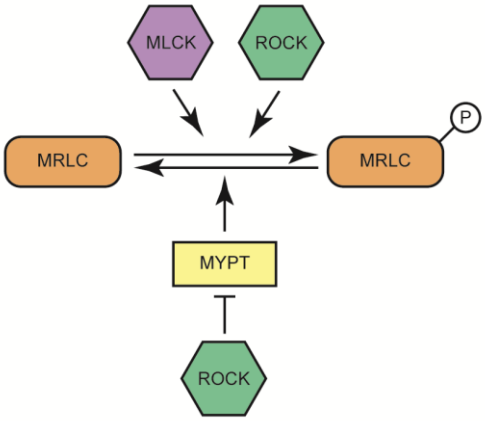

Figure 24: Phosphorylation of MRLC is mainly regulated through the interplay of the kinases MLCK, ROCK, and the phosphatase MYPT. Both ROCK and MLCK phosphorylate MRLC directly. Additionally, ROCK regulates MRLC phosphorylation indirectly through inhibition of MYPT, which dephosphorylates pMRLC.

Since the PCP pathway is a known activator of Ca^{2+} signaling, it is reasonable to assume PCP signaling might act as an effector of MLCK activity. Three types of muscle MLCKs have been identified: smooth muscle (smMLCK), skeletal (skMLCK), and cardiac (cMLCK) MLCK, which are products of genes *mylk*1, *mylk*2, and *mylk*3, respectively (Chan et al., 2008; Takashima, 2009; Watterson et al., 1999). The cardiac specific MLCK (Mylk3) contains a unique N-terminal sequence (Chan et al., 2008).

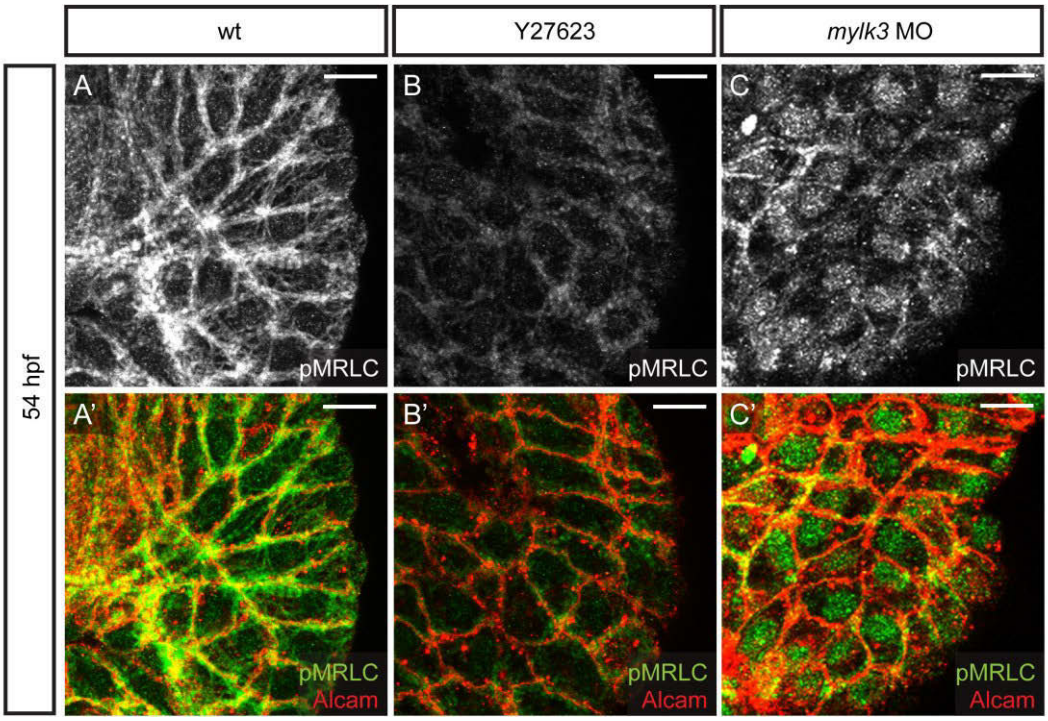

Figure 25: Localization of phosphorylated MRLC is regulated by Mylk3. (A-C, A'-C') Confocal images of OC region of hearts at 54 hpf stained for pMRLC (green) and Alcam (red). (A, A') In wild-type hearts at 54 hpf pMRLC localizes to sarcomeric structures along the cell membrane. (B, B') In hearts treated with ROCK inhibitor Y27623 the level of pMRLC is reduced drastically. (C, C') Decreased levels of Mylk3 lead to accumulation of pMRLC within the nuclear compartment of the zebrafish myocardium.

To investigate the role of kinases that regulate MRLC activity in the context of cardiac remodeling, function of both upstream regulators ROCK and MLCK was inhibited (Figure 25 A-C, A'-C'). Dissected hearts at 54 hpf were treated for 1h with the ROCK inhibitor Y27623 leading to decreased overall pMRLC abundance (Figure 25 B, B'). In contrast, reduction in Mylk3 levels via morpholino knockdown increased nuclear localization of pMRLC with concomitant reduction in its sarcomeric localization (Figure 25 C, C'). This finding reveals that pMRLC activity within the myocardium is regulated by upstream kinases through either abundance or localization.

2.8 Pk1a is a Potential Nuclear Transporter

2.8.1 Pk1 Localizes to Nucleus During Cardiac Remodeling

Changes in localization of pMRLC to the nuclear compartment observed in *pk1a*- and *mylk3*-deficient hearts suggest a novel function of PCP-signaling and downstream kinases in targeting nuclear transport. Pk1 is a PET and LIM domain containing protein that features several nuclear localization sites (NLS) as well as a C-terminal farnesylation motif CAAX that was shown to facilitate association with the membranes (Figure 26) (Ahearn et al., 2011). The N-terminal PET domain has been suggested to play a role in protein-protein interactions with proteins involved in planar polarity signaling or organization of the cytoskeleton (Gubb et al., 1999). The following LIM domains are zinc finger structures that were found in several types of proteins, including transcription factors and kinases that play essential roles in a diverse set of developmental processes such as cytoskeletal organization, cell lineage specification and organogenesis (Bach, 2000). Interestingly, the Pk1 nuclear localization is not only facilitated by NLS domain, but also by its C-terminal farnesylation motif (Mapp et al., 2010).

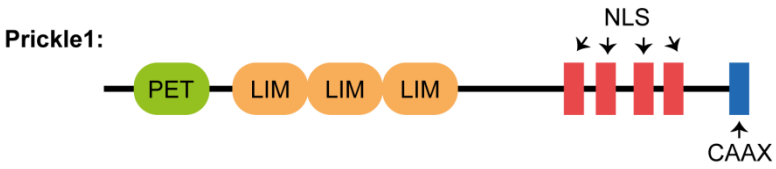

Figure 26: Pk1 is a LIM-domain containing protein with several nuclear localization signals (NLS). The N-terminal PET and LIM domains have been suggested to play a role in protein-protein interactions with proteins involved in planar polarity signaling or organization of the cytoskeleton. Nuclear localization is facilitated by nuclear localization sites (NLS) and CAAX, a farnesylation signal, that also mediates Pk1 membrane binding.

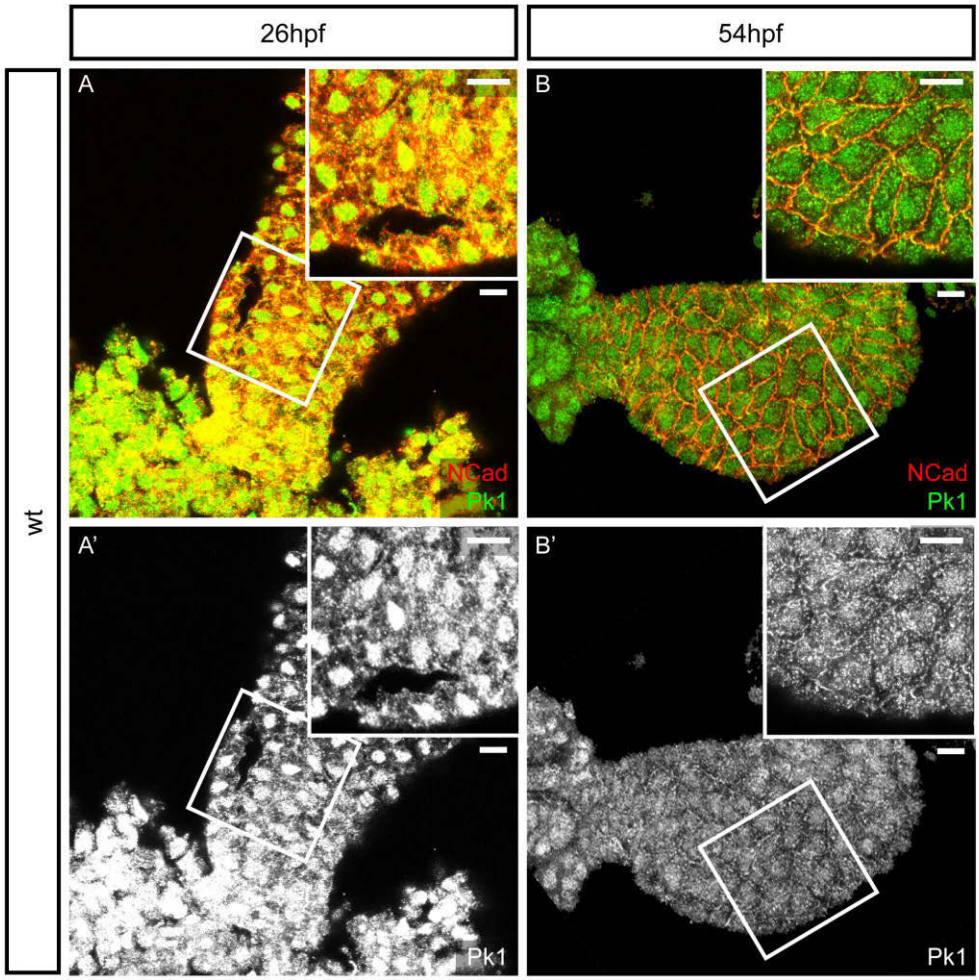

Figure 27: Pk1 is predominantly localized in the nucleus at 26 hpf and both at the cell membrane and in the nucleus at 54 hpf. Localization of Pk1 at 26 hpf (green in A, greyscale in A') and at 54 hpf (green in B, greyscale in B') in wild-type hearts. Myocardial plasma membrane is stained for N-Cadherin (red in A, B). Scale bar = 10 µm.

Several studies provided evidence that Pk1 is directly interacting with the nuclear transcriptional repressor RE1-silencing TF (REST), which is involved in the repression of neuronal genes in non-neuronal cells and the regulation of neuronal differentiation (Shimojo and Hersh, 2003; Shimojo and Hersh, 2006). In addition, during facial branchiomotor neurons migration, Pk1b isoform regulates the nuclear localization of the REST via its C-terminal farnesylation motif (Mapp et al., 2010; Yang et al., 2014). Thus, it has been proposed that Pk1 can function as a nuclear transporter (Mapp et al., 2010).

First, to assess whether Pk1 might play a functional role in the nuclear compartment its localization in the developing myocardium was analyzed by immunostaining with an antibody specific to Pk1a and Pk1b.

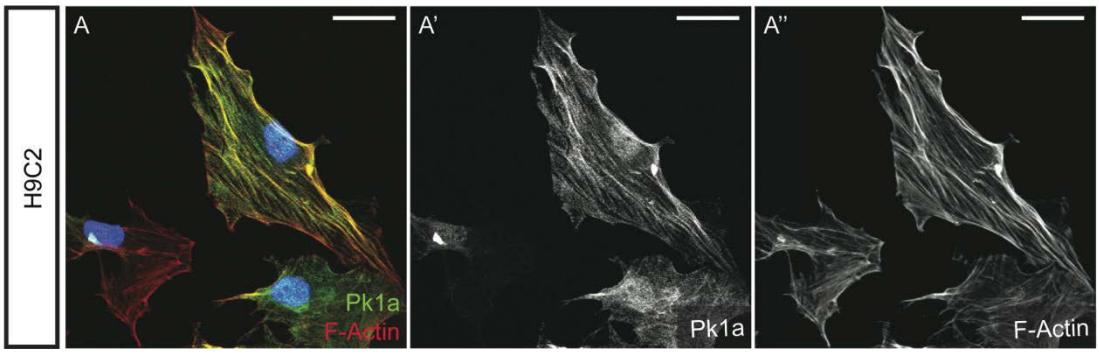

Figure 28: In H9c2 rat cardiomyoblasts Pk1 accumulates within the nucleus and co-localizes with filamentous actin (F-Actin). (A-A'') Confocal images of H9c2 rat cardiomyoblasts stained for Pk1 (green in A, greyscale in A'), F-Actin (red in A, greyscale in A''), and the nucleus (blue in A). Scale bar = 20 µm.

At LHT stage Pk1 localizes predominantly to the nucleus of ventricular cardiomyocytes with little protein at the cell membranes (Figure 27 A, A'), while at 54 hpf after completed chamber formation Pk1 localizes in presumably equal amounts to the cell membrane and the nuclear compartment (Figure 27 B, B'). These data suggest, that Pk1 may be involved in mechanisms within the nucleus during early cardiac development and that its role could change after the two chambers have formed.

Next, to corroborate the data and to resolve the subcellular localization of Pk1 in greater detail, rat H9c2 cardiomyoblasts were stained for Pk1. Here, the protein co-localized with actin filaments and accumulated within the nucleus (Figure 28). This suggests that Pk1 nuclear localization is not specific to zebrafish cardiomyocytes, but can be observed in cardiomyocytes of different species. This enforces further the hypothesis that Pk1 has a role in nuclear processes.

2.8.2 SRF Localizes to Nucleus During Cardiac Remodeling

Cardiac muscle differentiation and maturation is regulated by several signaling pathways including mechanosensitive SRF signaling. Nuclear localization of pMRLC, G-actin and Pk1 in the early LHT myocardium and their subsequent translocation to the cytoplasm, formation of actomyosin cables followed by sarcomere formation, and Pk1 actin association suggests a role of these proteins not only in the cardiac chamber remodeling, but also in the maturation of the contractile myocardium. First, G-actin was implicated in activation of SRF/MRTF-A signaling, which is pivotal to myogenic and cytoskeletal gene expression in cardiac, smooth and skeletal muscle (Sun, 2005).

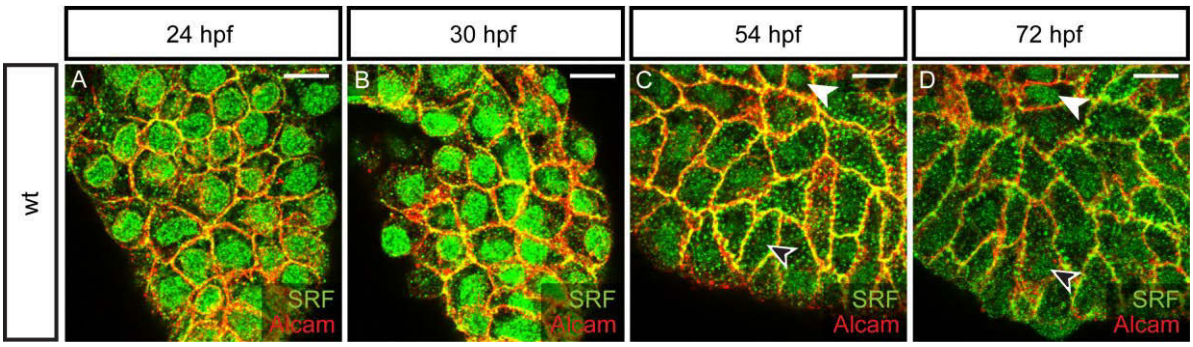

Figure 29: SRF translocates from nucleus to sarcomeres between 24 hpf and 72 hpf. (A-D) Confocal images of wild type hearts at different stages during cardiac development stained for SRF and Alcam. (A, B) At LHT stage SRF is highly abundant in the nucleus. (C) After chamber formation is completed SRF localizes not only in the nucleus, but also to sarcomeric structures. SRF remains more abundant within IC cardiomyocytes (full arrowheads) compared to OC cardiomyocytes (empty arrowheads). (D) Nuclear localization of SRF is further diminished at 72 hpf. Scale bar = 10 µm.

Secondly, previous studies implicated other members of the LIM protein family in mechanisms regulating muscle-specification. Specifically, members of the CRP family were shown to interact with the SRF and members of the GATA family to achieve smooth-muscle differentiation (Chang et al., 2003). Lastly, changes in intracellular localization of pMRLC are likely accompanied by differences in local tension as indicated through decreasing solidity from early LHT stage to the beginning of cardiac chamber formation (Figure 22 A-C). Tensional homeostasis and mechanosensitivity was linked to SRF signaling on various occasions (McGee et al., 2011; Somogyi and Rørth, 2004).

To investigate the role of SRF signaling during cardiac chamber formation in more detail, the early zebrafish myocardium was stained for SRF at different stages. During LHT stage, at 24 hpf and 30 hpf, SRF is clearly localized within the nucleus of the ventricular cardiomyocytes (Figure 29 A, B). In the course of cardiac chamber formation SRF translocates from the nucleus to sarcomeric structures. At 54 hpf, SRF can be detected within the nuclei of the ventricular cardiomyocytes to a much lesser extent, with cells at the inner curvature often retaining more SRF than those of the outer curvature (Figure 29 C, arrowheads). At 72 hpf, after chamber formation is completed, SRF signal in the ventricular nuclei is further depleted (Figure 29 D). From 54 hpf onwards, SRF is clearly localized to sarcomeric structures of cardiomyocytes (Figure 29 C, D). Thus, SRF behaves similarly in regard to nuclear localization and translocation to the cytosol when compared to pMRLC, G-actin and Pk1, further enforcing the potential role of these proteins in cardiac muscle maturation.

2.8.3 Pk1a and Mylk3 Might Mediate SRF Nuclear Export

The aforementioned data show that Pk1, Mylk3 and SRF are exported out of the nucleus during cardiac chamber formation. Previously, an isoform of Pk1 was reported to facilitate nuclear export of a transcriptional regulator (Shimojo and Hersh, 2003; Shimojo and Hersh, 2006). Another study reported members of the LIM-protein family as both nuclear SRF transcriptional cofactors and cytoplasmic scaffold proteins, that shuttle between the two compartments during differentiation processes of smooth muscle cells from proepicardial cells (Chang et al., 2003). Additionally, previous studies showed that MLCK is required for nuclear translocation of NFκB and RelA/p65 (Kimelman and Xu, 2006; Wadgaonkar et al., 2005)

It was reported previously that SRF is regulated by changes in nuclear tension (Swift et al., 2013). Since reduction in both Pk1a and Mylk3 resulted in pMRLC retention in the nucleus, local tensions could be affected leading to changes in SRF localization. To that end, SRF localization was analyzed in hearts with decreased levels of Pk1a and Mylk3. In hearts with reduction in either Pk1a or Mylk3, SRF signal within the nucleus is distinctly stronger than in wild-type hearts (Figure 30 A-C). Furthermore, localization of SRF into sarcomeric structures is reduced, particularly in *mylk3*-deficient hearts (Figure 30 C). Thus, both Pk1 and Mylk3 are involved in regulation of SRF localization.

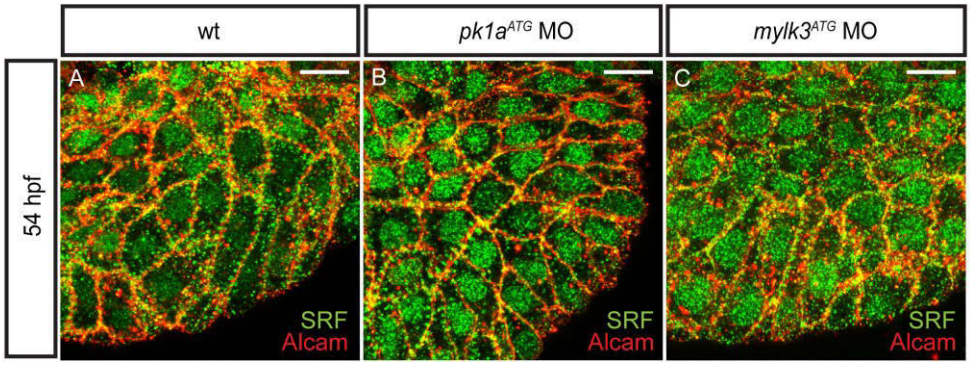

Figure 30: Pk1 and Mylk3 are involved in SRF nuclear localization. (A-C) Confocal images of OC myocardium at 54 hpf stained for SRF (green) and Alcam (red). (A) In wild type hearts SRF is localized both at sarcomeres and in nuclei albeit in lower levels. In a number of cells SRF nuclear localization is not detectable indicating a dynamic change in its localization during cardiac remodeling. (B, C) In hearts with decreased levels of *pk1a* (B) or *mylk3* (C) the abundance of SRF within nuclei is markedly increased. Scale bar = 10 µm.

2.9 PCP Mediates SRF-Regulated Myogenic Differentiation

2.9.1 Acta2 Expression is Heavily Increased During Cardiogenesis

Changes in tensional homeostasis accompanied by changes in SRF localization during cardiac remodeling are likely to affect SRF-regulated transcription. SRF target genes comprise several proteins of the contractile machinery such as smooth muscle, skeletal and cardiac α-actin (*acta2*, *acta1b* and *actc1b*), β-myosin heavy chain (*β-mhc*) and myosin light chain 2 (*myl2*) (Davey et al., 1995; Gustafson and Kedes, 1989; Henderson et al., 1989; Molkentin, 1996). Actins are highly conserved among animal species and play crucial roles during cell division, migration, cytoskeletal composition, and contraction. Higher eukaryotes express six different actins: skeletal, cardiac and smooth muscle α-actins, β-actin, γ-actin, and γ-enteric actin (Vandekerckhove and Weber, 1978). While β-actin and γ-actin are expressed ubiquitously, smooth muscle actin (*acta2*) is highly abundant in smooth muscle cells, and cardiac α-actin (*actc1b*) and skeletal α-actin (*acta1b*) are predominantly expressed in striated muscle. During early avian cardiogenesis smooth muscle α-actin is the first actin to be strongly expressed in the heart, and precedes following co-expression of skeletal and cardiac α-actin (Ruzicka, 1988). In zebrafish, *in-situ* hybridization revealed that apart from *acta1b* and *actc1b*, smooth muscle α-actin is also highly expressed in the LHT (Thisse et al., 2004).

To determine the spatiotemporal changes in expression of smooth muscle, skeletal and cardiac α-actin during cardiogenesis in zebrafish, cells were sorted for cardiomyocytes and non-cardiomyocytes by fluorescence-activated cell sorting (FACS) from *Tg(myl7:GFP)* line labeling all myocardial cells. Subsequently, both populations were analyzed for the expression of *acta1b*, *actc1b*, and *acta2* at LHT stage (26 hpf), shortly after the cardiac chambers have formed (54 hpf), in the beginning of trabeculation (72 hpf) and at 120 hpf (Figure 31). The data were collected in collaboration with Anne Merks. Fold expressions were calculated in relation to 26 hpf stage. During early zebrafish development expression levels of *acta1b*, *actc1b*, and *acta2* change between different stages of cardiogenesis. In the GFP-positive cardiomyocytes, *acta1b* expression increases to 4.7-fold at 54 hpf and then drops gradually to 3.3-fold at 72 hpf and 1.7-fold at 120 hpf. Levels of *actc1b* mRNA increase to 8.4-fold at 54 hpf and remain more or less constant with 7.3-fold induction at 72 hpf and 7.8-fold increase at 120 hpf. In contrast, *acta2* mRNA levels are nearly unchanged at 54 hpf with a 1.4-fold induction, but expression increases strongly at 72 hpf with an 18-fold induction and is enhanced further at 120 hpf to 72-fold (Figure 31, cardiomyocytes). In the GFP-negative cells mRNA levels of *acta1b* are increased to 5.2-fold and remain stable

until 72 hpf (4.9-fold induction). Expression levels decrease strongly within the next hours to 1.7-fold. Similarly, levels of *actc1b* mRNA are increased to 4.2-fold at 54 hpf with a mild increase to 5.2-fold at 72 hpf, but are decreased strongly at 120 hpf to a 1.7-fold expression. In contrast, mRNA levels of *acta2* are increased to 36-fold at 54 hpf and expression is further enhanced to 1700-fold at 72 hpf dropping to 1000-fold at 120 hpf (Figure 31, non-cardiomyocytes). These results suggest, that the different actin isoforms are important during different stages of cardiac development. While *acta1b* and *actc1b* are more abundant at LHT stage and during early cardiac chamber formation, *acta2* expression increases mainly after the two cardiac chambers have formed. Thus, unlike in other vertebrates, in zebrafish myocardial *acta2* expression markedly increases only after the two cardiac chambers are formed.

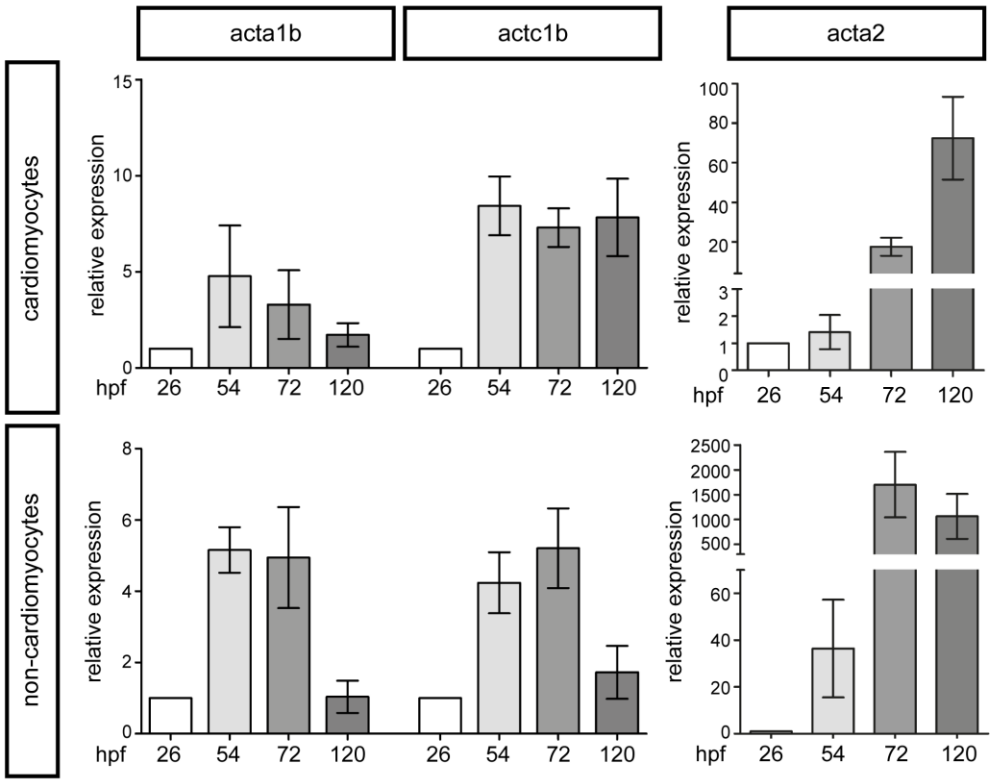

Figure 31: Skeletal, smooth muscle, and cardiac actin are differentially expressed during cardiogenesis. In cardiomyocytes expression of skeletal (*acta1b*) and cardiac actin (*actc1b*) are increased at 54 and 72 hpf, but are downregulated after chamber formation has completed (120 hpf). Smooth muscle actin (*acta2*) expression in myocardial cells is increased by 18-fold at 72 hpf and by 72-fold at 120 hpf. Results of three independent experiments.

2.9.2 PCP Dysregulation Affects SRF Target Gene Expression

SRF signal transduction is crucial to proper cardiac development. Several studies show that both loss and overexpression of SRF leads to cardiomyopathies and that changes in actin distribution in the embryonic heart are associated with impaired development of cardiac structure and function (Kumar et al., 1997; Niu et al., 2008; Parlakian et al., 2004).

To investigate the function of PCP signaling in cardiac-specific SRF/MRTF-A-mediated signal transduction, target gene expression was analyzed using quantitative real-time PCR in embryos with reduced Vangl2 and Pk1a levels. Reduction in Pk1a results in decrease of *acta1b* levels to 82% and *acta2* mRNA levels to 80%, while expression levels of *actc1b*, *tgln* and *srfb* are not significantly affected (Figure 32). Furthermore, loss of Pk1a leads to a mild, but not significant decrease of *pk1b* mRNA levels (Figure 32). The control genes *ETS translocation variant 4* (*etv4*) and *fibroblast growth factor 4* (*fgf4*) which regulate MRTF-A independent cardiac gene expression through SRF (Liang et al., 2001; Znosko et al., 2010), were not affected by *pk1a* knockdown (Figure 32).

Analysis of SRF target gene expression in *vangl2*-mutants revealed a decrease in *acta1b* mRNA levels to 70 % and *fgf4* levels to 64 % (Figure 33). In contrast to *pk1a*-deficient zebrafish, *acta2* expression is increased by 40 % in *vangl2*-mutants (Figure 33). Expression levels of *actc1b, tgln*, *srfb* and *pk1b* are mildly decreased (n.s.) and no effect on *etv4* and *pk1a* expression was observed (Figure 33). Taken together, both loss of Pk1a and Vangl2 result in deficient SRF target gene expression mainly affecting *acta1b* and *acta2* mRNA levels.

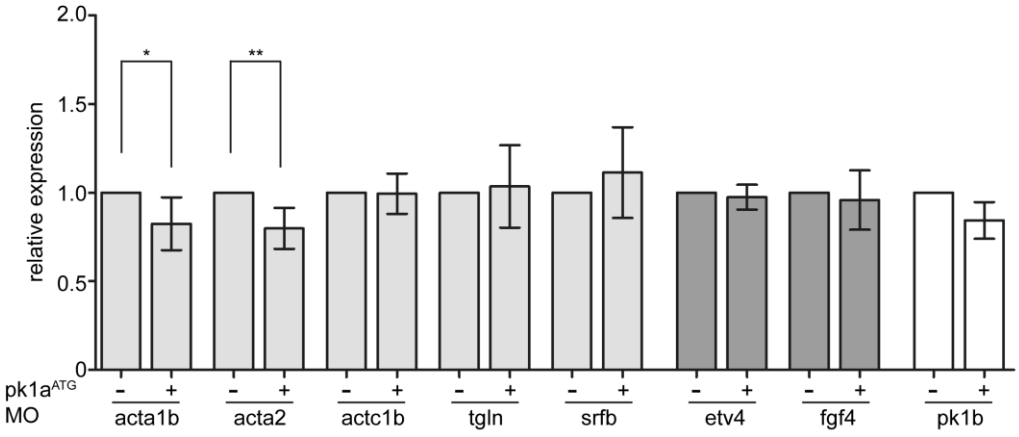

Figure 32: Pk1 is crucial to SRF signal transduction. Quantitative RT-PCR results in whole zebrafish embryos with reduced levels of *pk1a* at 54hpf. Loss of Pk1a leads to decreased amounts of *acta1b* and *acta2*, but not *actc1b*, *tgln* and *srfb*. Expression of *etv4* and *fgf4* is not affected in *pk1a*-deficient zebrafish. Results of eight independent experiments. * = $P < 0.05$, ** = $P < 0.01$; t-test.

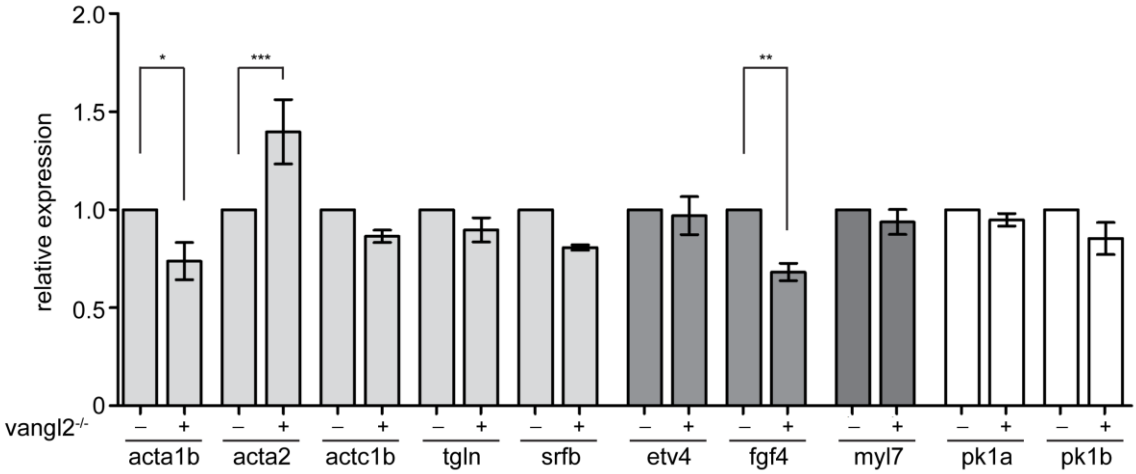

Figure 33: Vangl2 affects myogenic SRF signaling transduction. In *vangl2* mutant hearts expression of *acta2* is increased by 40%, while *acta1b* expression is reduced to 70 % and *fgf4* expression decreases to 64 %. Gene expression of *actc1b*, *tgln*, *srfb* and *pk1b* is reduced mildly. Levels of *pk1a* and *etv4* are unchanged. Results of three independent experiments. * = P < 0.05, *** = P < 0.001; t-test.

2.9.3 Proper Sarcomerogenesis Requires PCP Signaling

Cardiac function is dependent on myogenic differentiation and maturation of the heart to ensure proper contraction and coupling of the myocardium. During cardiac chamber formation sarcomeres start to assemble around 48 hpf, but fully structured sarcomeres are not visible by electron microscopy before 96 hpf (Becker et al., 2011; Huang et al., 2009; Sehnert and Stainier, 2002). Myofibrils of striated muscle, such as cardiac and skeletal muscle, are formed through the assembly of small contractile units, the sarcomeres.

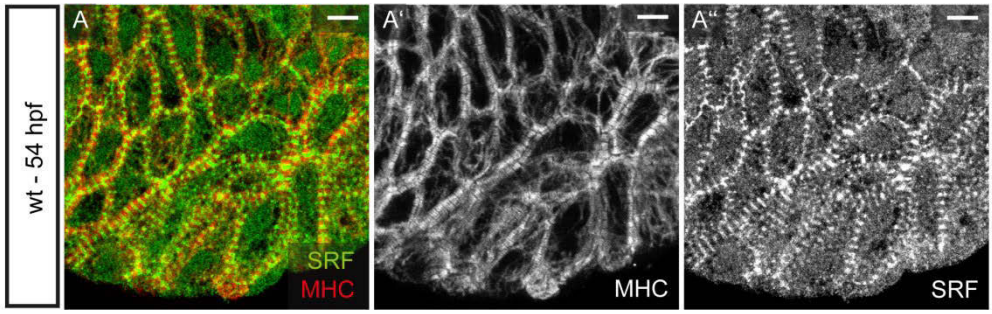

Figure 34: SRF localizes to Z-discs during cardiac chamber formation. (A) Confocal images of OC myocardium at 54 hpf stained for MHC (A', red in A) and SRF (A'', green in A). Scale bar = 10 µm.

SRF function was shown to be required for sarcomerogenesis in many instances (Balza and Misra, 2006; Lahoute et al., 2008; Parlakian et al., 2005). Additionally, regulators of SRF signaling were implicated in sarcomere assembly. In zebrafish, loss of Mylk3 resulted in failure to form proper sarcomeric structures and overexpression of activated MLCK improved sarcomere organization in neonatal rat ventricular myocytes (Aoki et al., 2000; Seguchi et al., 2007). Another study showed that ROCK inhibition delayed sarcomere assembly (Stepanova et al., 2011).

First, to address a potential function of SRF during sarcomere assembly, its localization within the sarcomeric structures of the early zebrafish myocardium was analyzed in more detail. Here, at 54 hpf SRF localizes to Z-discs between M-bands as visualized by myosin heavy chain (MHC) (Figure 34). Next, it was addressed whether PCP-mediated changes in early actomyosin organization and altered SRF target gene expression result in maturation defects. In zebrafish, sarcomere structure assembly is initiated at about 48 hpf (Huang et al., 2009; Sehnert and Stainier, 2002). Sarcomeric structures in PCP-deficient hearts at 72 hpf were visualized by MHC staining to ensure potential defects are not due to a delay in development. In wild-type hearts myosin-containing thick filaments form highly ordered structures that often span several cells (Figure 35 A, A').

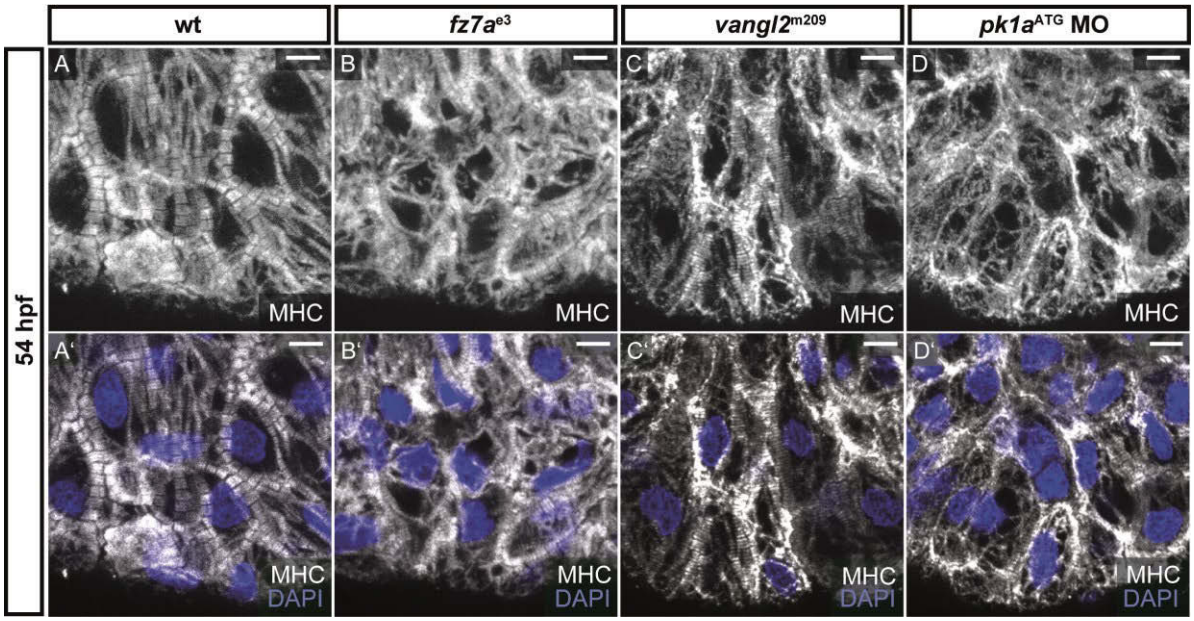

Figure 35: Deficient PCP signaling leads to failure in maturation of cardiac muscle. (A-D, A'-D') Confocal images of hearts at 72 hpf stained for myosin heavy chain (MHC), and DAPI in blue (A'-D'). (A, A') Sarcomeres in wild-type cardiomyocytes are highly organized, often forming cables along cell membranes spanning several cells. (B-D, B'-D') In *fzd7a*$^{-/-}$, *vangl2*$^{-/-}$ mutant and *pk1a*-morphant hearts thick filaments are highly disorganized and fail to form intercellular connections. Scale bar = 10 µm.

In contrast, sarcomere assembly was severely disturbed in ventricles of *fzd7a*$^{-/-}$, *vangl2*$^{-/-}$ and *pk1a* morphant hearts. Thick filaments were not properly organized, often forming filamentous structures or accumulations instead of myosin bundles (Figure 35 B-D, B'-D'). Observed defects in sarcomere organization strongly corroborate the hypothesis that PCP mediates cardiac maturation through effects on myogenic SRF target gene expression.

3 Discussion

The PCP pathway is known as a master regulator of morphogenesis of a variety of organs. Previous studies mainly addressed effects of impaired PCP signaling on gastrulation movements and tissue architecture during organ formation of the kidney, eye, and lung (Babayeva et al., 2011; Classen et al., 2005; Nagaoka et al., 2014; Ulrich et al., 2005; Zallen, 2007). Although several studies show the importance of functional PCP signaling during heart development by attributing the congenital heart defects to the absence of non-canonical Wnt ligands or core components of this pathway, its precise role during cardiogenesis remains incompletely understood (Henderson and Chaudry, 2011). Importantly, formation of the heart requires not only establishment of proper myocardial architecture, but also differentiation into a functional syncytium of cardiomyocytes that are electrically coupled and able to contract in a coordinative manner. Cardiomyocyte differentiation is dependent on myogenic signaling through the SRF transduction cascade. Although it has been inferred that PCP might affect SRF signal transduction through its downstream effectors such as Rho GTPases, experimental proof for the involvement of the PCP core components was not yet brought forward (Hill et al., 1995; Olson and Nordheim, 2010). The present study reveals a novel function of Wnt non-canonical PCP signaling during cardiac remodeling that couples changes in tensional tissue homeostasis to cardiomyocyte differentiation regulated by SRF.

3.1 Mutants Correspond to Morphant Phenotypes

Recently, biomedical research experienced revolutionary changes in technical advancements to target the function of genes through the discovery of CRISPR (Clustered regularly interspaced short palindromic repeats) - Cas9 mediated mutagenesis. The CRISPR/Cas9 system was discovered first in bacteria and archaea where it provides adaptive immunity against invading nucleic acids of viruses and plasmids (Jinek et al., 2012). In zebrafish, like in other model systems, it allows fast and efficient generation of knock-out models (Bassett et al., 2013; Burger et al., 2016; Gagnon et al., 2014; Lindsay et al., 2016). Briefly, during CRISPR-Cas9 mutagenesis short guided RNAs that are homologous to target sequences within the genomic DNA facilitate opening of the double stranded structure. Secondary structures within the sgRNA allow binding of Cas9 endonuclease, that then cleaves 3 nt upstream of a mandatory protospacer adjacent motif (PAM) sequence NGG that follows the 20 nt target sequence within the DNA sequence. The PAM sequence is a 2 - 6 bp DNA sequence targeted by the Cas9 nuclease to facilitate the cleavage. In zebrafish, these cleaved sites are mainly repaired via the error-prone process of non-homologous end

joining (NHEJ) that frequently induces insertions or deletions (indels) (Sander and Joung, 2014; Wang et al., 2013). Generation of indels that consist of a number of nucleotides not divisible by three leads to a shift of the open reading frame resulting in nonsense mutations or a premature stop codon.

Earlier studies mainly relied on morpholino-induced blockage of translation to investigate protein function, since the generation of a full gene knock-out required either time-consuming methods like TALEN mutagenesis or discovery of relevant mutations induced by ENU-mutagenesis in the Sanger Mutation Project (Hwang et al., 2014; Kettleborough et al., 2013). With growing availability of mutants, data that were obtained using morpholino knockdown technology became the center of attention as several mutant phenotypes reportedly did not correspond to those of morphant zebrafish. For instance, in a study that focused mainly on vascular morphogenesis, only about 20% of morphant phenotypes were also observed in mutant embryos (Kok et al., 2015). However, few studies of morphant knockdown technology showed reliability, albeit with observed differences between morphant and mutants phenotypes. For instance, *egfl7* mutants did not display vascular phenotypes that were observed in *egfl7* morphant fish. However, detailed analysis of both mutants and morphants revealed that complete loss of *egfl7* was compensated by increase in Emilin2/Emilin3 that was not induced in *egfl7* morphant zebrafish and that overexpression of Emilin 2 partially rescued morphant phenotypes (Rossi et al., 2015).

In the present study initial analysis of phenotypic effects on zebrafish cardiac development after PCP pathway disruption was carried out using morpholino knockdown technology. Later, additional data were obtained by analyzing mutant and CRISPant phenotypes. Here, CRISPants (CRISPR-mediated somatic mutants) were generated by injection of CRISPR/Cas9 protein complexes, which yields up to 100% efficiency of transient mutagenesis of target genes and can be used for immediate phenotypic screening (Supplement Figure 37) (Burger et al., 2016; Lindsay et al., 2016; Shah et al., 2015). Off-target and toxic effects were minimized by identification of threshold levels through dose-response curves in both zebrafish morphants and CRISPants. Importantly, quantification of transitory states during cardiac remodeling as well as imaging of SRF localization and sarcomere organization was highly reproducible when comparing *vangl2*, *fzd7a*, and *pk1a* morphants with *vangl2*, *fzd7a* mutants and *pk1a* CRISPants. For this reason, the analysis of mutant, morphant or CRISPant phenotypes was used interchangeably. However, it is important to take into account that variability is increased in CRISPants and most consistent results are achieved in stable mutants such as the *vangl2*^{m209} mutant.

3.2 PCP-Dependent Epithelial Remodeling Guides Cardiac Chamber Formation

During vertebrate cardiogenesis the chambered and looped heart is formed from a simple linear tube through a process that to date is termed cardiac ballooning (van den Berg and Moorman, 2009). While specification of cardiac precursors, migration patterns of cardiac progenitors to the ventral midline and the formation of the LHT have been studied extensively, the understanding of subsequent processes that underlie cardiac looping and chamber formation remains limited (Staudt and Stainier, 2012).

3.2.1 PCP Drives Myocardial Remodeling through Regulation of Cell Rearrangements

One of the first obvious changes in tissue architecture during cardiac chamber formation is the emergence of region-specific differences in cardiomyocyte size and shape within the IC and OC of the ventricle. Differences in outer and inner curvature regions have been described previously (Auman et al., 2007; Panáková et al., 2010). This study verifies the previous results, albeit the circularity values of both, outer and inner curvature cardiomyocytes, slightly deviate from those reported. This is very likely due to the increased accuracy achieved by the software-based definition of cell outlines labeled with anti-Alcam stainings and quantification of all cells within the respective regions.

These region-specific differences in tissue architecture, but more importantly the expansion of the cardiac chambers are achieved via cell rearrangements. The initial evidence was brought forward from *in vivo* time-lapse imaging of the LHT myocardium, in which formation of rosettes and their subsequent resolution was observed. This finding strongly suggests that mechanisms of epithelial remodeling, that were shown to be crucial for organogenesis of several organs, also underlie cardiac chamber formation. However, live imaging of epithelial remodeling in cardiac tissue could only be performed in non-contractile hearts of *tnnt2*-morphant embryos, since spatial-temporal resolution was limited in beating hearts using the methods at hand. Actomyosin modulation is pivotal to mechanisms that guide cell rearrangements. For instance, previous studies have shown that MRLC phospho-variants can influence number, speed, and nature of cell rearrangements (Kasza et al., 2014). Since in the absence of *tnnt2* actomyosin contraction is impaired, it is likely that the observed time-span of 5 hours of rosette resolution does not completely reflect the timing of this process. However, recently developed methods that utilize high-speed selective plane illumination microscopy (SPIM) together with brief interruption of the heart beat using optogenetics will

allow for high resolution reconstructions as well as shed more light on the dynamics of processes that underlie cardiac remodeling (Mickoleit et al., 2014).

It was previously proposed that the number of points in which four or more cells converge into a central junction reflects the activity of a single-layered tissue undergoing remodeling via cellular rearrangements (Blankenship et al., 2006; Farhadifar et al., 2007; Villasenor et al., 2010). The LHT myocardium features a high number of transitory states, which indicate the presence of intercalating cells within the myocardial cell layer. The number of rosettes and T1-transitions decreases significantly within the following 24 h until the two cardiac chambers form suggesting that early cardiac remodeling is driven by cell rearrangements at LHT stage. As PCP signaling drives epithelial remodeling in many instances, its potential role in directing cell rearrangements within the early myocardium was tested. Indeed, in loss-of-function studies using morpholino knockdown, CRISPants and PCP-mutants, dysregulation of PCP signaling results in altered number of transitory states at 54 hpf. Here, Wnt11 and Wnt5b are main regulators of myocardial remodeling. Down-regulation of either Wnt5b or Wnt11 results in a mild increase of transitory states. However, simultaneous knockdown of Wnt5b and Wnt11 led to an increase of transitory states suggesting that they function synergistically to regulate cardiomyocyte rearrangement. This observation is supported by a study that shows that complexes between Wnt11 homodimers and Wnt5a homodimers are required for *Xenopus* axis formation (Cha et al., 2008).

Decrease in Fzd7a, Dvl2, and Pk1a levels results in an increase in transitory states, while down-regulation of Vangl2 leads to mild reduction in transitory states. The number of transitory states in absence of Fzd7a is comparable to that observed in Wnt5b/Wnt11 morphants indicating that Fzd7a is the main receptor mediating the non-canonical Wnt signaling. However, whether the observed increase transitory states caused by down-regulation of Fzd7a or Wnt11 and Wnt5b are due to their more frequent formation or because they fail to resolve can only be determined by live imaging and tracking of fluorescently labeled cells. Furthermore, it remains to be determined whether transitory states resolve stochastically or asymmetrically, and thus shape the cardiac chambers' axes. Whether PCP signaling could play a role in such a polarized mechanism remains to be determined.

3.2.2 PCP Establishes Regionally Restricted Cardiomyocyte Characteristics

Previous studies have not addressed regional differences in cardiomyocyte orientation, although cardiomyocyte elongation in accordance with the stretching direction seems to be prerequisite for the normal function of these cells (Wang et al., 2014). This study describes

myocardial architecture in more detail by analyzing cardiomyocyte orientation in regard to IC and OC position. During cardiac chamber formation elongation and alignment of cardiomyocytes along the curvatures is crucial for establishing the overall shape of the ventricle. Here, especially positioning of OC cardiomyocytes in a radial pattern defines distinct ventricular shape. Thus, investigation of cardiomyocyte shape and organization within specified regions of the ventricle allows assessment of the effects of impaired PCP signaling on ventricular shape. This study shows that PCP signaling is indispensable for cell orientation within the ventricular chamber. Specifically, disruption of PCP signaling leads to defects in cardiomyocyte positioning in OFT regions. This finding underlines the importance of PCP during OFT remodeling in accordance with several other studies that found that CHDs related to mutations of PCP core components usually result in OFT region defects (Hamblet, 2002; Henderson and Chaudhry, 2011; Henderson et al., 2001; Phillips, 2005; Schleiffarth et al., 2007; Wu et al., 2011). Taken together, the data presented in this study indicate that failure to establish typical ventricular shape and remodel OFT may be due to impaired cell rearrangements regulated by PCP signaling.

3.2.3 Fzd7a and Vangl2 Function Determines FHF/SHF Contribution

Several studies in the recent years have proven the existence of a SHF in the zebrafish heart despite only primitive OFT region and the absence of a right ventricle, which are the main compartments of the heart formed through addition of SHF cardiomyocytes in higher vertebrates. In zebrafish, the primitive LHT arises from cardiomyocytes of the FHF, and a second population of cells from the SHF contributes to the formation of the myocardium of the arterial and venous poles (de Pater et al., 2009; Hami et al., 2011; Mosimann et al., 2015).

The data obtained in this study suggest that core components of the PCP pathway control mechanisms that regulate the pool of undifferentiated cardiac precursors of the FHF or SHF. Specifically, the myocardium of hearts with decreased levels of the Wnt receptor Fzd7a consists of a higher proportion of FHF derived cardiomyocytes, while Vangl2 deficient hearts show larger portions of cells that are presumably of SHF origin. However, whether Wnt/PCP signaling targets cardiac precursor proliferation, their differentiation or migration remains to be answered.

Previous studies were able to show that expansion and allocation of early heart progenitors is dependent on Wnt/β-Catenin signaling, since genetic activation of the pathway using a stabilized form of β-Catenin resulted in marked proliferation of SHF progenitors (Ai et al., 2007; Kwon et al., 2007). Potential downstream targets of β-Catenin comprise *isl1* and *fgf10* suggesting a link between Wnt and FGF signaling pathways in SHF specification (Lin et al.,

2007; Luo et al., 2015). Elevated FGF8 signaling with downstream targets such as FGF4 (Sun et al., 1999), has been associated with excessive proliferation of secondary heart field progenitors and failure of the myocardial cells to be added to the heart (Waldo et al., 2005). If FGF8 induced FGF4 expression in cardiac progenitors, observed reduction in *fgf4* mRNA expression levels in the absence of Vangl2 were in disagreement with increased number of SHF derived cardiomyocytes when Vangl2 is missing. Moreover, a recent study shows that loss of Vangl2 results in SHF progenitor reduction and premature differentiation in the distal outflow tract (Ramsbottom et al., 2014). The contrasting results presented in this study with those reported previously demonstrate that more detailed studies are required to address the spatial as well as temporal requirement of PCP signaling during FHF/SHF specification. In addition, the defects in cardiac looping together with decreased SHF cell number in *fzd7a*-deficient hearts suggests that PCP might be involved in regulating cardiac looping through changes in SHF migration. To that end, cell-tracing experiments could be performed to follow migration of cardiomyocytes in PCP-deficient hearts to confirm defective addition of SHF cardiomyocytes into the developing heart. Altogether, the results indicate a putative role of the PCP core components in cardiac precursor proliferation, specification or migration. However, future studies should address what cellular process is targeted by non-canonical PCP signaling.

3.3 PCP Targets Tensional Homeostasis by Regulation of Actomyosin Contractility

Cell intercalation in single-layered tissues is driven either through remodeling of cadherin rich adherens junction or protrusion formation similar to filopodia in migratory cells (Walck-Shannon and Hardin, 2013). Thus, I next elucidated the mechanism that underlies the regulation of cell rearrangements through PCP signaling in the heart. Since loss of Fzd7a and Vangl2 led to opposing effects on the amount of transitory states within the myocardium at 54 hpf, I focused on analyzing junctional integrity and actomyosin organization in the hearts with decreased levels of Fzd7a or Vangl2.

3.3.1 PCP Signaling Does Not Affect N-Cadherin Localization

Cells need to be mechanically coupled in order to transmit force effectively. Cadherins at the cell-cell contacts mediate the mechanical linkage and through modulation of F-actin regulate tissue stiffness and tissue surface tension (Gumbiner, 2005). Cadherin-mediated cell adhesion and signal transduction is pivotal during cardiomyogenesis and cardiac disease (Piven et al., 2011; Resink et al., 2009). Several studies showed direct control of N-Cadherin

through Wnt non-canonical signaling components in diverse contexts (Nagaoka et al., 2014; Tufan et al., 2002).

In the ventricular myocardium of *fzd7a* or *vangl2* morphant hearts no change in N-cadherin localization or abundance was detected at 54 hpf. However, it cannot be excluded that dysregulation of the PCP pathway has an effect on rate of N-cadherin endosomal recycling as the regulation of cell rearrangements could be regulated by cadherin turnover rates in a number of instances (Bentley et al., 2014; Classen et al., 2005; Ulrich and Heisenberg, 2008). Additionally, it was shown that conformational change of cadherins at cellular junctions affects their stability resulting in changes of the strength of adhesive bonds between cells (Hong et al., 2011). It remains to be addressed if cadherin mobility or stability at cellular junctions has an impact on cell rearrangements through changes in cell adhesion. Besides cadherin dynamics, changes in intercellular adhesion are mediated via availability of Ca^{2+} (Takeichi et al., 1981). Thus, the PCP pathway could act on adhesion processes through effects on intercellular as well as intracellular Ca^{2+} concentrations.

3.3.2 PCP Signaling Organizes Polarized Actomyosin

It is well known that cell shape changes are driven by actomyosin-induced contractions to establish new tissue morphologies. PCP signaling is indispensable for organization of cytoskeletal components in all cells (Tada and Kai, 2009). Transient expression of a membrane-associated form of EGFP in morphant hearts revealed that reduction in Fzd7a levels results in increased formation of basal protrusions and apical constriction. Cellular protrusion formation is crucial for oriented cell migration. Hence, it is likely that cardiomyocyte migration is affected in hearts with reduced levels of Fzd7a. The fact that ventricles of *fzd7a* deficient hearts might incorporate fewer SHF cardiomyocytes could support this claim. Additionally, recent concepts evolve around the function of Wnt intercellular signaling through basal cytoplasmic projections (Stanganello and Scholpp, 2016); one of the studies shows a central function of Fzd7 during signaling between ectodermal and somatic epithelia (Sagar et al., 2015). Given that Wnt11 is expressed in the pharyngeal mesoderm, in a tissue juxtaposed to the heart tube's arterial pole, and has to instruct the ventricular cells several cell diameters away, Fzd7 regulated basal cell protrusions could facilitate the communications between Wnt11 producing and receiving cells.

Proper formation of the apical actomyosin network is specified by correct establishment of the apical domain, and regulated by apicobasal polarized proteins like Par6 and Par3 and aPKC (Putzke and Rothman, 2003; Sawyer et al., 2010). PCP is known to establish apicobasal polarity, for instance through binding of Dvl to aPKC. (Zhang et al., 2007). Through this mechanism, PCP mediates the formation of contractile actomyosin at the cell

cortex at apical tight junctions. Actomyosin structures within *fzd7a* deficient cardiomyocytes show irregular protrusive patterns that are enriched at the basolateral compartment of cardiomyocytes. This finding strongly suggest that PCP signaling is crucial to establish and maintain polarized actomyosin structures in the developing vertebrate heart.

3.3.3 PCP Controls Spatially Restricted Myosin Regulatory Light Chain Contractility

In heart, coordinated contractility by actomyosins is fundamental for its proper function and encompasses not only tight regulation of cardiac myosins, but also non-muscle myosins (Vicente-Manzanares et al., 2009). Non-muscle myosin II (NMII), a member of the myosin II subfamily that includes cardiac, skeletal, and smooth muscle myosin, was shown to be the key regulator of cell intercalation movements. The protein is enriched at disassembling cell-cell junctions and becomes localized to temporary junctions and rosettes, where it appears to drive the formation of new junctions by preventing reversion to the original cell orientation (Bertet et al., 2004; Zallen and Wieschaus, 2004). NMII localization or activity is regulated by phosphorylation and dephosphorylation of its regulatory light chain (pMRLC) involving a tightly regulated interplay between ROCK, MLCK, and myosin phosphatase (MYPT) activity (Matsumura et al., 2001; Riento and Ridley, 2003).

This study provides evidence for a novel role of coordinated activity of NMII regulatory light chain (MRLC) during cardiac chamber formation through rapid relocalization of pMRLC from the nucleus to the cell junctions between 26 and 28 hpf. At 24 hpf pMRLC is localized predominantly in the nucleus of ventricular cardiomyocytes. However, at 54 hpf, after the cardiac chambers have formed, pMRLC is no longer present in the nuclei, but localizes to actomyosin fibers within the cytoplasm and at the vicinity of plasma membrane. Here, a distinct accumulation of pMRLC to points of active cell rearrangements suggests its role in epithelial remodeling during cardiac chamber formation. The importance of this relocalization seems to be specific to active MRLC, since its unphosphorylated form exclusively localizes to cell membranes and is never present in the nuclear compartment. During body axis elongation in *Drosophila*, unphosphorylated MRLC resulted in fewer, slower cell rearrangements, while phosphomimetic MRLC accelerated cell rearrangements and incorporated more cells into rosette structures (Kasza et al., 2014). Further studies should aim at a deeper understanding of the role of MRLC phosphorylation during cardiac chamber formation by investigating the effects of overexpression of MRLC variants that prevent or mimic phosphorylation on transitory states as well as ventricular shape.

The antibody used to detect the phosphorylated and non-phosphorylated form of MRLC is specific to myosin regulatory light chain 12b and 9b. Results acquired by using the antibody against the phosphorylated form of MRLC could not be reproduced after acquiring another antibody batch for which processes during its production were modified by the manufacturer. However, in immunostainings with this antibody batch decreased signal of pMRLC after treatment with the ROCK inhibitor Y27623 indicates that the signal is specific to MRLC phosphorylation and that results acquired using this antibody batch allow for meaningful interpretation.

Wnt non-canonical signaling was implicated in mechanisms that differentially regulate myosin II-based contractile forces in various contexts mainly through downstream effectors of PCP signaling such as ROCK or aPKC (Blankenship et al., 2006; Lee et al., 2012). Recently, it was shown in *Ciona intestinalis* that MRLC co-localizes with the PCP core protein Vangl and Pk (Newman-Smith et al., 2015). Thus, the PCP pathway likely targets either NMII localization or its activity in the developing heart and during cardiac chamber formation in particular. Indeed, in loss of function studies, defective PCP signaling results in altered pMRLC localization and abundance at 26 hpf. Here, reduction in Fzd7a and Dvl2 leads to decreased levels of pMRLC, which is likely caused by effects of defective Wnt non-canonical signaling on MRLC phosphorylation through ROCK (Strutt et al., 1997). In contrast, knockdown of Vangl2 or Pk1a results in changes in pMRLC localization. Here, pMRLC relocalizes to cell membranes more rapidly in hearts with reduced levels of *vangl2*, whereas pMRLC nuclear localization is increased in *pk1a* morphant hearts. However, it remains uncertain, if PCP targets pMRLC localization, transport or spatially restricted phosphorylation of MRLC.

Translocation of pMRLC from the nucleus to the cell membrane likely affects tensional homeostasis within the early zebrafish myocardium. Phosphorylation of MRLC was repeatedly shown to affect localized tension (Cai et al., 2006; Lecuit et al., 2011). Nuclear tension was determined through analysis of solidity at 24 hpf and 30 hpf. Here, high nuclear tension corresponds to high abundance of both pMRLC and G-actin in the nucleus at early LHT stage, while reduction in these proteins responds to decreased tension in the nuclear compartment. With initiation of cardiac chamber formation at around 30 hpf, pMRLC localizes to cell junctions. Several studies confirm a role of MRLC during epithelial remodeling through accumulation at central junctions of cell clusters during cell rearrangements (Blankenship et al., 2006; Zallen and Blankenship, 2008).

Actin dynamics within the nucleus were shown before to regulate myogenic SRF target gene expression through changes in MAL/MRTF-A localization (Baarlink et al., 2013; Vartiainen et al., 2007). Crm1-mediated export of MRTF-A is dependent on binding of G-actin to MRTF-

A, and nuclear actin prevents SRF activation (Olson and Nordheim, 2010; Vartiainen et al., 2007). Here, G-actin levels are regulated by F-actin formation in the cytoplasm, for example due to RhoA-induced stress fiber formation (Lundquist et al., 2014; Vartiainen et al., 2007). This underlines the potential significance of G-actin translocation from the nucleus to filamentous structures during early cardiac development. Additionally, MRLC was suggested to act as a core transcription factor that is regulated by control of its phosphorylation status, which in turn coordinates relative motion between DNA bound to myosin II and RNA polymerase II bound to actins and nucleoskeleton (Li and Sarna, 2009). In future studies, the role of MRLC or pMRLC during cardiac gene expression should be explored.

3.3.4 MRLC Phosphorylation is Spatially Regulated by Mylk3

Activity of MRLC is controlled by interaction between ROCK, MLCK, and the myosin phosphatase (MYPT), that regulate its phosphorylation and dephosphorylation status in a complex interaction network. Briefly, ROCK and MLCK directly phosphorylate MRLC, while MYPT reduces MRLC phosphorylation (Loirand, 2006). Expectedly, inhibition of Rock using Y27623 decreases the amount of MRLC phosphorylation in zebrafish hearts. On the other hand, inhibition of Mylk3, the cardiac isoform of MLCK in zebrafish, using morpholino knockdown resulted in restricted localization of pMRLC within the nucleus. This finding suggests a role of this kinase in spatially controlled phosphorylation or in mechanisms controlling its translocation. Spatially restricted phosphorylation by ROCK and MLCK was observed in 3T3 fibroblasts (Totsukawa et al., 2000). Here, Rock was shown to inhibit MYPT and phosphorylate MRLC directly at the center of the cells, while MLCK activity induced phosphorylation of MRLC at the cell periphery. As a result, induction of peripheral pMRLC induced fibroblast migration (Totsukawa et al., 2004). Further studies should address whether Mylk3 targets spatially restricted phosphorylation or pMRLC transport from the nucleus.

MLCK is activated in response to Ca^{2+} release from intracellular stores. In both skeletal and cardiac myocytes binding of Ca^{2+} to Calmodulin induces MLCK to phosphorylate MRLC on serine 19. This in turn increases the contractile strength of actomyosin. Since PCP is known to affect Ca^{2+} release from intracellular stores and actomyosin contractility, its effect on MLCK activity through Calmodulin is likely. Hence, nuclear pMRLC in both *mylk3*- and *pk1a*-deficient hearts further enforces a role of PCP signaling in spatially restricted phosphorylation of MRLC as a downstream effector. Further studies should address whether loss of Pk1 and Mylk3 in fact increases nuclear tension and whether Pk1a acts upstream of Mylk3 activity.

Future studies should aim at understanding the role of Pk1 within the complex network of pMRLC regulation. Phosphorylation of MRLC involves tight regulation of various processes

not only dependent on various kinases, but also on the phosphatase MYPT1 and Ca^{2+} signaling (Riento and Ridley, 2003). For instance, ROCK not only increases MRLC phosphorylation directly, but also indirectly through phosphorylation of MYPT1, which inhibits its phosphatase activity, and results in elevated pMRLC levels (Somlyo and Somlyo, 2004). Interestingly, MYPT1 translocation was implicated in regulation of cardiac differentiation of mouse embryonic stem cells, where MYPT1 was shown to function as a nuclear exporter of Nkx2.5 (Ryan et al., 2013). Loss of function studies targeting MYPT1 should explore potential effects on nuclear translocation of pMRLC and SRF signal transduction to determine whether the phosphatase acts downstream of PCP signaling. Furthermore, Wnt non-canonical signaling is known to act upstream of Calmodulin through its effects on Ca^{2+}. Calmodulin is activated after binding of Ca^{2+}, which leads to increased interaction and activation of several kinases and phosphatases (Kühl et al., 2000; Kühl et al., 2001; Sheldahl et al., 2003; Shimizu et al., 2006).

3.4 PCP Signaling Acts Upstream of SRF Signal Transduction

Wnt non-canonical signaling fulfils many functions during heart development. Among other things, this study shows that it targets actomyosin localization during embryonic cardiac remodeling. In general, PCP-mediated effects on actomyosin are well described; mostly through studies on its role in regulation of Rho signal transduction and Ca^{2+} release from intracellular stores. This study describes a novel role of this pathway that involves regulation of mechanisms within the nuclear compartment that are crucial to myogenic differentiation.

3.4.1 Nuclear-Specific Processes During Cardiac Development Require Pk1 Function

Whereas various functions of the PCP signaling core components Fzd7, Dvl2 and Vangl2 have been described, less is known about the function of Pk1. For instance its involvement in control of the directionality of tissue polarity during Drosophila wing or vertebrate limb growth has been addressed only recently (Sharp and Axelrod, 2016; Yang et al., 2013). In this study, it was revealed that Pk1 localizes to the nuclei of cardiomyocytes of the developing zebrafish myocardium as well as to those of H9c2 cells. The role of Pk1 in the nucleus is not very well understood. Shimojo and Hersh suggested that Pk1 could act as a nuclear receptor which is involved in nuclear trafficking of the transcription repressors REST/NRSF and REST4 (Shimojo and Hersh, 2006). Additionally, it was shown that its nuclear localization is required for facial branchiomotor neuron migration (Mapp et al., 2010). As reduction in Pk1a results in increased nuclear localization of both pMRLC and SRF, Pk1 might play a role

during nuclear transport mechanisms of these factors. Nuclear localization of Pk1 depends not only on its nuclear localization signals (NLS), but also on a farnesylation motif in the C-terminal part of the protein (Mapp et al., 2010). To confirm a nuclear function of Pk1, further studies should assess whether inhibition of Pk1 translocation through deletion of its NLS and farnesylation motifs leads to effects on SRF and pMRLC localization similar to those observed in hearts with complete loss of the protein. In contrast to a potential function of Pk1 as shuttle protein, SRF translocation might be mediated indirectly through changes in nuclear tension after pMRLC export, decrease in nuclear kinase activity or localized actomyosin contractility in the course of myocardial maturation. Future studies should aim at elucidating the role of Pk1 in tensional homeostasis and its effects on SRF translocation.

Apart from spatially regulated effects on tension, kinase activity and actomyosin contractility, Pk1 itself could act either as a transcriptional co-activator of SRF, similar to MRTF-A or it could regulate the SRF co-factor switching. In *pk1a* morphants SRF remains longer within the nucleus, however, its target gene expression is reduced. Previous studies show, that SRF signal transduction is not only controlled by nuclear localization, but also by cofactor association. SRF-DNA complexes are bound by at least two different co-factors – MRTF and TCF (Posern and Treisman, 2006). Strong evidence for regulated SRF cofactor exchange was provided *in vivo*, where smooth muscle differentiation was reduced by platelet-derived growth factor (PDGF) induced ERK signaling. This exchange was initiated by phosphorylated Elk-1 that switched places with Myocardin at SRF target promoters, such as *tgln* (Wang et al., 2004). Elk-1 phosphorylation is regulated by phosphorylated JNK, a known target of PCP signaling (Pellicer, 1998). Thus, Pk1 could facilitate the binding of a distinct co-factor to SRF indirectly via downstream PCP targets. Alternatively, Pk1a itself might act as a cofactor for SRF as it was shown for the LIM-only proteins CRP1 and CRP2, that both associate with SRF and GATA4 and bind to actin structures within the nucleus to control smooth muscle differentiation (Chang et al., 2003). Other LIM-domain containing proteins were shown to act on SRF signal transduction through changes in actin dynamics. Limk1, for instance, is able to activate SRF through its ability to regulate actin treadmilling (Sotiropoulos et al., 1999). However, another member of the LIM protein family, four-and-a-half LIM domain 1 (Fhl1) was shown to be crucial to induce myogenesis in mouse C2C12 myoblasts by binding to TCF/LEF (Lee et al., 2012). Thus, in the context of early cardiogenesis it remains unclear if and how SRF is differentially controlled in regard to MRTF / TCF co-factor binding. For this reason, both proposed roles of Pk1 in modulating SRF signaling should be explored in future investigations.

3.4.2 Changes in Cellular Tension are Coupled to SRF-Mediated Cardiac Maturation

Tight regulation of SRF target gene expression is crucial for proper sarcomere assembly and cardiac contractile function. Whereas SRF function as nuclear regulator has been described since decades, its function within the cytosolic fraction of skeletal myocytes remains elusive (Flück et al., 1999; Rech et al., 1994). Although most components of sarcomeres are known, it remains poorly understood how is the assembly and patterning of sarcomeric protein complexes regulated.

From the studies of avian sarcomere assembly, both smooth (Acta2) and skeletal α-actin (Acta1b) localize to developing sarcomeres. During early development overall expression of smooth muscle actin decreases with regionalized accumulation in inflow and outflow tract regions, while skeletal α-actin expression remains high over the whole ventricle (Ruzicka, 1988; Sugi and Lough, 2005). Thus, both smooth muscle and skeletal α-actins are involved in sarcomere assembly with a specific role of smooth muscle actin during early sarcomerogenesis. Interestingly, expression levels of actin isoforms in zebrafish cardiomyocytes during early cardiogenesis seem to variate from those observed in mouse cardiomyocytes. Here, *acta2* is expressed in high amounts right after differentiation into cardiomyocytes at E9.5 and drops at E17, while expression of *acta1b* increases at E13 and is reduced only after 2 weeks. All this time, *actc1b* mRNA remains at a high expression level (Clement et al., 2007).

Sarcomere assembly leads to increased tension within the myocardium; a process that might be inducing SRF translocation from the nucleus. During cardiac development several mechanical forces are exerted on the tissue. Firstly, blood flow generates frictional force on the surface of the myocardium. This process was shown to be essential during cell fate specification of cardiomyocytes (Huang et al., 2010). Secondly, stretching of cardiac chambers activates transcription factors such as GATA4 (Hautala et al., 2002; Hautala et al., 2001). Effects of PCP-mediated changes in tensional homeostasis on SRF target gene expression should be investigated further to elucidate the importance of force during cardiac tissue morphogenesis in more depth.

In zebrafish hearts, SRF is highly abundant in the nucleus at LHT stage and translocates to sarcomeric structures between 52 and 58 hpf. This correlates with the onset of increased *acta2* expression and decreased *acta1b* expression. Reduction in *pk1a* results in decreased levels of both *acta1b* and *acta2.* In contrast, loss of Vangl2 leads to decreased levels of *acta1b*, but induces *acta2* expression. In both *vangl2*-and *pk1a*-deficient hearts no change in expression of two other SRF target genes, *actc1b* and *tgln*, was observed. Formation of a

complex between Pk1 and Vangl2 is crucial to functional Wnt signaling (Jenny, 2003). It is possible, that loss of Vangl2 releases now unbound Pk1a that in turn is capable to prolong SRF-mediated *acta2*-expression. To verify this, knockdown of both *pk1a* and *vangl2* using subthreshold levels of morpholino should be performed to investigate their potential interaction. Taken together, these data suggest that tightly regulated *acta2*-expression seems to be pivotal to cardiac maturation. During avian cardiogenesis Acta2 was reported to be spatially restricted to OFT regions early after cardiac chamber formation (Ruzicka, 1988; Sugi and Lough, 2005). In line with these reports, OFT defects observed in PCP-deficient zebrafish hearts could correspond to changes in *acta2* expression levels. Additionally, *acta1b* and *actc1b* share significant sequence homology that allows either one of them to at least partially rescue loss-of-function of the other (Kumar et al., 1997; Nowak et al., 2009).

Earlier studies showed that cardiomyocyte differentiation is dependent on Dkk/Wnt11 activity (Tzahor, 2007). Loss of Vangl2, Pk1a and Fzd7 results in disturbed sarcomere formation that was visualized by staining for cardiac MHC. Thus, functional PCP signaling is pivotal for cardiomyocyte differentiation and cardiac maturation. In particular, SRF-mediated cardiac maturation is likely dependent on downstream effectors of PCP-signaling. In 2007, Seguchi et al. reported that sarcomere assembly in the zebrafish heart is regulated by a cardiac specific myosin light chain kinase (cMLCK). In this context, decreased phosphorylation of MRLC inhibited epinephrine-induced activation of sarcomere reassembly (Seguchi et al., 2007). Since Mylk3 reduction leads to increased SRF abundance in nuclei of hearts at 54 hpf, a potential role of this kinase during cardiac maturation should be investigated in further studies. Thus, the mechanisms underlying PCP-mediated cardiac maturation remain to be elucidated.

3.5 Conclusion and Outlook

This study provides evidence that early cardiac remodeling and maturation of the zebrafish myocardium is mediated heavily by activation of the non-canonical Wnt/PCP pathway through Wnt11/Fzd7a. Specifically, PCP signaling guides cardiac chamber formation through effects on cell rearrangements mediated mainly through Fzd7a and Wnt11/Wnt5b. Cardiac remodeling through Wnt non-canonical signaling ensures formation of proper myocardial tissue architecture of the ventricular chamber and looping of the heart. Additionally, cardiac shape is established by control of SHF contribution through Fzd7a. On a cellular level, PCP affects cardiomyocyte shape through effects on actomyosin. A novel function of Wnt non-canonical signaling was identified for pMRLC localization during early phases of cardiac chamber formation. Notably, both Vangl2 and Pk1a take roles in translocation of pMRLC

from the nucleus to cell junctions at LHT stage. Translocation of pMRLC and G-actin from nucleus to cell junctions is accompanied by changes in nuclear tension and LMNA localization. SRF signal transduction, a process responsive to changes in tensional homeostasis, is affected in hearts with deficient PCP signaling (Figure 36). The presented findings reveal a novel function of the PCP-specific core components Vangl2 and Pk1a in modulation of SRF-mediated myogenic gene expression. Dysregulation of PCP signaling results in defective cardiac maturation and sarcomerogenesis. Collectively, these data support the concept that the Wnt non-canonical pathway couples changes in actomyosin tension with myocyte differentiation during cardiac chamber formation through effects on SRF signaling.

Interaction of PCP core components has been described extensively. Thus, future studies should aim at understanding the distinct roles of PCP core components of this complex network during cardiogenesis. For instance, Prickle and Vangl2 have been shown to interact both biochemically and genetically (Jenny, 2003). Decreased levels of *pk1* result in reduction in *wnt5b* and *vangl2* (Yang et al., 2013). Myosin II is involved of feedback regulation of Vangl2 polarity (Ossipova et al., 2015). Further investigation should explore possible feedback loops between Vangl2, Pk1 and MRLC which control myocardial differentiation. Double knockdown experiments could aim at understanding whether one of these proteins acts upstream of the other. Wnt non-canonical signaling not only affects cytoskeletal structures, but also Ca^{2+} dependent signal transduction. Effects on SRF signaling through the Ca^{2+}/calmodulin-dependent kinase (CaMK) have been reported previously and should be explored as potential target of Wnt non-canonical signaling (McKinsey, 2007).

Further studies should aim at a broader understanding of the function of forces in the context of transcriptional regulation during organ development. To this end, tension sensors can be utilized to visualize mechanical forces that act on specific molecules involved in force transduction and also transcriptional regulation (Grashoff et al., 2010). Lastly, apart from proteins of the contractile apparatus, SRF also targets non-contractile proteins involved in cardiac function such as the sarcoplasmic reticulum Ca^{2+}-ATPase (SERCA) and the Na^{+}/Ca^{2+} exchanger Ncx1 (Argentin et al., 1994; Cheng et al., 1999). Previous data show changes in velocity of action potential propagation in *vangl2* mutants and *pk1a* morphant zebrafish hearts (Panáková et al., 2010). Thus, it will be interesting to explore the role of SRF during the formation of proper electrical coupling across the developing ventricular myocardium.

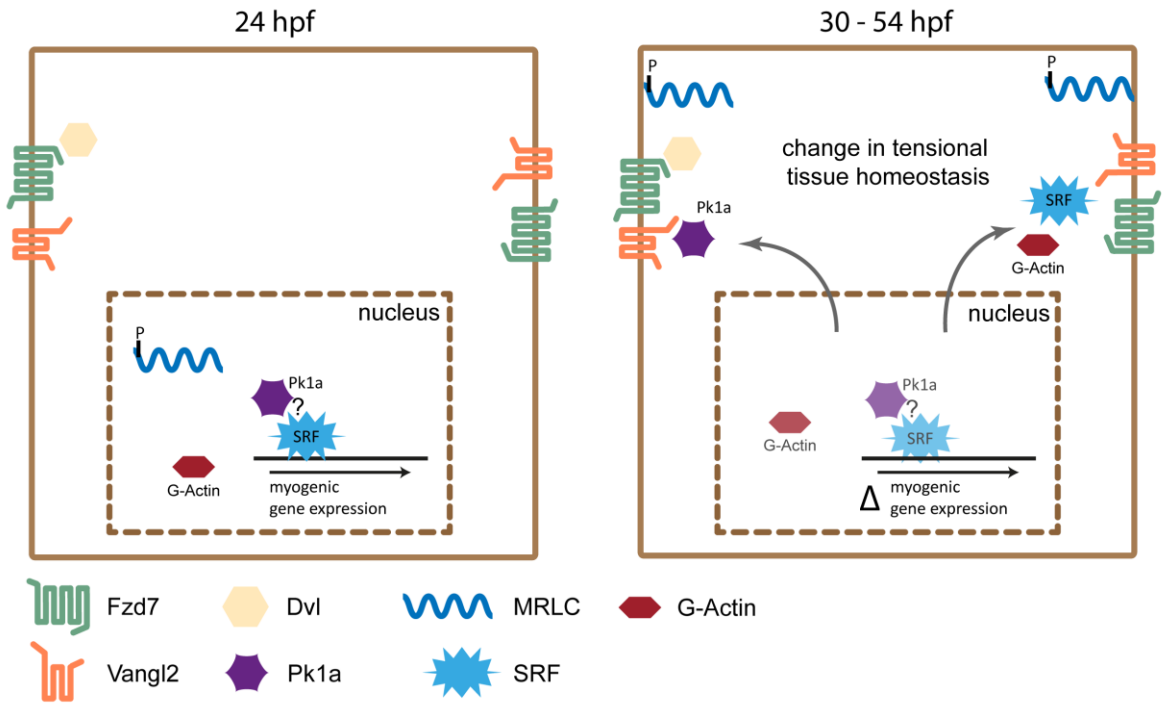

Figure 36: Model of SRF signal transduction regulated by PCP signaling. At LHT stage (24 hpf) nuclear tension is high due to accumulation of proteins of the contractile machinery such as pMRLC and G-actin. At the same time Pk1a and SRF are highly abundant in the nucleus. With onset of cardiac chamber formation (30 hpf) pMRLC localizes to central junctions of cell clusters to facilitate cell rearrangements. This process requires tight regulation of PCP signal transduction. During cardiac chamber formation, tensional tissue homeostasis is altered due to changes in actomyosin localization resulting in partial SRF translocation and modified myogenic gene expression. Simultaneously, Pk1 translocates to cell membranes which presumably effects cardiac target gene expression.

4 Materials and Methods

4.1 Materials

4.1.1 Equipment and Software

Table 1: Overview of Equipment.

Equipment	Purpose	Manufacturer
FACSAria™ I Flow Cytometer	FACS Sorting	BD Biosciences
FemtoJet	Microinjection	Eppendorf
M165	Fluorescent Microscopy	Leica
MD G33	Brightfield Microscopy	Leica
SP5	Confocal Microscopy	Leica
SP8	Confocal Microscopy	Leica
ViiA™ 7	Quantitative Real-Time PCR	Life Technologies

Table 2: Overview of Software.

Equipment	Purpose	Vendor / URL
A Plasmid Editor (APE)	Plasmid Editor	http://biologylabs.utah.edu/jorgensen/wayned/ape/
Adobe Illustrator	Illustration of Data	Adobe Systems, Inc. (San Jose, US)
Adobe Photoshop	Image Processing	Adobe Systems, Inc. (San Jose, US)
ClustalW2	Sequence Alignment	www.ebi.ac.uk/Tools/msa/clustalw2/
GraphPad Prism 5	Statistical Analysis	GraphPad Software, Inc. (La Jolla, US)
ImageJ	Image Processing	http://imagej.nih.gov/ij/
MATLAB	Cell Orientation	http://de.mathworks.com/products/matlab/
Packing Analyzer	Image Analysis	https://idisk-srv1.mpi-cbg.de/~eaton/

Papers 3	Reference Manager	http://www.papersapp.com/mac/
Past	Rose Plots	http://folk.uio.no/ohammer/past/

4.1.2 Kits

Table 3: List of kits.

Kits	Purpose	Manufacturer
GeneJET Gel Extraction Kit	PCR Purification	Thermo Scientific
mMESSAGE mMACHINE ® T7 Kit	RNA Transcription	Ambion
pGEM®-T Easy Vector System	Subcloning	Promega
RNeasy Mini Kit	RNA Extraction	Qiagen

4.1.3 Chemicals and Reagents

Unless otherwise stated chemicals, enzymes, markers, and oligonucleotides were purchased from Ambion, Applied Biosystems, Biorad, Biozym, Calbiochem, Life Technologies, New England Biolabs, Qiagen, Promega, Roche, Roth, R&D Systems, Sigma-Aldrich, Stratagene, Thermo-Scientific, and VWR.

4.1.4 Buffers and Solutions

Buffers and solutions listed in Table 4 are indicated in bold in the following Chapters.

Table 4: Overview of buffers and solutions.

Name	Composition
Blocking Buffer	PBS; 5% Normal Goat Serum; 1% DMSO; 0.1% Tween-20; 2 mg/mL BSA
Tyrode's Solution	136 mM NaCl; 5.4 mM KCl; 1 mM $MgCl_2$; 1.8 mM $CaCl_2$; 10 mM HEPES; 5 mM D(+) Glucose; 0.3 mM Na_2HPO_4; pH 7.4
Danieau's Buffer	17.4 mM NaCl; 0.21 mM KCl; 0.12 mM $MgSO_4$; 0.18 mM $Ca(NO_3)$; 1.5 mM HEPES; pH 7.6

E3 Medium	5mM NaCl; 0.17 mM KCl; 0.33mM CaCl; 0.33mM $MgSO_4$; pH 7.4
PEM	0.1 M PIPES (pH 6.95); 2 mM EGTA; 1 mM $MgSO_4$

4.1.5 Oligonucleotides

Oligonucleotides were purchased from BioTeZ Berlin Buch GmbH (Berlin, DE). They were synthesized in 10 nmol scale, dissolved in destilled water and stored as 100 mM stock and 10 µM solutions at -20°C.

4.1.5.1 Genotyping

Table 5: List of oligos used for genotyping of mutants and CRISPants.

Gene	Oligo	Sequence	Size
Fz7a	fw rv	CAAACCCGACGCCCTAC ATGAGGTACCGATGAAGAGG	765 bp
Pk1a	fw rv	GGCAGCGCTGAGCATCATAG GCGAATGTTGTCTGTTTTGGAGC	462 bp

4.1.5.2 sgRNA Synthesis

Table 6: Overview of oligos for sgRNA synthesis.

Target-Gene	Sequence
Pk1a	GAAATTAATACGACTCACTATA GGAGCTGGAGAATCACGGTG GTTTTAGAGCTAGAAATAGC
sgRNA rv	AAAAGCACCGACTCGGTGCCACTTTTTCAAGTTGATAACGGACTAGC CTTATTTTAACTT GCTATTTCTAGCTCTAAAAC

4.1.5.3 Morpholino Oligonucleotides

Table 7: Morpholino antisense oligonucleotides from GeneTools.

Morpholino	$[c]_E$	Target	Sequence 5'-3'
MO1-dvl2	3.5 ng	ATG of *dvl2*	TAAATTATCTTGGTCTCCGCCATGT
MO1-fzd7a	1.5 ng	5'UTR of *fz7a*	ATAAACCAACAAAAACCTCCTCGTC
MO1-mylk3	3.5 ng	ATG of *mylk3*	TACAGCGAGGTCCCCATCATGCCCT
MO1-pk1a	1.5 ng	ATG of *pk1a*	GCCCACCGTGATTCTCCAGCTCCAT
MO1-tnnt2	1 ng	ATG of *tnnt2*	CATGTTTGCTCTGATCTGACACGCA
MO1-vangl2	2 ng	ATG of *vangl2*	GTACTGCGACTCGTTATCCATGTC
MO2-wnt11	1.5 ng; 0.7 ng	ATG of *wnt11*	GTTCCTGTATTCTGTCATGTCGCTC
MO2-wnt5b	1.5 ng; 0.7 ng	exon 6 splice acceptor of wnt5b	TGTTTATTTCCTCACCATTCTTCCG

4.1.6 Vectors

4.1.6.1 Gateway Cloning

Table 8: Overview of vectors utilized for generation of expression constructs.

Gateway Cloning Vectors	Description
pDONR221	backbone for middle entry vector
pDEST crystalline-YFP	backbone for destination vector with YFP marker gene expression in the eye
myl7 p5'E	myocardial promoter
polyA p3'E	polyA tailing

4.1.6.2 Vectors

Table 9: List of expression constructs.

Expression Construct	Description
***myl7:*lck-eGFP**	myocardial expression of membrane tethered eGFP
***myl7:*lifeact-RFP**	myocardial expression of actin-binding RFP

4.1.7 Antibodies

4.1.7.1 Primary Antibodies

Table 10: Overview of applied primary antibodies.

Primary Antibody	Dilution / Quantity	Origin	Supplier	Order No.
Alcam a	1:25	Mouse	DSHB	zn-8
DNaseI (Alexa Fluor® 488 Conjugate)	1:100		Life Technologies	D-12371
GFP	1:200	Rabbit	Sigma-Aldrich	G1544
GFP	1:200	Rabbit	Abcam	ab290
MHC	1:50	Mouse	DSHB	MF-20
Myl12/9	1:100	Rabbit	Abcam	ab64161
N-Cadherin	1:50	Mouse	BD Biosciences	610920
phospho-Myl9 (phospho S20)	1:100	Rabbit	Abcam	ab2480
Pk1a	1:100	Rabbit	Abcam	Ab15577
SRFa	1:100	Rabbit	Abcam	ab101246

4.1.7.2 Secondary Antibodies

Table 11: List of applied secondary antibodies.

Secondary Antibody	Dilution / Quantity	Origin	Supplier	Order No.
Anti-mouse IgG Alexa Fluor® 488 Conjugate	1:500	Donkey	Life Technologies	A-21202
Anti-mouse IgG Alexa Fluor® 555 Conjugate	1:500	Goat	Life Technologies	A-21422
Anti-mouse IgG Alexa Fluor® 633 Conjugate	1:500	Goat	Life Technologies	A-21050
Anti-rabbit IgG Alexa Fluor® 488 Conjugate	1:500	Donkey	Life Technologies	A-21206
Anti-rabbit IgG Alexa Fluor® 555 Conjugate	1:500	Goat	Life Technologies	A-21428
Anti-rabbit IgG Alexa Fluor® 647 Conjugate	1:500	Goat	Life Technologies	A-21246
Zenon® IgG Alexa Fluor® 488 Conjugate			Life Technologies	Z-25302
Zenon® IgG Alexa Fluor® 555 Conjugate			Life Technologies	Z-25305

4.1.8 TaqMan Probes for qPCR

Table 12: List of TaqMan probes for qRT-PCR.

Gene	Order No.	Amplicon Length	Exon Boundary
acta1b	Dr03440340_m1	62 nt	1 - 2
acta2	Dr03088509_mH	68 nt	6 - 7
actc1b	Dr03451294_s1	151 nt	8 - 8
eef1α	Dr03432748_m1	106 nt	1 - 2
etv4	Dr03138282_m1	76 nt	1 - 2

fgf4	Dr03080033_m1	78 nt	1 - 2
myl7	Dr03105697_m1	75 nt	2 - 3
pk1a	Dr03112723_m1	97 nt	3 - 4
pk1b	Dr03141824_m1	68 nt	2 - 3
srfb	Dr03106979_m1	82 nt	-
tagln2	Dr03151758_m1	102 nt	3 - 4

4.1.9 Eukaryotic Cells

Table 13: H9c2 cell line information.

Cell Line	Description	Culture Medium	Vendor	Article Number
H9c2	Rat Cardiac Myoblast Cell Line	DMEM + 2mM Glutamine + 10% Fetal Bovine Serum (FBS)	ATCC	ATCC® CRL-1446™

4.1.10 siRNA

Table 14: Information on fzd7a siRNA.

Target	Manufacturer	Order No.	Target Sequences
fzd7a	DharmaFECT	ON-TARGETplus SMARTpool LOC100360552 L-115723-00-0005	GCUAAGACUUGCAGGACGA; GCCCAAAUGAAAAGGCGAA; GCGAGAACUUCCCGGUGCA; GCUAGAGUCCUAACGCAGA

4.1.11 Transgenic Zebrafish Lines

Table 15: Transgenic Zebrafish Lines

Transgenic Zebrafish Line	Function
Tg(*myl7*:eGFP)	Myocardial marker (cytosolic GFP)
Tg(*drl*:eGFP)	FHF marker
Tg(*myl7*:lck-eGFP)*	Myocardial expression of membraneous GFP

fzd7a^{e3}	Non-Sense Mutation in Fzd7a
vangl2^{m209}	Non-Sense Mutation in Vangl2
slb	Non-Sense Mutation in Wnt11
ppt	Non-Sense Mutation in Wnt5b

*provided by Alexander Meyer, MDC Berlin (previously unpublished)

4.2 Methods

4.2.1 Zebrafish Methods

4.2.1.1 Zebrafish husbandry

Zebrafish were bred, raised and maintained at 28°C following standard procedures according to the German Animal Welfare Act (Nüsslein-Volhard et al., 2003). Zebrafish strains AB, TüLF, wik, and TU were used for analysis of wild type phenotypes and for injection of constructs and CRISPR sgRNA / Cas9 protein. Embryos were kept in **E3 medium** (Table 4) with or without 1% methylene blue. At around 24 hpf embryos were treated with 0.003% PTU to prevent pigmentation if required (Burrill and Easter, 1994). Staging was performed as described previously by hours post fertilization (hpf) or by counting somites (Kimmel et al., 2005). The experiments were declared and approved by the Landesamt für Gesundheit und Soziales.

4.2.1.2 Expression Vector Generation

Expression vectors were generated using the Gateway® cloning system (Invitrogen). In brief, genes of interest were amplified from genomic DNA or commercially available expression vectors (addgene) using specific oligonucleotides that add attB sites to the 5' and 3' ends of the sequence. The resulting product was inserted via recombination into a donor vector (pDONR221) containing the corresponding attP sites in the Gateway-specific BP reaction using BP clonase. In a subsequent LR reaction the DONR plasmid containing the gene of interest flanked by attL sites is recombined into a destination vector (pDEST) comprising the homologous attR sites. Furthermore, recombination into pDEST requires addition of a 5' entry vector containing the desired promoter sequence and a 3' entry vector containing a polyA sequence. Additionally, both 5' entry and 3' entry vectors can carry sequences for addition of N- or C-terminal tags. A detailed description of the Gateway® cloning system can be found in the manufacturer's instructions. Vectors used for generation of expression constructs are listed in Table 8. Expression vectors used in this study are listed in Table 9.

4.2.1.3 Microinjections and Morpholino Mediated Gene Knockdown

Genetic manipulations were performed by injection of in-vitro transcribed mRNA, expression constructs, antisense morpholino oligonucleotides or sgRNA-Cas9 protein complexes (CRISPR-Cas9 mutagenesis) into Zebrafish embryos at one-cell stage. Morpholino antisense oligonucleotides block translation by complementary binding to mRNA. Fertilized eggs were mounted on 1.5% agarose moulds and injected either into the yolk (morpholino

knockdown) or directly into the cell (mRNA, expression constructs, sgRNA-Cas9 complexes) using a FemtoJet® microinjector (Eppendorf). 10 pg of expression constructs were injected with 25 pg of Transposase mRNA for promoter driven transient expression of specific genes. Morpholino oligonucleotides and expression constructs were diluted in **Danieau buffer** (Table 4). Morpholino end concentrations are indicated in Table 7. CRISPR-Cas9 Mutagenesis is described in detail in the following paragraph.

4.2.1.4 CRISPR-Cas9 Mutagenesis

Targeted mutagenesis using the CRISPR-Cas9 system was performed in collaboration with the group of C. Mosimann (University of Zurich, Switzerland). Transient somatic and germline mutations were achieved by injection of sgRNA-Cas9 protein mix into cytoplasm of one-cell stage zebrafish embryos. Synthesis of sgRNA was performed by PCR amplification and subsequent in-vitro transcription. A unique oligonucleotide contained the T7 polymerase binding site, the sgRNA target sequence, and part of the hairpin structure important for Cas9 binding, while a common oligonucleotide comprised the remaining sequence to generate the hairpin structure. The unique and common oligonucleotides were designed to overlap and allow to perform the subsequent PCR for the sgRNA synthesis without a template. PCR was performed using Phusion polymerase in HF buffer in 100 µL reaction volumes (oligos for amplification: Table 6). Amplification was performed on an Eppendorf Mastercycler ep Gradient S with the following program: 98°C – 30 s; 40 cycles of 98°C – 10 s, 60°C – 30 s, 72°C – 15 s; 72°C 10 min; 10°C infinite. Purification of PCR products was performed using a PCR purification kit. In-vitro transcription was performed using the Ambion MEGAscript T7 Kit with 300 ng purified DNA template over night at 37°C. sgRNA was purified using the Qiagen RNeasy Mini Kit, diluted to 600 ng / µL and stored in aliquots at -80°C.
Cas9 protein was expressed from the plasmid pET-28b-Cas9-His (Addgene plasmid #47327; (Gagnon et al., 2014) by Anja Schütz from the Helmholtz Protein Sample Production Facility at MDC. The injection mix was adjusted for optimal KCl concentration and sgRNA / Cas9 protein ratio using the "CrispantCal: CRISPR/Cas9 Injection Mix Calculator" (https://lmwebr.shinyapps.io/CRISPR_Cas9_mix_calc/). Single embryos showing mild or severe phenotypes were selected and analyzed to determine mutagenesis efficiency (oligos for genotyping: Table 5).

4.2.1.5 Isolation of Genomic DNA from Zebrafish Fins and Single Embryos

Adult fish and 24 hpf to 72 hpf old embryos were anaesthetized in 0.016% Tricaine in E3 medium before taking fin samples and collecting single embryos. The tissue was lysed in 50 µL of 50 mM NaOH solution by boiling for 20 min at 95°C. The reaction was stopped by adding 5 µL of 1M Tris buffer (pH 8.0). Samples were used for PCR amplification and stored at 4°C.

4.2.1.6 Analysis of Efficiency of Transient CRISPR/Cas9 Mutagenesis

Genomic DNA from wild type and zebrafish showing mild or severe phenotypes was isolated as described in Chapter 4.2.6. A region of approx. 500 bp spanning the CRISPR / Cas9 target sequence was amplified with specific oligonucleotides (Table 6) using Taq polymerase in 25 µL reaction volumes on an Eppendorf Mastercycler ep Gradient S with the following program: 98°C – 30 s; 35 cycles of 98°C – 10 s, 60°C – 30 s, 72°C – 15 s; 72°C 10 min; 10°C infinite. Fragments were cloned into the pGEM T-easy vector, transformed into the *E. coli* strain DH5α and spread on ampicillin containing plates (100 µg/mL). Single colonies were dissolved into LB medium and 1 µL was used for colony PCR using Taq polymerase in 25 µL. Amplification was performed with T7 fw and SP6 oligonucleotides on a Eppendorf Mastercycler ep Gradient S using the above mentioned program. Products were diluted 1:3 and sent for sequencing (Source BioScience, Berlin) (oligos for genotyping: Table 5). Bioinformatic analysis to determine frequency and length of insertions and deletions was performed by Helen Lindsay (University of Zurich, Switzerland).

4.2.1.7 Genotyping of Mutant Strains

Genomic DNA was extracted from Zebrafish fins as described in Chapter 4.2.6. The PCR reaction contained 1-2 µL gDNA, 2.5 µL 10x DreamTaq Buffer, 0.5 µL dNTPs (10 mM each), 0.25 µL fw-Primer (50 µM), 0.25 µL rv-Primer (50 µM), 2 µL $MgCl_2$, and 0.2 µL DreamTaq Polymerase (Thermo Scientific) in a volume of 25 µL. Amplification was performed on an Eppendorf Mastercycler ep Gradient S with the following program: 98°C – 30 s; 40 cycles of 98°C – 10 s, 60°C – 30 s, 72°C – 15 s; 72°C 10 min; 10°C infinite. PCR products were analyzed on an 1.5% agarose gel and diluted 1:3 and sent for sequencing (Source BioScience, Berlin).

4.2.1.8 Fluorescent-Activated Cell Sorting

Embryos were treated with 0.25% Trypsin until homogenous cell suspension was achieved. Cell suspension was put through cell strainer (70 µm Nylon) and centrifuged by 200g for 20 min at 4°C. Supernatant was removed until 1ml and 100 µl 100% FCS added to stop trypsinization. Cell pellet was resuspended and centrifuged at 200g for 10 min at 4°C. Supernatant was removed and pellet washed with 2% FCS. After centrifugation at 200g for 10 min at 4°C, pellet was resuspended in 100 – 100 µl 1x PBS. FACS sorting was performed after final filtration of cell suspension.

4.2.1.9 RNA Isolation, cDNA Synthesis and Quantitative PCR (qRT-PCR)

Total RNA was isolated from 24 hpf, 54 hpf, 72 hpf or 120 hpf old embryos using TRIzol® reagent (Life Technologies). The tissue was homogenized using 23- and 27-gauge needles and RNA was precipitated with Chloroform/Isopropanol and GlycoBlue™ (Life Technologies). On-column DNaseI treatment, clean-up and concentration of RNA were performed according to RNeasy MicroKit (Qiagen). Reverse transcription was done using First-Strand cDNA Synthesis Kit (Thermo Scientific). For reverse transcription of mRNA into cDNA a mix of random hexamers and oligo dT primers (1:1), Reaction Buffer (5x), Ribolock RNase inhibitor (20 u/µl), dNTP Mix (10 mM) and M-MuLV Reverse Transcriptase (20 u/µl) was added to 200 – 2000 ng of RNA. The reverse transcription reaction was incubated for 5 min at 25°C followed by 60 minutes at 37°C on an Eppendorf Mastercycler ep Gradient S. Quantitative RT-PCR was performed on 50 – 75 ng cDNA using FAM™ dye-labeled TaqMan® MGB probes (Table 12) and Gene Expression Master Mix (Applied Biosystems) on a ViiA7 PCR system. The following conditions were used: annealing at 50°C for 2 min; denaturation at 95°C for 10 min; denaturation at 95°C for 15 s; amplification at 60°C for 1 min. Data were analyzed using ViiA™ 7 RUO software (Life Technologies). Fold induction was determined using ΔΔCt calculation. The data were normalized to the internal housekeeping gene eef1a1l labeled with VIC™ dye. Fold induction was determined using ΔΔCt calculation.

4.2.1.10 *In Vivo* Imaging

Embryos were anaesthetized with 0.016% Tricaine and embedded in a ventral position in 1% low melting agarose for immobilization in glass bottom dishes. *In vivo* imaging was performed using a Leica SP8 microscope with a 20 x (NA=0.8) water immersion objective. During acquisition embedded zebrafish were kept in a chamber with 28°C and covered with E3 medium containing 0.016% Tricaine.

4.2.1.11 Immunofluorescence Stainings

Hearts were dissected in **Tyrode's solution** (Table 4) with 20 mg/mL BSA and subsequently fixed in 4% FA in **PEM** (Table 4) or Glyo-Fixx™ for 20 min (Thermo Scientific). Subsequently, hearts were washed and stored up to one week in PBST (0.1% Tween-20). For ROCK-inhibition dissected hearts were treated for 1 h with 200 µM Y-27632. Treated and untreated hearts were incubated in **blocking solution** (Table 4) for 1 h. Hearts were incubated with primary antibodies (Table 10) diluted in blocking buffer over night at 4°C. After three washing steps in blocking buffer á 30 min hearts were incubated with Alexa-conjugated secondary antibodies (Table 11) diluted in blocking buffer for 2 h at RT. Finally, hearts were washed over night in PBS and 0.1% Tween-20 before mounting in ProLong Antifade with DAPI (Life Technologies).

4.2.1.12 Confocal Microscopy

Immunostainings of fixed hearts were analyzed using the Leica SP5 or SP8 confocal laser scanning microscope with 63x (NA=1.4) oil or 63x (NA=1.3) glycerol objective. Images were analyzed using ImageJ (NIH), Fiji (http://fiji.sc/Fiji) and Packing Analyzer (Aigouy et al., 2010). Statistical analysis was performed using Prism (GraphPad) (Table 1 & 2).

4.2.2 Cell Culture Methods

4.2.2.1 Culturing of H9C2 Rat Myoblast Cell Line

H9c2 cells were grown in DMEM medium (Gibco) and subcultured twice a week. Cells that reached 70% confluency were washed in ice-cold PBS and incubated with 1x Trypsin-EDTA for 2-10 min at 37°C. Trypsinization was stopped after detachment of cells with FBS containing DMEM. A defined volume of cell suspension was transferred into a new cell culture flask with fresh DMEM. Cell counting was performed with a ScepterTM 2.0 pipette with 60 µM tips. Only cells of 9-21 µM size were counted.

4.2.2.2 Immunofluorescence Microscopy of H9c2

Cells were plated and cultured on sterile coverglasses in 24-well plates and fixed at approx. 70% confluency in 4% PFA / 4% Sucrose in PBS for 20 min. Two washing steps with PBS were performed after every subsequent treatment if not stated otherwise. PFA-reaction was quenched with 50 mM Ammoniumchloride for 10 min. Subsequently, cells were permeabilized with 0.2% Triton for 5 min and washed with 0.2% Gelatine for 5 min. Unspecific sites were blocked with 1% Gelatine for 1 h. Cells were incubated with primary antibodies

(Table 10) diluted in 1% Gelatine for 1 h in a wet chamber. Cells were washed twice in 1% Gelatine before treatment with secondary antibody in 1% Gelatine for 30-45 min (Table 11). Nuclei were stained with 5µM Hoechst in PBS for 10 min. Final fixation was performed with 4% PFA / 4% Sucrose in PBS for 5 min and subsequent treatment with NH_4Cl for 5 min. Final washing was performed with 1% Gelatine, 0.2% Gelatine and PBS for 5 min each. Coverslides were mounted on 4 µL of ProLong Antifade with DAPI (Life Technologies) and stored at 4°C.

4.2.2.3 siRNA Transfection of H9c2

H9c2 cells (Table 13) were seeded onto a 24-well plate, pre-coated with poly-D-Lysine, at $3x10^4$ cells per well and cultured for 24 hours. The transfection has been achieved using DharmaFECT TM siRNA Transfection Reagent (GE Healthcare Dharmacon) according to manufacturer's instructions. Briefly, 100 nM ON-TARGETplus SMARTpool Fzd7a siRNA (GE Healthcare Dharmacon) was added to serum-free DMEM and then mixed with DharmaFECT™ (1 µl per well) (Table 14). After incubation over 30 min at RT the DharmaFECT™ / siRNA mixture was added to the cells. 24 hours after transfection, cells were harvested.

4.2.3 Statistics

Statistical analysis was performed using GraphPad Prism5 (Table 2). Unpaired t-test or one-way ANOVA with Bonferonni Multiple Comparison were applied. Significant differences are indicated as $P \leq 0.05$ = *, $P \leq 0.01$ = **, $P \leq 0.001$ = ***. For transitory states boxplots with minimum to maximum value whiskers and median are plotted. Otherwise, data are plotted as mean plus standard error of mean (SEM). Rayleigh's R values were determined using Past software (Table 2).

5 Supplement

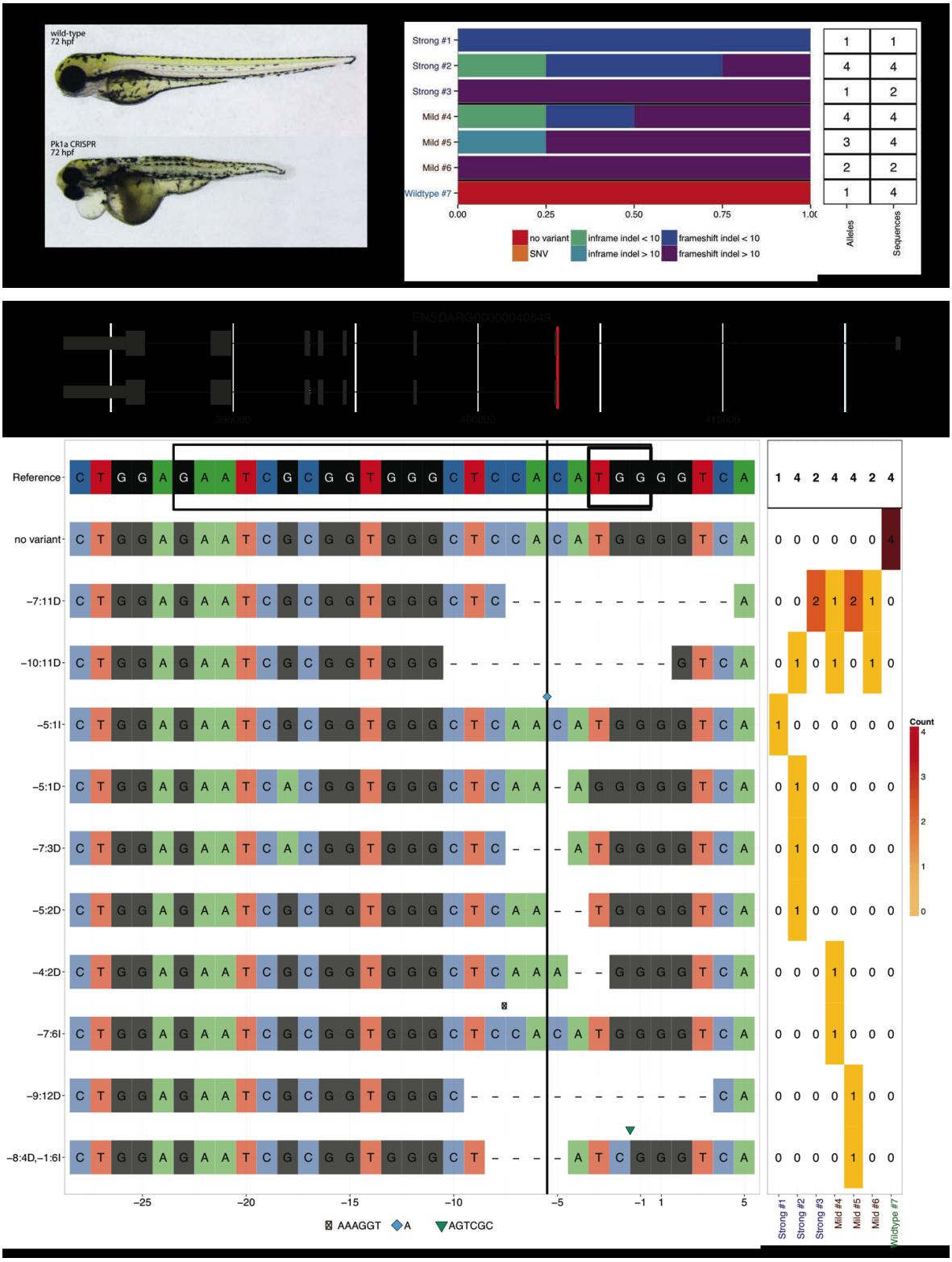

Figure 37: CRISPR-mediated mutagenesis of the pk1a locus with information on phenotype and indel frequency (Lindsay et al., 2016).

6 References

Aberle, H., Bauer, A., Stappert, J., Kispert, A. and Kemler, R. (1997). β-catenin is a target for the ubiquitin–proteasome pathway. *EMBO J* **16**, 3797–3804.

Adler, P. N., Krasnow, R. E. and Liu, J. (1997). Tissue polarity points from cells that have higher Frizzled levels towards cells that have lower Frizzled levels. *Current Biology* **7**, 940–949.

Afouda, B. A., Martin, J., Liu, F., Ciau-Uitz, A., Patient, R. and Hoppler, S. (2008). GATA transcription factors integrate Wnt signalling during heart development. *Development* **135**, 3185–3190.

Ahearn, I. M., Haigis, K., Bar-Sagi, D. and Philips, M. R. (2011). Regulating the regulator: post-translational modification of RAS. *Nature Reviews Molecular Cell Biology* **13**, 39–51.

Ahmad, N. (2004). A Southpaw Joins the Roster: The Role of the Zebrafish nodal-related Gene Southpaw in Cardiac LR Asymmetry. *Trends in Cardiovascular Medicine* **14**, 43–49.

Ai, D., Fu, X., Wang, J., Lu, M. F., Chen, L., Baldini, A., Klein, W. H. and Martin, J. F. (2007). Canonical Wnt signaling functions in second heart field to promote right ventricular growth. *Proceedings of the National Academy of Sciences* **104**, 9319–9324.

Aigouy, B., Farhadifar, R., Staple, D. B., Sagner, A., Röper, J.-C., Jülicher, F. and Eaton, S. (2010). Cell Flow Reorients the Axis of Planar Polarity in the Wing Epithelium of Drosophila. *Cell* **142**, 773–786.

Aisagbonhi, O., Rai, M., Ryzhov, S., Atria, N., Feoktistov, I. and Hatzopoulos, A. K. (2011). Experimental myocardial infarction triggers canonical Wnt signaling and endothelial-to-mesenchymal transition. *Disease Models & Mechanisms* **4**, 469–483.

Alsan, B. H. and Schultheiss, T. M. (2002). Regulation of avian cardiogenesis by Fgf8 signaling. *Development* **129**, 1935–1943.

Aoki, H., Sadoshima, J. and Izumo, S. (2000). Myosin light chain kinase mediates sarcomere organization during cardiac hypertrophy in vitro. *Nature medicine* **6**, 183–188.

Argentin, S., Ardati, A., Tremblay, S., Lihrmann, I., Robitaille, L., Drouin, J. and Nemer, M. (1994). Developmental stage-specific regulation of atrial natriuretic factor gene transcription in cardiac cells. *Molecular and Cellular Biology* **14**, 777–790.

Arsenian, S., Weinhold, B., Oelgeschläger, M., Rüther, U. and Nordheim, A. (1998). Serum response factor is essential for mesoderm formation during mouse embryogenesis. *EMBO J* **17**, 6289–6299.

Asem, M., Buechler, S., Wates, R., Miller, D. and Stack, M. (2016). Wnt5a Signaling in Cancer. *Cancers* **8**, 79.

Ateshian, G. A. and Humphrey, J. D. (2012). Continuum Mixture Models of Biological Growth and Remodeling: Past Successes and Future Opportunities. *Annu. Rev. Biomed. Eng.* **14**, 97–111.

Auman, H. J., Coleman, H., Riley, H. E., Olale, F., Tsai, H.-J. and Yelon, D. (2007). Functional Modulation of Cardiac Form through Regionally Confined Cell Shape Changes. *PLoS biology* **5**, e53.

Axelrod, J. D., Miller, J. R., Shulman, J. M., Moon, R. T. and Perrimon, N. (1998). Differential recruitment of Dishevelled provides signaling specificity in the planar cell polarity and Wingless signaling pathways. *Genes & Development* **12**, 2610–2622.

Baarlink, C., Wang, H. and Grosse, R. (2013). Nuclear Actin Network Assembly by Formins Regulates the SRF Coactivator MAL. *Science* **340**, 864–867.

Babayeva, S., Zilber, Y. and Torban, E. (2011). Planar cell polarity pathway regulates actin rearrangement, cell shape, motility, and nephrin distribution in podocytes. *AJP: Renal Physiology* **300**, F549–F560.

Bach, I. (2000). The LIM domain: regulation by association. *Mechanisms of development* **91**, 5–17.

Balza, R. O. and Misra, R. P. (2006). Role of the Serum Response Factor in Regulating Contractile Apparatus Gene Expression and Sarcomeric Integrity in Cardiomyocytes. *Journal of Biological Chemistry* **281**, 6498–6510.

Barron, M. R., Belaguli, N. S., Zhang, S. X., Trinh, M., Iyer, D., Merlo, X., Lough, J. W., Parmacek, M. S., Bruneau, B. G. and Schwartz, R. J. (2005). Serum Response Factor, an Enriched Cardiac Mesoderm Obligatory Factor, Is a Downstream Gene Target for Tbx Genes. *Journal of Biological Chemistry* **280**, 11816–11828.

Bassett, A. R., Tibbit, C., Ponting, C. P. and Liu, J.-L. (2013). Highly Efficient Targeted Mutagenesis of Drosophila with the CRISPR/Cas9 System. *Cell reports* **4**, 220–228.

Bassuk, A. G., Wallace, R. H., Buhr, A., Buller, A. R., Afawi, Z., Shimojo, M., Miyata, S., Chen, S., Gonzalez-Alegre, P., Griesbach, H. L., et al. (2008). A Homozygous Mutation in Human PRICKLE1 Causes an Autosomal-Recessive Progressive Myoclonus Epilepsy-Ataxia Syndrome. *The American Journal of Human Genetics* **83**, 572–581.

Bazellières, E., Conte, V., Elosegui-Artola, A., Serra-Picamal, X., Bintanel-Morcillo, M., Roca-Cusachs, P., Muñoz, J. J., Sales-Pardo, M., Guimerà, R. and Trepat, X. (2015). Control of cell–cell forces and collective cell dynamics by the intercellular adhesome. *Nature cell biology* **17**, 409–420.

Becker, J. R., Deo, R. C., Werdich, A. A., Panáková, D., Coy, S. and MacRae, C. A. (2011). Human cardiomyopathy mutations induce myocyte hyperplasia and activate hypertrophic pathways during cardiogenesis in zebrafish. *Disease Models & Mechanisms* **4**, 400–410.

Behrens, J., Kries, von, J. P., Kühl, M., Bruhn, L., Wedlich, D., Grosschedl, R. and Birchmeier, W. (1996). Functional interaction of β-catenin with the transcription factor LEF-1. *Nature* **382**, 638–642.

Behringer, R. R., Bradley, A., Liu, P., Wakamiya, M., Shea, M. J. and Albrecht, U. (1999). *Nature Genetics* **22**, 361–365.

Beis, D. (2005). Genetic and cellular analyses of zebrafish atrioventricular cushion and valve development. *Development* **132**, 4193–4204.

Belaguli, N. S., Sepulveda, J. L., Nigam, V., Charron, F., Nemer, M. and Schwartz, R. J. (2000). Cardiac Tissue Enriched Factors Serum Response Factor and GATA-4 Are Mutual Coregulators. *Molecular and Cellular Biology* **20**, 7550–7558.

Ben-Shachar, G., Arcilla, R. A., Lucas, R. V. and Manasek, F. J. (1985). Ventricular trabeculations in the chick embryo heart and their contribution to ventricular and muscular septal development. *Circulation Research* **57**, 759–766.

Benson, C. C., Zhou, Q., Long, X. and Miano, J. M. (2011). Identifying functional single nucleotide polymorphisms in the human CArGome. *Physiological Genomics* **43**, 1038–1048.

Bentley, K., Franco, C. A., Philippides, A., Blanco, R., Dierkes, M., Gebala, V., Stanchi, F., Jones, M., Aspalter, I. M., Cagna, G., et al. (2014). The role of differential VE-cadherin dynamics in cell rearrangement during angiogenesis. *Nature cell biology* **16**, 309–321.

Bertet, C., Sulak, L. and Lecuit, T. (2004). Myosin-dependent junction remodelling controls planar cell intercalation and axis elongation. *Nature* **429**, 667–671.

Blankenship, J. T., Backovic, S. T., Sanny, J. S. P., Weitz, O. and Zallen, J. A. (2006). Multicellular Rosette Formation Links Planar Cell Polarity to Tissue Morphogenesis. *Developmental Cell* **11**, 459–470.

Boheler, K. R., Carrier, L., Chassagne, C., la Bastie, de, D., Mercadier, J. J. and Schwartz, K. (1991). Regulation of myosin heavy chain and actin isogenes expression during cardiac growth. In *Molecular Mechanisms of Cellular Growth*, pp. 101–107. Boston, MA: Springer US.

Booth, A. J. R., Blanchard, G. B., Adams, R. J. and Röper, K. (2014). A Dynamic Microtubule Cytoskeleton Directs Medial Actomyosin Function during Tube Formation. *Developmental Cell* **29**, 562–576.

Bosoi, C. M., Capra, V., Allache, R., Trinh, V. Q.-H., De Marco, P., Merello, E., Drapeau, P., Bassuk, A. G. and Kibar, Z. (2011). Identification and characterization of novel rare mutations in the planar cell polarity gene PRICKLE1in human neural tube defects. *Hum. Mutat.* **32**, 1371–1375.

Boutros, M., Paricio, N., Strutt, D. I. and Mlodzik, M. (1998). Dishevelled Activates JNK and Discriminates between JNK Pathways in Planar Polarity and wingless Signaling. *Cell* **94**, 109–118.

Bovellan, M., Romeo, Y., Biro, M., Boden, A., Chugh, P., Yonis, A., Vaghela, M., Fritzsche, M., Moulding, D., Thorogate, R., et al. (2014). Cellular Control of Cortical Actin Nucleation. *Current Biology* **24**, 1628–1635.

Brade, T., Männer, J. and Kühl, M. (2006). The role of Wnt signalling in cardiac development and tissue remodelling in the mature heart. *Cardiovascular Research* **72**, 198–209.

Buckingham, M., Meilhac, S. and Zaffran, S. (2005). Building the mammalian heart from two sources of myocardial cells. *Nat Rev Genet* **6**, 826–837.

Buckley, C. D., Tan, J., Anderson, K. L., Hanein, D., Volkmann, N., Weis, W. I., Nelson, W. J. and Dunn, A. R. (2014). The minimal cadherin-catenin complex binds to actin filaments under force. *Science* **346**, 1254211–1254211.

Burger, A., Lindsay, H., Felker, A., Hess, C., Anders, C., Chiavacci, E., Zaugg, J., Weber, L. M., Catena, R., Jinek, M., et al. (2016). Maximizing mutagenesis with solubilized CRISPR-Cas9 ribonucleoprotein complexes. *Development* **143**, 2025–2037.

Burggren, W. W. and Pinder, A. W. (1991). Ontogeny of Cardiovascular and Respiratory Physiology in Lower Vertebrates. *Annual Review of Physiology* **53**, 107–135.

Burrill, J. D. and Easter, S. S. (1994). Development of the retinofugal projections in the embryonic and larval zebrafish (Brachydanio rerio). *J. Comp. Neurol.* **346**, 583–600.

Bussmann, J., Bakkers, J. and Schulte-Merker, S. (2007). Early Endocardial Morphogenesis Requires Scl/Tal1. *PLoS Genet* **3**, e140.

Buxboim, A., Swift, J., Irianto, J., Spinler, K. R., Dingal, P. C. D. P., Athirasala, A., Kao, Y.-R. C., Cho, S., Harada, T., Shin, J.-W., et al. (2014). Matrix Elasticity Regulates Lamin-A,C Phosphorylation and Turnover with Feedback to Actomyosin. *Current Biology* **24**, 1909–1917.

Cai, C.-L., Liang, X., Shi, Y., Chu, P.-H., Pfaff, S. L., Chen, J. and Evans, S. (2003). Isl1 Identifies a Cardiac Progenitor Population that Proliferates Prior to Differentiation and Contributes a Majority of Cells to the Heart. *Developmental Cell* **5**, 877–889.

Cai, Y., Biais, N., Giannone, G., Tanase, M., Jiang, G., Hofman, J. M., Wiggins, C. H., Silberzan, P., Buguin, A., Ladoux, B., et al. (2006). Nonmuscle Myosin IIA-Dependent Force Inhibits Cell Spreading and Drives F-Actin Flow. *Biophysical Journal* **91**, 3907–3920.

Cantley, L. C. (2002). The Phosphoinositide 3-Kinase Pathway. *Science* **296**, 1655–1657.

Carrier, L., Boheler, K. R., Chassagne, C., la Bastie, de, D., Wisnewsky, C., Lakatta, E. G. and Schwartz, K. (1992). Expression of the sarcomeric actin isogenes in the rat heart with development and senescence. *Circulation Research* **70**, 999–1005.

Carvajal-Gonzalez, A., Leite, M. I., Waters, P., Woodhall, M., Coutinho, E., Balint, B., Lang, B., Pettingill, P., Carr, A., Sheerin, U. M., et al. (2014). Glycine receptor antibodies in PERM and related syndromes: characteristics, clinical features and outcomes. *Brain* **137**, 2178–2192.

Cervantes, S., Yamaguchi, T. P. and Hebrok, M. (2009). Wnt5a is essential for intestinal elongation in mice. *Developmental biology* **326**, 285–294.

Cha, S. W., Tadjuidje, E., Tao, Q., Wylie, C. and Heasman, J. (2008). Wnt5a and Wnt11 interact in a maternal Dkk1-regulated fashion to activate both canonical and non-canonical signaling in Xenopus axis formation. *Development* **135**, 3719–3729.

Chae, J., Kim, M. J., Goo, J. H., Collier, S., Gubb, D., Charlton, J., Adler, P. N. and Park, W. J. (1999). The Drosophila tissue polarity gene starry night encodes a member of the protocadherin family. *Development* **126**, 5421–5429.

Chan, J. Y., Takeda, M., Briggs, L. E., Graham, M. L., Lu, J. T., Horikoshi, N., Weinberg, E. O., Aoki, H., Sato, N., Chien, K. R., et al. (2008). Identification of Cardiac-Specific Myosin Light Chain Kinase. *Circulation Research* **102**, 571–580.

Chang, C.-P., Neilson, J. R., Bayle, J. H., Gestwicki, J. E., Kuo, A., Stankunas, K., Graef, I. A. and Crabtree, G. R. (2004). A Field of Myocardial-Endocardial NFAT Signaling Underlies Heart Valve Morphogenesis. *Cell* **118**, 649–663.

Chang, D. F., Belaguli, N. S., Iyer, D., Roberts, W. B., Wu, S.-P., Dong, X.-R., Marx, J. G., Moore, M. S., Beckerle, M. C., Majesky, M. W., et al. (2003). Cysteine-Rich LIM-Only Proteins CRP1 and CRP2 Are Potent Smooth Muscle Differentiation Cofactors. *Developmental Cell* **4**, 107–118.

Chen, C. Y. and Schwartz, R. J. (1996). Recruitment of the tinman homolog Nkx-2.5 by serum response factor activates cardiac alpha-actin gene transcription. *Molecular and Cellular Biology* **16**, 6372–6384.

Chen, F., Kook, H., Milewski, R., Gitler, A. D., Lu, M. M., Li, J., Nazarian, R., Schnepp, R., Jen, K., Biben, C., et al. (2002). Hop Is an Unusual Homeobox Gene that Modulates Cardiac Development. *Cell* **110**, 713–723.

Chen, J. N. and Fishman, M. C. (1996). Zebrafish tinman homolog demarcates the heart field and initiates myocardial differentiation. *Development* **122**, 3809–3816.

Cheng, G., Hagen, T. P., Dawson, M. L., Barnes, K. V. and Menick, D. R. (1999). The Role of GATA, CArG, E-box, and a Novel Element in the Regulation of Cardiac Expression of the Na+-Ca2+ Exchanger Gene. *Journal of Biological Chemistry* **274**, 12819–12826.

Choi, S.-C. and Han, J.-K. (2002). Xenopus Cdc42 Regulates Convergent Extension Movements during Gastrulation through Wnt/Ca2+ Signaling Pathway. *Developmental biology* **244**, 342–357.

Christodoulides, C. (2006). The Wnt antagonist Dickkopf-1 and its receptors are coordinately regulated during early human adipogenesis. *Journal of Cell Science* **119**, 2613–2620.

Christoffels, V. M., Habets, P. E. M. H., Franco, D., Campione, M., de Jong, F., Lamers, W. H., Bao, Z.-Z., Palmer, S., Biben, C., Harvey, R. P., et al. (2000). Chamber Formation and Morphogenesis in the Developing Mammalian Heart. *Developmental biology* **223**, 266–278.

Christoffels, V. M., Smits, G. J., Kispert, A. and Moorman, A. F. M. (2010). Development of the Pacemaker Tissues of the Heart. *Circulation Research* **106**, 240–254.

Ciruna, B., Jenny, A., Lee, D., Mlodzik, M. and Schier, A. F. (2006). Planar cell polarity signalling couples cell division and morphogenesis during neurulation. *Nature* **439**, 220–224.

Clark, K., Langeslag, M., Figdor, C. G. and van Leeuwen, F. N. (2007). Myosin II and mechanotransduction: a balancing act. *Trends in Cell Biology* **17**, 178–186.

Classen, A.-K., Anderson, K. I., Marois, E. and Eaton, S. (2005). Hexagonal Packing of Drosophila Wing Epithelial Cells by the Planar Cell Polarity Pathway. *Developmental Cell* **9**, 805–817.

Clement, S., Stouffs, M., Bettiol, E., Kampf, S., Krause, K. H., Chaponnier, C. and Jaconi, M. (2007). Expression and function of -smooth muscle actin during embryonic-stem-cell-derived cardiomyocyte differentiation. *Journal of Cell Science* **120**, 229–238.

Cohen, E. D., Miller, M. F., Wang, Z., Moon, R. T. and Morrisey, E. E. (2012). Wnt5a and Wnt11 are essential for second heart field progenitor development. *Development* **139**, 1931–1940.

Cohen, E. D., Tian, Y. and Morrisey, E. E. (2008). Wnt signaling: an essential regulator of cardiovascular differentiation, morphogenesis and progenitor self-renewal. *Development* **135**, 789–798.

Cripps, R. M. and Olson, E. N. (2002). Control of Cardiac Development by an Evolutionarily Conserved Transcriptional Network. *Developmental biology* **246**, 14–28.

Davey, H. W., Kelly, J. K. and Wildemann, A. G. (1995). The Nucleotide Sequence, Structure, and Preliminary Studies on the Transcriptional Regulation of the Bovine α Skeletal Actin Gene. *DNA and Cell Biology* **14**, 609–618.

De Ferrari, G. V. and Moon, R. T. (2006). The ups and downs of Wnt signaling in prevalent neurological disorders. *Oncogene* **25**, 7545–7553.

de Pater, E., Clijsters, L., Marques, S. R., Lin, Y. F., Garavito-Aguilar, Z. V., Yelon, D. and Bakkers, J. (2009). Distinct phases of cardiomyocyte differentiation regulate growth of the zebrafish heart. *Development* **136**, 1633–1641.

De, A. (2011). Wnt/Ca2+ signaling pathway: a brief overview. *Acta Biochimica et Biophysica Sinica* **43**, 745–756.

Dietrich, A.-C., Lombardo, V. A., Veerkamp, J., Priller, F. and Abdelilah-Seyfried, S. (2014). Blood Flow and Bmp Signaling Control Endocardial Chamber Morphogenesis.

Developmental Cell **30**, 367–377.

Dolk, H., Loane, M., Garne, E.a European Surveillance of Congenital Anomalies (EUROCAT) Working Group (2011). Congenital Heart Defects in Europe: Prevalence and Perinatal Mortality, 2000 to 2005. *Circulation* **123**, 841–849.

Du, K. L., Ip, H. S., Li, J., Chen, M., Dandre, F., Yu, W., Lu, M. M., Owens, G. K. and Parmacek, M. S. (2003). Myocardin Is a Critical Serum Response Factor Cofactor in the Transcriptional Program Regulating Smooth Muscle Cell Differentiation. *Molecular and Cellular Biology* **23**, 2425–2437.

Elul, T. and Keller, R. (2000). Monopolar Protrusive Activity: A New Morphogenic Cell Behavior in the Neural Plate Dependent on Vertical Interactions with the Mesoderm in Xenopus. *Developmental biology* **224**, 3–19.

Faienza, M. F., Luce, V., Lonero, A., Ventura, A., Colaianni, G., Colucci, S., Cavallo, L., Grano, M. and Brunetti, G. (2014). Treatment of osteoporosis in children with glucocorticoid-treated diseases. *Expert Review of Endocrinology & Metabolism* **9**, 525–534.

Farhadifar, R., Röper, J.-C., Aigouy, B., Eaton, S. and Jülicher, F. (2007). The Influence of Cell Mechanics, Cell-Cell Interactions, and Proliferation on Epithelial Packing. *Current Biology* **17**, 2095–2104.

Feiguin, F., Hannus, M., Mlodzik, M. and Eaton, S. (2001). The Ankyrin Repeat Protein Diego Mediates Frizzled-Dependent Planar Polarization. *Developmental Cell* **1**, 93–101.

Fernandez-Gonzalez, R., Simoes, S. de M., Röper, J.-C., Eaton, S. and Zallen, J. A. (2009). Myosin II Dynamics Are Regulated by Tension in Intercalating Cells. *Developmental Cell* **17**, 736–743.

Ferrante, M. I., Romio, L., Castro, S., Collins, J. E., Goulding, D. A., Stemple, D. L., Woolf, A. S. and Wilson, S. W. (2008). Convergent extension movements and ciliary function are mediated by ofd1, a zebrafish orthologue of the human oral-facial-digital type 1 syndrome gene. *Human Molecular Genetics* **18**, 289–303.

Ferreira-Cornwell, M. C., Luo, Y., Narula, N., Lenox, J. M., Lieberman, M. and Radice, G. L. (2002). Remodeling the intercalated disc leads to cardiomyopathy in mice misexpressing cadherins in the heart. *Journal of Cell Science* **115**, 1623–1634.

Fletcher, A. G., Osterfield, M., Baker, R. E. and Shvartsman, S. Y. (2014). Vertex models of epithelial morphogenesis. *Biophysical Journal* **106**, 2291–2304.

Flück, M., Carson, J. A., Schwartz, R. J. and Booth, F. W. (1999). SRF protein is upregulated during stretch-induced hypertrophy of rooster ALD muscle. *J. Appl. Physiol.* **86**, 1793–1799.

Forouhar, A. S. (2006). The Embryonic Vertebrate Heart Tube Is a Dynamic Suction Pump. *Science* **312**, 751–753.

Fournier, M. F., Sauser, R., Ambrosi, D., Meister, J.-J. and Verkhovsky, A. B. (2010). Force transmission in migrating cells. *The Journal of Cell Biology* **188**, 287–297.

Franze, K., Gerdelmann, J., Weick, M., Betz, T., Pawlizak, S., Lakadamyali, M., Bayer, J., Rillich, K., Gögler, M., Lu, Y.-B., et al. (2009). Neurite Branch Retraction Is Caused by a Threshold-Dependent Mechanical Impact. *Biophysical Journal* **97**, 1883–1890.

Freund, J. B., Goetz, J. G., Hill, K. L. and Vermot, J. (2012). Fluid flows and forces in development: functions, features and biophysical principles. *Development* **139**, 3063–3063.

Gagnon, J. A., Valen, E., Thyme, S. B., Huang, P., Ahkmetova, L., Pauli, A., Montague, T. G., Zimmerman, S., Richter, C. and Schier, A. F. (2014). Efficient Mutagenesis by Cas9 Protein-Mediated Oligonucleotide Insertion and Large-Scale Assessment of Single-Guide RNAs. *PloS one* **9**, e98186.

Gao, C. and Chen, Y.-G. (2010). Dishevelled: The hub of Wnt signaling. *Cellular Signalling* **22**, 717–727.

Garriock, R. J., D'Agostino, S. L., Pilcher, K. C. and Krieg, P. A. (2005). Wnt11-R, a protein closely related to mammalian Wnt11, is required for heart morphogenesis in Xenopus. *Developmental biology* **279**, 179–192.

Garrity, D. M., Childs, S. and Fishman, M. C. (2002). The heartstrings mutation in zebrafish causes heart/fin Tbx5 deficiency syndrome. *Development* **129**, 4635–4645.

Georgiou, M. and Baum, B. (2010). Polarity proteins and Rho GTPases cooperate to spatially organise epithelial actin-based protrusions. *Journal of Cell Science* **123**, 1089–1098.

Gessert, S. and Kühl, M. (2010). The Multiple Phases and Faces of Wnt Signaling During Cardiac Differentiation and Development. *Circulation Research* **107**, 186–199.

Gessert, S. and Kühl, M. (2009). Comparative gene expression analysis and fate mapping studies suggest an early segregation of cardiogenic lineages in Xenopus laevis. *Developmental biology* **334**, 395–408.

Gessert, S., Maurus, D., Brade, T., Walther, P., Pandur, P. and Kühl, M. (2008). DM-GRASP/ALCAM/CD166 is required for cardiac morphogenesis and maintenance of cardiac identity in first heart field derived cells. *Developmental biology* **321**, 150–161.

Giles, R. H., van Es, J. H. and Clevers, H. (2003). Caught up in a Wnt storm: Wnt signaling in cancer. *Biochimica et Biophysica Acta (BBA) - Reviews on Cancer* **1653**, 1–24.

Glickman, N. S. and Yelon, D. (2002). Cardiac development in zebrafish: coordination of form and function. *Seminars in cell & developmental biology* **13**, 507–513.

Gong, Y., Mo, C. and Fraser, S. E. (2004). Planar cell polarity signalling controls cell division orientation during zebrafish gastrulation. *Nature* **430**, 689–693.

Grant, S. F. A., Thorleifsson, G., Reynisdottir, I., Benediktsson, R., Manolescu, A., Sainz, J., Helgason, A., Stefansson, H., Emilsson, V., Helgadottir, A., et al. (2006). Variant of transcription factor 7-like 2 (TCF7L2) gene confers risk of type 2 diabetes. *Nature Genetics* **38**, 320–323.

Grashoff, C., Hoffman, B. D., Brenner, M. D., Zhou, R., Parsons, M., Yang, M. T., McLean, M. A., Sligar, S. G., Chen, C. S., Ha, T., et al. (2010). Measuring mechanical tension across vinculin reveals regulation of focal adhesion dynamics. *Nature* **466**, 263–266.

Gray, R. S., Roszko, I. and Solnica-Krezel, L. (2011). Planar Cell Polarity: Coordinating Morphogenetic Cell Behaviors with Embryonic Polarity. *Developmental Cell* **21**, 120–133.

Grummt, I. and Pikaard, C. S. (2003). Epigenetic silencing of RNA polymerase I transcription. *Nature Reviews Molecular Cell Biology* **4**, 641–649.

Gubb, D. and García-Bellido, A. (1982). A genetic analysis of the determination of cuticular polarity during development in Drosophila melanogaster. *Journal of embryology and experimental morphology* **68**, 37–57.

Gubb, D., Green, C., Huen, D., Coulson, D., Johnson, G., Tree, D., Collier, S. and Roote, J. (1999). The balance between isoforms of the Prickle LIM domain protein is critical for planar polarity in Drosophila imaginal discs. *Genes & Development* **13**, 2315–2327.

Gumbiner, B. M. (2005). Regulation of cadherin-mediated adhesion in morphogenesis. *Nature Reviews Molecular Cell Biology* **6**, 622–634.

Gustafson, T. A. and Kedes, L. (1989). Identification of multiple proteins that interact with functional regions of the human cardiac alpha-actin promoter. *Molecular and Cellular Biology* **9**, 3269–3283.

Halbleib, J. M. and Nelson, W. J. (2006). Cadherins in development: cell adhesion, sorting, and tissue morphogenesis. *Genes & Development* **20**, 3199–3214.

Halcox, J. and Deanfield, J. E. (2007). Endothelial cell function testing: how does the method help us in evaluating vascular status? *Acta Paediatrica* **93**, 48–54.

Hamblet, N. S. (2002). Dishevelled 2 is essential for cardiac outflow tract development, somite segmentation and neural tube closure. *Development* **129**, 5827–5838.

Hami, D., Grimes, A. C., Tsai, H. J. and Kirby, M. L. (2011). Zebrafish cardiac development requires a conserved secondary heart field. *Development* **138**, 2389–2398.

Harris, T. J. C. and Tepass, U. (2010). Adherens junctions: from molecules to morphogenesis. *Nature Reviews Molecular Cell Biology* **11**, 502–514.

Harvey, R. P., Lai, D., Elliott, D., Biben, C., Solloway, M., Prall, O., Stennard, F., Schindeler, A., Groves, N., Lavulo, L., et al. (2002). Homeodomain Factor Nkx2-5 in Heart Development and Disease. *Cold Spring Harbor Symposia on Quantitative Biology* **67**, 107–114.

Hautala, N., Tenhunen, O., Szokodi, I. and Ruskoaho, H. (2002). Direct left ventricular wall stretch activates GATAff4 binding in perfused rat heart: involvement of autocrine/paracrine pathways. *Pflügers Archiv* **443**, 362–369.

Hautala, N., Tokola, H., Luodonpää, M., Puhakka, J., Romppanen, H., Vuolteenaho, O. and Ruskoaho, H. (2001). Pressure Overload Increases GATA4 Binding Activity via Endothelin-1. *Circulation* **103**, 730–735.

He, A., Kong, S. W., Ma, Q. and Pu, W. T. (2011). Co-occupancy by multiple cardiac transcription factors identifies transcriptional enhancers active in heart. *Proceedings of the National Academy of Sciences* **108**, 5632–5637.

He, W., Zhang, L., Ni, A., Zhang, Z., Mirotsou, M., Mao, L., Pratt, R. E. and Dzau, V. J. (2010). Exogenously administered secreted frizzled related protein 2 (Sfrp2) reduces fibrosis and improves cardiac function in a rat model of myocardial infarction. *Proceedings of the National Academy of Sciences* **107**, 21110–21115.

Heisenberg, C.-P. and Bellaïche, Y. (2013). Forces in Tissue Morphogenesis and Patterning. *Cell* **153**, 948–962.

Heisenberg, C.-P., Tada, M., Rauch, G.-J., Saúde, L., Concha, M. L., Geisler, R., Stemple, D. L., Smith, J. C. and Wilson, S. W. (2000). Silberblick/Wnt11 mediates convergent extension movements during zebrafish gastrulation. *Nature* **405**, 76–81.

Henderson, D. J. and Chaudhry, B. (2011). Getting to the heart of planar cell polarity signaling. *Birth Defects Research Part A: Clinical and Molecular Teratology* **91**, 460–467.

Henderson, D. J., Conway, S. J., Greene, N. D. E., Gerrelli, D., Murdoch, J. N., Anderson, R. H. and Copp, A. J. (2001). Cardiovascular Defects Associated With Abnormalities in Midline Development in the Loop-tail Mouse Mutant. *Circulation Research* **89**, 6–12.

Henderson, D. J., Phillips, H. M. and Chaudhry, B. (2006). Vang-like 2 and Noncanonical Wnt Signaling In Outflow Tract Development. *Trends in Cardiovascular Medicine* **16**, 38–45.

Henderson, S. A., Spencer, M., Sen, A., Kumar, C., Siddiqui, M. A. and Chien, K. R. (1989). Structure, organization, and expression of the rat cardiac myosin light chain-2 gene. Identification of a 250-base pair fragment which confers cardiac-specific expression. *Journal of Biological Chemistry* **264**, 18142–18148.

High, F. A., Jain, R., Stoller, J. Z., Antonucci, N. B., Lu, M. M., Loomes, K. M., Kaestner, K. H., Pear, W. S. and Epstein, J. A. (2009). Murine Jagged1/Notch signaling in the second heart field orchestrates Fgf8 expression and tissue-tissue interactions during outflow tract development. *J. Clin. Invest.* **119**, 1986–1996.

Hill, C. S., Wynne, J. and Treisman, R. (1995). The Rho family GTPases RhoA, Racl , and CDC42Hsregulate transcriptional activation by SRF. *Cell* **81**, 1159–1170.

Hinton, R. B. and Yutzey, K. E. (2011). Heart Valve Structure and Function in Development and Disease. *Annual Review of Physiology* **73**, 29–46.

Hofmann, W. A. and de Lanerolle, P. (2006). Nuclear actin: to polymerize or not to polymerize. *The Journal of Cell Biology* **172**, 495–496.

Holtzinger, A. and Evans, T. (2007). Gata5 and Gata6 are functionally redundant in zebrafish for specification of cardiomyocytes. *Developmental biology* **312**, 613–622.

Hong, S., Troyanovsky, R. B. and Troyanovsky, S. M. (2011). Cadherin exits the junction by switching its adhesive bond. *The Journal of Cell Biology* **192**, 1073–1083.

Hoogaars, W. M. H., Barnett, P., Moorman, A. F. M. and Christoffels, V. M. (2007). Cardiovascular development: towards biomedical applicability. *Cell. Mol. Life Sci.* **64**, 646–660.

Howard, J. and Clark, R. L. (2002). Mechanics of Motor Proteins and the Cytoskeleton. *Appl. Mech. Rev.* **55**, B39.

Hsu, S.-C., Galceran, J. and Grosschedl, R. (1998). Modulation of Transcriptional Regulation by LEF-1 in Response to Wnt-1 Signaling and Association with β-Catenin. *Molecular and Cellular Biology* **18**, 4807–4818.

Hu, N., Sedmera, D., Yost, H. J. and Clark, E. B. (2000). Structure and function of the developing zebrafish heart. *The Anatomical record* **260**, 148–157.

Hu, Q., Kwon, Y. S., Nunez, E., Cardamone, M. D., Hutt, K. R., Ohgi, K. A., Garcia-Bassets, I., Rose, D. W., Glass, C. K., Rosenfeld, M. G., et al. (2008). Enhancing nuclear receptor-induced transcription requires nuclear motor and LSD1-dependent gene networking in interchromatin granules. *Proceedings of the National Academy of Sciences* **105**, 19199–19204.

Huang, W., Zhang, R. and Xu, X. (2009). Myofibrillogenesis in the developing zebrafish heart: A functional study of tnnt2. *Developmental biology* **331**, 237–249.

Huang, Y., Jia, X., Bai, K., Gong, X. and Fan, Y. (2010). Effect of Fluid Shear Stress on Cardiomyogenic Differentiation of Rat Bone Marrow Mesenchymal Stem Cells. *Archives of Medical Research* **41**, 497–505.

Huber, F., Boire, A., López, M. P. and Koenderink, G. H. (2015). Cytoskeletal crosstalk: when three different personalities team up. *Current Opinion in Cell Biology* **32**, 39–47.

Hurlstone, A. F. L., Haramis, A.-P. G., Wienholds, E., Begthel, H., Korving, J., Van Eeden, F., Cuppen, E., Zivkovic, D., Plasterk, R. H. A. and Clevers, H. (2003). The Wnt/β-catenin pathway regulates cardiac valve formation. *Nature* **425**, 633–637.

Hutson, M. R., Zeng, X. L., Kim, A. J., Antoon, E., Harward, S. and Kirby, M. L. (2010). Arterial pole progenitors interpret opposing FGF/BMP signals to proliferate or differentiate. *Development* **137**, 3001–3011.

Hwang, W. Y., Peterson, R. T. and Yeh, J.-R. J. (2014). Methods for targeted mutagenesis in zebrafish using TALENs. *Methods* **69**, 76–84.

Ikeda, S. (1998). Axin, a negative regulator of the Wnt signaling pathway, forms a complex with GSK-3beta and beta -catenin and promotes GSK-3beta -dependent phosphorylation of beta -catenin. *EMBO J* **17**, 1371–1384.

Jenny, A. (2003). Prickle and Strabismus form a functional complex to generate a correct axis during planar cell polarity signaling. *EMBO J* **22**, 4409–4420.

Jenny, A., Reynolds-Kenneally, J., Das, G., Burnett, M. and Mlodzik, M. (2005). Diego and Prickle regulate Frizzled planar cell polarity signalling by competing for Dishevelled binding. *Nature cell biology* **7**, 691–697.

Jinek, M., Chylinski, K., Fonfara, I., Hauer, M., Doudna, J. A. and Charpentier, E. (2012). A Programmable Dual-RNA-Guided DNA Endonuclease in Adaptive Bacterial Immunity. *Science* **337**, 816–821.

Kamm, K. E. and Stull, J. T. (2001). Dedicated Myosin Light Chain Kinases with Diverse Cellular Functions. *Journal of Biological Chemistry* **276**, 4527–4530.

Kasza, K. E., Farrell, D. L. and Zallen, J. A. (2014). Spatiotemporal control of epithelial remodeling by regulated myosin phosphorylation. *Proceedings of the National Academy of Sciences* **111**, 11732–11737.

Katoh, M. and Katoh, M. (2003). Identification and characterization of human PRICKLE1 and PRICKLE2 genes as well as mouse Prickle1 and Prickle2 genes homologous to Drosophila tissue polarity gene prickle. *Int J Mol Med* **11**, 249–256.

Keegan, B. R. (2004). Organization of cardiac chamber progenitors in the zebrafish blastula. *Development* **131**, 3081–3091.

Keegan, B. R. (2005). Retinoic Acid Signaling Restricts the Cardiac Progenitor Pool. *Science* **307**, 247–249.

Keller, R. and Shih, J. (1992). Mediolateral Intercalation of Mesodermal Cells in the Xenopus Laevis Gastrula. In *Formation and Differentiation of Early Embryonic Mesoderm*, pp. 47–61. Boston, MA: Springer US.

Keller, R. E., Danilchik, M., Gimlich, R. and Shih, J. (1985). The function and mechanism of convergent extension during gastrulation of Xenopus laevis. *Journal of embryology and experimental morphology* **89**, 185–209.

Kelly, R. G. (2012). The Second Heart Field. In *Heart Development*, pp. 33–65. Elsevier.

Kettleborough, R. N. W., Busch-Nentwich, E. M., Harvey, S. A., Dooley, C. M., de Bruijn, E., van Eeden, F., Sealy, I., White, R. J., Herd, C., Nijman, I. J., et al. (2013). A systematic genome-wide analysis of zebrafish protein-coding gene function. *Nature* **496**, 494–497.

Kikuchi, Y., Trinh, L. A., Reiter, J. F., Alexander, J., Yelon, D. and Stainier, D. Y. (2000). The zebrafish bonnie and clyde gene encodes a Mix family homeodomain protein that regulates the generation of endodermal precursors. *Genes & Development* **14**, 1279–1289.

Kimelman, D. and Xu, W. (2006). β-Catenin destruction complex: insights and questions from a structural perspective. *Oncogene* **25**, 7482–7491.

Kimmel, C. B., Ballard, W. W., Kimmel, S. R., Ullmann, B. and Schilling, T. F. (2005). Stages of embryonic development of the zebrafish. *Developmental Dynamics* **203**, 253–310.

Kimura, K., Ito, M., Amano, M., Chihara, K., Fukata, Y., Nakafuku, M., Yamamori, B., Feng, J., Nakano, T., Okawa, K., et al. (1996). Regulation of Myosin Phosphatase by Rho and Rho-Associated Kinase (Rho-Kinase). *Science* **273**, 245–248.

Kitagawa, M., Hatakeyama, S., Shirane, M., Matsumoto, M., Ishida, N., Hattori, K., Nakamichi, I., Kikuchi, A., Nakayama, K.-I. and Nakayama, K. (1999). An F-box protein, FWD1, mediates ubiquitin-dependent proteolysis of β-catenin. *EMBO J* **18**, 2401–2410.

Kitajima, S., Takagi, A., Inoue, T. and Saga, Y. (2000). MesP1 and MesP2 are essential for the development of cardiac mesoderm. *Development* **127**, 3215–3226.

Klaus, A., Muller, M., Schulz, H., Saga, Y., Martin, J. F. and Birchmeier, W. (2012). Wnt/ -catenin and Bmp signals control distinct sets of transcription factors in cardiac progenitor cells. *Proceedings of the National Academy of Sciences* **109**, 10921–10926.

Klein, T. J. and Mlodzik, M. (2005). Planar Cell Polarization: An Emerging Model Points in the Right Direction. *Annual Review of Cell and Developmental Biology* **21**, 155–176.

Kok, F. O., Shin, M., Ni, C.-W., Gupta, A., Grosse, A. S., van Impel, A., Kirchmaier, B. C., Peterson-Maduro, J., Kourkoulis, G., Male, I., et al. (2015). Reverse Genetic Screening Reveals Poor Correlation between Morpholino-Induced and Mutant Phenotypes in Zebrafish. *Developmental Cell* **32**, 97–108.

Krasnow, R. E., Wong, L. L. and Adler, P. N. (1995). Dishevelled is a component of the frizzled signaling pathway in Drosophila. *Development* **121**, 4095–4102.

Krendel, M. (2005). Myosins: Tails (and Heads) of Functional Diversity. *Physiology* **20**, 239–251.

Kumar, A., Crawford, K., Close, L., Madison, M., Lorenz, J., Doetschman, T., Pawlowski, S., Duffy, J., Neumann, J., Robbins, J., et al. (1997). Rescue of cardiac -actin-deficient mice by enteric smooth muscle -actin. *Proceedings of the National Academy of Sciences* **94**, 4406–4411.

Kühl, M., Geis, K., Sheldahl, L. C., Pukrop, T., Moon, R. T. and Wedlich, D. (2001). Antagonistic regulation of convergent extension movements in Xenopus by Wnt/beta-catenin and Wnt/Ca2+ signaling. *Mechanisms of development* **106**, 61–76.

Kühl, M., Sheldahl, L. C., Malbon, C. C. and Moon, R. T. (2000). Ca(2+)/calmodulin-dependent protein kinase II is stimulated by Wnt and Frizzled homologs and promotes ventral cell fates in Xenopus. *Journal of Biological Chemistry* **275**, 12701–12711.

Kwon, C., Arnold, J., Hsiao, E. C., Taketo, M. M., Conklin, B. R. and Srivastava, D. (2007). Canonical Wnt signaling is a positive regulator of mammalian cardiac progenitors. *Proceedings of the National Academy of Sciences* **104**, 10894–10899.

Kwon, C., Qian, L., Cheng, P., Nigam, V., Arnold, J. and Srivastava, D. (2009). A regulatory pathway involving Notch1/β-catenin/Isl1 determines cardiac progenitor cell fate. *Nature cell biology* **11**, 951–957.

Lahoute, C., Sotiropoulos, A., Favier, M., Guillet-Deniau, I., Charvet, C., Ferry, A., Butler-Browne, G., Metzger, D., Tuil, D. and Daegelen, D. (2008). Premature Aging in Skeletal Muscle Lacking Serum Response Factor. *PloS one* **3**, e3910.

Le A Trinh, Yelon, D. and Stainier, D. Y. R. (2005). Hand2 Regulates Epithelial Formation during Myocardial Differentiation. *Current Biology* **15**, 441–446.

Lecuit, T., Lenne, P.-F. and Munro, E. (2011). Force Generation, Transmission, and Integration during Cell and Tissue Morphogenesis. *Annual Review of Cell and Developmental Biology* **27**, 157–184.

Lee, J.-Y., Chien, I.-C., Lin, W.-Y., Wu, S.-M., Wei, B.-H., Lee, Y.-E. and Lee, H.-H. (2012). Fhl1 as a downstream target of Wnt signaling to promote myogenesis of C2C12 cells. *Molecular and Cellular Biochemistry* **365**, 251–262.

Lee, R. K., Stainier, D. Y., Weinstein, B. M. and Fishman, M. C. (1994). Cardiovascular development in the zebrafish. II. Endocardial progenitors are sequestered within the heart field. *Development* **120**, 3361–3366.

Levayer, R., Pelissier-Monier, A. and Lecuit, T. (2011). Spatial regulation of Dia and Myosin-II by RhoGEF2 controls initiation of E-cadherin endocytosis during epithelial morphogenesis. *Nature cell biology* **13**, 529–540.

Li, Q. and Sarna, S. K. (2009). Nuclear Myosin II Regulates the Assembly of Preinitiation Complex for ICAM-1 Gene Transcription. *Gastroenterology* **137**, 1051–1060.e3.

Liang, D., Chang, J. R., Chin, A. J., Smith, A., Kelly, C., Weinberg, E. S. and Ge, R. (2001). The role of vascular endothelial growth factor (VEGF) in vasculogenesis, angiogenesis, and hematopoiesis in zebrafish development. *Mechanisms of development* **108**, 29–43.

Lienkamp, S. S., Liu, K., Karner, C. M., Carroll, T. J., Ronneberger, O., Wallingford, J. B. and Walz, G. (2012). Vertebrate kidney tubules elongate using a planar cell polarity–dependent, rosette-based mechanism of convergent extension. *Nature Genetics* **44**, 1382–1387.

Lim, X. and Nusse, R. (2013). Wnt Signaling in Skin Development, Homeostasis, and Disease. *Cold Spring Harbor Perspectives in Biology* **5**, a008029–a008029.

Lin, L., Cui, L., Zhou, W., Dufort, D., Zhang, X., Cai, C. L., Bu, L., Yang, L., Martin, J., Kemler, R., et al. (2007). beta-Catenin directly regulates Islet1 expression in cardiovascular progenitors and is required for multiple aspects of cardiogenesis. *Proceedings of the National Academy of Sciences* **104**, 9313–9318.

Linask, K. K. (1992). N-cadherin localization in early heart development and polar expression of Na+, K+-ATPase, and integrin during pericardial coelom formation and epithelialization of the differentiating myocardium. *Developmental biology* **151**, 213–224.

Lindsay, H., Burger, A., Biyong, B., Felker, A., Hess, C., Zaugg, J., Chiavacci, E., Anders, C., Jinek, M., Mosimann, C., et al. (2016). CrispRVariants charts the mutation spectrum of genome engineering experiments. *Nat Biotechnol* **34**, 701–702.

Lindsley, R. C. (2006). Canonical Wnt signaling is required for development of embryonic stem cell-derived mesoderm. *Development* **133**, 3787–3796.

Liu, C., Liu, W., Palie, J., Lu, M. F., Brown, N. A. and Martin, J. F. (2002). Pitx2c patterns anterior myocardium and aortic arch vessels and is required for local cell movement into atrioventricular cushions. *Development* **129**, 5081–5091.

Liu, J. and Stainier, D. Y. R. (2010). Tbx5 and Bmp Signaling Are Essential for Proepicardium Specification in Zebrafish. *Circulation Research* **106**, 1818–1828.

Liu, J., Bressan, M., Hassel, D., Huisken, J., Staudt, D., Kikuchi, K., Poss, K. D., Mikawa, T. and Stainier, D. Y. R. (2010). A dual role for ErbB2 signaling in cardiac trabeculation. *Development* **137**, 3867–3875.

Loirand, G. (2006). Rho Kinases in Cardiovascular Physiology and Pathophysiology. *Circulation Research* **98**, 322–334.

Luga, V., Zhang, L., Viloria-Petit, A. M., Ogunjimi, A. A., Inanlou, M. R., Chiu, E., Buchanan, M., Hosein, A. N., Basik, M. and Wrana, J. L. (2012). Exosomes Mediate Stromal Mobilization of Autocrine Wnt-PCP Signaling in Breast Cancer Cell Migration. *Cell* **151**, 1542–1556.

Lundquist, M. R., Storaska, A. J., Liu, T.-C., Larsen, S. D., Evans, T., Neubig, R. R. and Jaffrey, S. R. (2014). Redox Modification of Nuclear Actin by MICAL-2 Regulates SRF Signaling. *Cell* **156**, 563–576.

Luo, W., Zhao, X., Jin, H., Tao, L., Zhu, J., Wang, H., Hemmings, B. A. and Yang, Z. (2015). Akt1 signaling coordinates BMP signaling and -catenin activity to regulate second heart field progenitor development. *Development* **142**, 732–742.

Luo, Y., Ferreira-Cornwell, M., Baldwin, H., Kostetskii, I., Lenox, J., Lieberman, M. and Radice, G. (2001). Rescuing the N-cadherin knockout by cardiac-specific expression of N- or E-cadherin. *Development* **128**, 459–469.

Malekar, P., Hagenmueller, M., Anyanwu, A., Buss, S., Streit, M. R., Weiss, C. S., Wolf, D., Riffel, J., Bauer, A., Katus, H. A., et al. (2010). Wnt Signaling Is Critical for Maladaptive Cardiac Hypertrophy and Accelerates Myocardial Remodeling. *Hypertension* **55**, 939–945.

Mapp, O. M., Wanner, S. J., Rohrschneider, M. R. and Prince, V. E. (2010). Prickle1b mediates interpretation of migratory cues during zebrafish facial branchiomotor neuron migration. *Developmental Dynamics* **239**, 1596–1608.

Markwald, R. R., Fitzharris, T. P. and Manasek, F. J. (1977). Structural development of endocardial cushions. *Am. J. Anat.* **148**, 85–119.

Markwald, R. R., Fitzharris, T. P. and Smith, W. N. A. (1975). Structural analysis of endocardial cytodifferentiation. *Developmental biology* **42**, 160–180.

Marlow, F., Topczewski, J., Sepich, D. and Solnica-Krezel, L. (2002). Zebrafish Rho Kinase 2 Acts Downstream of Wnt11 to Mediate Cell Polarity and Effective Convergence and Extension Movements. *Current Biology* **12**, 876–884.

Marques, S. R. and Yelon, D. (2009). Differential requirement for BMP signaling in atrial and ventricular lineages establishes cardiac chamber proportionality. *Developmental biology* **328**, 472–482.

Marques, S. R., Lee, Y., Poss, K. D. and Yelon, D. (2008). Reiterative roles for FGF signaling in the establishment of size and proportion of the zebrafish heart. *Developmental biology* **321**, 397–406.

Martin-Belmonte, F. and Perez-Moreno, M. (2011). Epithelial cell polarity, stem cells and cancer. *Nat Rev Cancer* **12**, 23–38.

Marvin, M. J. (2001). Inhibition of Wnt activity induces heart formation from posterior mesoderm. *Genes & Development* **15**, 316–327.

Matsui, T. (2005). Noncanonical Wnt signaling regulates midline convergence of organ primordia during zebrafish development. *Genes & Development* **19**, 164–175.

Matsumura, F. (2005). Regulation of myosin II during cytokinesis in higher eukaryotes. *Trends in Cell Biology* **15**, 371–377.

Matsumura, F., Totsukawa, G., Yamakita, Y. and Yamashiro, S. (2001). Role of Myosin Light Chain Phosphorylation in the Regulation of Cytokinesis. *Cell Structure and Function* **26**, 639–644.

Männer, J., Wessel, A. and Yelbuz, T. M. (2010). How does the tubular embryonic heart work? Looking for the physical mechanism generating unidirectional blood flow in the valveless embryonic heart tube. *Developmental Dynamics* **239**, 1035–1046.

McDonald, D., Carrero, G., Andrin, C., de Vries, G. and Hendzel, M. J. (2006). Nucleoplasmic β-actin exists in a dynamic equilibrium between low-mobility polymeric species and rapidly diffusing populations. *The Journal of Cell Biology* **172**, 541–552.

McGee, K. M., Vartiainen, M. K., Khaw, P. T., Treisman, R. and Bailly, M. (2011). Nuclear transport of the serum response factor coactivator MRTF-A is downregulated at tensional homeostasis. *EMBO Rep* **12**, 963–970.

McGreevy, E. M., Vijayraghavan, D., Davidson, L. A. and Hildebrand, J. D. (2015). Shroom3 functions downstream of planar cell polarity to regulate myosin II distribution and cellular organization during neural tube closure. *Biology Open* **4**, 186–196.

McKinsey, T. A. (2007). Derepression of pathological cardiac genes by members of the CaM kinase superfamily. *Cardiovascular Research* **73**, 667–677.

Miano, J. M., Long, X. and Fujiwara, K. (2006). Serum response factor: master regulator of the actin cytoskeleton and contractile apparatus. *AJP: Cell Physiology* **292**, C70–C81.

Mickoleit, M., Schmid, B., Weber, M., Fahrbach, F. O., Hombach, S., Reischauer, S. and Huisken, J. (2014). High-resolution reconstruction of the beating zebrafish heart. *Nature Methods* **11**, 919–922.

Mirotsou, M., Zhang, Z., Deb, A., Zhang, L., Gnecchi, M., Noiseux, N., Mu, H., Pachori, A. and Dzau, V. (2007). Secreted frizzled related protein 2 (Sfrp2) is the key Akt-mesenchymal stem cell-released paracrine factor mediating myocardial survival and repair. *Proceedings of the National Academy of Sciences* **104**, 1643–1648.

Molkentin, J. (1996). α-myosin Heavy Chain Gene Regulation: Delineation and Characterization of the Cardiac Muscle-specific Enhancer and Muscle-specific Promoter. *Journal of Molecular and Cellular Cardiology* **28**, 1211–1225.

Moon, R. T., Slusarski, D. C. and Corces, V. G. (1997). Interaction of Wnt and a Frizzled homologue triggers G-protein-linked phosphatidylinositol signalling. *Nature* **390**, 410–413.

Moore, S. W., Zhang, X., Lynch, C. D. and Sheetz, M. P. (2012). Netrin-1 Attracts Axons through FAK-Dependent Mechanotransduction. *Journal of Neuroscience* **32**, 11574–11585.

Moorman, A. (2003). Development of the heart: (1) formation of the cardiac chambers and arterial trunks. *Heart* **89**, 806–814.

Mosimann, C., Panáková, D., Werdich, A. A., Musso, G., Burger, A., Lawson, K. L., Carr, L. A., Nevis, K. R., Sabeh, M. K., Zhou, Y., et al. (2015). Chamber identity programs drive early functional partitioning of the heart. *Nature Communications* **6**, 8146.

Mueller, C. G. and Nordheim, A. (1991). A protein domain conserved between yeast MCM1 and human SRF directs ternary complex formation. *EMBO J* **10**, 4219–4229.

Nagaoka, T., Inutsuka, A., Begum, K., Hafiz, K. M. B. and Kishi, M. (2014). Vangl2 Regulates E-Cadherin in Epithelial Cells. *Scientific Reports* **4**, 6940.

Naito, A. T., Shiojima, I., Akazawa, H., Hidaka, K., Morisaki, T., Kikuchi, A. and Komuro, I. (2006). Developmental stage-specific biphasic roles of Wnt/beta-catenin signaling in cardiomyogenesis and hematopoiesis. *Proceedings of the National Academy of Sciences* **103**, 19812–19817.

Newman-Smith, E., Kourakis, M. J., Reeves, W., Veeman, M. and Smith, W. C. (2015). Reciprocal and dynamic polarization of planar cell polarity core components and myosin. *eLife* **4**, 1302.

Nishimura, T. and Takeichi, M. (2009). Chapter 2 Remodeling of the Adherens Junctions During Morphogenesis.pp. 33–54. Elsevier.

Nishimura, T., Honda, H. and Takeichi, M. (2012). Planar Cell Polarity Links Axes of Spatial Dynamics in Neural-Tube Closure. *Cell* **149**, 1084–1097.

Niu, Z., Iyer, D., Conway, S. J., Martin, J. F., Ivey, K., Srivastava, D., Nordheim, A. and Schwartz, R. J. (2008). Serum response factor orchestrates nascent sarcomerogenesis and silences the biomineralization gene program in the heart. *Proceedings of the National Academy of Sciences* **105**, 17824–17829.

Niu, Z., Li, A., Zhang, S. X. and Schwartz, R. J. (2007). Serum response factor micromanaging cardiogenesis. *Current Opinion in Cell Biology* **19**, 618–627.

Norden, J. and Kispert, A. (2012). Wnt/Ctnnb1 Signaling and the Mesenchymal Precursor Pools of the Heart. *Trends in Cardiovascular Medicine* **22**, 118–122.

Norden, J., Greulich, F., Rudat, C., Taketo, M. M. and Kispert, A. (2011). Wnt/ -Catenin Signaling Maintains the Mesenchymal Precursor Pool for Murine Sinus Horn Formation. *Circulation Research* **109**, e42–e50.

Norman, C., Runswick, M., Pollock, R. and Treisman, R. (1988). Isolation and properties of cDNA clones encoding SRF, a transcription factor that binds to the c-fos serum response element. *Cell* **55**, 989–1003.

North, T. E., Goessling, W., Peeters, M., Li, P., Ceol, C., Lord, A. M., Weber, G. J., Harris, J., Cutting, C. C., Huang, P., et al. (2009). Hematopoietic Stem Cell Development Is Dependent on Blood Flow. *Cell* **137**, 736–748.

Novak, K. D. and Titus, M. A. (1997). Myosin I Overexpression Impairs Cell Migration. *The Journal of Cell Biology* **136**, 633–647.

Nowak, K. J., Ravenscroft, G., Jackaman, C., Filipovska, A., Davies, S. M., Lim, E. M., Squire, S. E., Potter, A. C., Baker, E., Clément, S., et al. (2009). Rescue of skeletal muscle α-actin–null mice by cardiac (fetal) α-actin. *The Journal of Cell Biology* **185**, 903–915.

Nusse, R. (2005). Wnt signaling in disease and in development. *Cell Res* **15**, 28–32.

Nusse, R. and Varmus, H. E. (1982). Many tumors induced by the mouse mammary tumor virus contain a provirus integrated in the same region of the host genome. *Cell* **31**, 99–109.

Nüsslein-Volhard, C. and Wieschaus, E. (1980). Mutations affecting segment number and

polarity in Drosophila. *Nature* **287**, 795–801.

Nüsslein-Volhard, C., Dahm, R. and Cunliffe, V. T. (2003). *Zebrafish: A Practical Approach.* Oxford University Press.

Odell, G., Oster, G., Burnside, B. and Alberch, P. (1980). A mechanical model for epithelial morphogenesis. *J. Math. Biology* **9**, 291–295.

Oerlemans, M. I. F. J., Goumans, M.-J., Middelaar, B., Clevers, H., Doevendans, P. A. and Sluijter, J. P. G. (2010). Active Wnt signaling in response to cardiac injury. *Basic Res Cardiol* **105**, 631–641.

Olson, E. N. (2006). Gene Regulatory Networks in the Evolution and Development of the Heart. *Science* **313**, 1922–1927.

Olson, E. N. and Nordheim, A. (2010). Linking actin dynamics and gene transcription to drive cellular motile functions. *Nature Reviews Molecular Cell Biology* **11**, 353–365.

Olson, E. N. and Srivastava, D. (1996). Molecular Pathways Controlling Heart Development. *Science* **272**, 671–676.

Ossipova, O., Kim, K. and Sokol, S. Y. (2015). Planar polarization of Vangl2 in the vertebrate neural plate is controlled by Wnt and Myosin II signaling. *Biology Open* **4**, 722–730.

Oteiza, P., Koppen, M., Krieg, M., Pulgar, E., Farias, C., Melo, C., Preibisch, S., Muller, D., Tada, M., Hartel, S., et al. (2010). Planar cell polarity signalling regulates cell adhesion properties in progenitors of the zebrafish laterality organ. *Development* **137**, 3459–3468.

Panáková, D., Werdich, A. A. and MacRae, C. A. (2010). Wnt11 patterns a myocardial electrical gradient through regulation of the L-type Ca2+ channel. *Nature* **466**, 874–878.

Pandur, P., Läsche, M., Eisenberg, L. M. and Kühl, M. (2002). Wnt-11 activation of a non-canonical Wnt signalling pathway is required for cardiogenesis. *Nature* **418**, 636–641.

Papusheva, E. and Heisenberg, C.-P. (2010). Spatial organization of adhesion: force-dependent regulation and function in tissue morphogenesis. *EMBO J* **29**, 2753–2768.

Park, E. J., Watanabe, Y., Smyth, G., Miyagawa-Tomita, S., Meyers, E., Klingensmith, J., Camenisch, T., Buckingham, M. and Moon, A. M. (2008). An FGF autocrine loop initiated in second heart field mesoderm regulates morphogenesis at the arterial pole of the heart. *Development* **135**, 3599–3610.

Parlakian, A., Charvet, C., Escoubet, B., Mericskay, M., Molkentin, J. D., Gary-Bobo, G., De Windt, L. J., Ludosky, M.-A., Paulin, D., Daegelen, D., et al. (2005). Temporally Controlled Onset of Dilated Cardiomyopathy Through Disruption of the SRF Gene in Adult Heart. *Circulation* **112**, 2930–2939.

Parlakian, A., Tuil, D., Hamard, G., Tavernier, G., Hentzen, D., Concordet, J. P., Paulin, D., Li, Z. and Daegelen, D. (2004). Targeted Inactivation of Serum Response Factor in the Developing Heart Results in Myocardial Defects and Embryonic Lethality. *Molecular and Cellular Biology* **24**, 5281–5289.

Pederson, T. (2008). As functional nuclear actin comes into view, is it globular, filamentous, or both? *The Journal of Cell Biology* **180**, 1061–1064.

Pellicer, A. (1998). RAS pathways to cell cycle control and cell transformation. *Front Biosci* **3**, d887–912.

Peralta, M., Steed, E., Harlepp, S., González-Rosa, J. M., Monduc, F., Ariza-Cosano, A., Cortés, A., Rayón, T., Gómez-Skarmeta, J.-L., Zapata, A., et al. (2013). Heartbeat-driven pericardiac fluid forces contribute to epicardium morphogenesis. *Curr. Biol.* **23**,

1726–1735.

Percipalle, P., Zhao, J., Pope, B., Weeds, A., Lindberg, U. and Daneholt, B. (2001). Actin Bound to the Heterogeneous Nuclear Ribonucleoprotein Hrp36 Is Associated with Balbiani Ring mRNA from the Gene to Polysomes. *The Journal of Cell Biology* **153**, 229–236.

Person, A. D., Klewer, S. E. and Runyan, R. B. (2005). Cell Biology of Cardiac Cushion Development. *International Review of Cytology* **243**, 287–335.

Peterkin, T., Gibson, A. and Patient, R. (2007). Redundancy and evolution of GATA factor requirements in development of the myocardium. *Developmental biology* **311**, 623–635.

Philippar, U., Schratt, G., Dieterich, C., Müller, J. M., Galgóczy, P., Engel, F. B., Keating, M. T., Gertler, F., Schüle, R., Vingron, M., et al. (2004). The SRF Target Gene Fhl2 Antagonizes RhoA/MAL-Dependent Activation of SRF. *Molecular Cell* **16**, 867–880.

Phillips, H. M. (2005). Vangl2 Acts via RhoA Signaling to Regulate Polarized Cell Movements During Development of the Proximal Outflow Tract. *Circulation Research* **96**, 292–299.

Pipes, G. C. T. (2006). The myocardin family of transcriptional coactivators: versatile regulators of cell growth, migration, and myogenesis. *Genes & Development* **20**, 1545–1556.

Piven, O. O., Kostetskii, I. E., Macewicz, L. L., Kolomiets, Y. M., Radice, G. L. and Lukash, L. L. (2011). Requirement for N-cadherin-catenin complex in heart development. *Experimental Biology and Medicine* **236**, 816–822.

Posern, G. and Treisman, R. (2006). Actin' together: serum response factor, its cofactors and the link to signal transduction. *Trends in Cell Biology* **16**, 588–596.

Putzke, A. P. and Rothman, J. H. (2003). Gastrulation: PARtaking of the Bottle. *Current Biology* **13**, R223–R225.

Qyang, Y., Martin-Puig, S., Chiravuri, M., Chen, S., Xu, H., Bu, L., Jiang, X., Lin, L., Granger, A., Moretti, A., et al. (2007). The Renewal and Differentiation of Isl1+ Cardiovascular Progenitors Are Controlled by a Wnt/β-Catenin Pathway. *Cell Stem Cell* **1**, 165–179.

Rackley, C. R. and Stripp, B. R. (2012). Building and maintaining the epithelium of the lung. *J. Clin. Invest.* **122**, 2724–2730.

Ramsbottom, S. A., Sharma, V., Rhee, H. J., Eley, L., Phillips, H. M., Rigby, H. F., Dean, C., Chaudhry, B. and Henderson, D. J. (2014). Vangl2-Regulated Polarisation of Second Heart Field-Derived Cells Is Required for Outflow Tract Lengthening during Cardiac Development. *PLoS Genet* **10**, e1004871.

Rana, M. S., Christoffels, V. M. and Moorman, A. F. M. (2013). A molecular and genetic outline of cardiac morphogenesis. *Acta Physiol* **207**, 588–615.

Rech, J., Barlat, I., Veyrune, J. L., Vie, A. and Blanchard, J. M. (1994). Nuclear import of serum response factor (SRF) requires a short amino-terminal nuclear localization sequence and is independent of the casein kinase II phosphorylation site. *Journal of Cell Science* **107**, 3029–3036.

Reckova, M. (2003). Hemodynamics Is a Key Epigenetic Factor in Development of the Cardiac Conduction System. *Circulation Research* **93**, 77–85.

Reiter, J. F., Alexander, J., Rodaway, A., Yelon, D., Patient, R., Holder, N. and Stainier, D. Y. R. (1999). Gata5 is required for the development of the heart and endoderm in zebrafish. *Genes & Development* **13**, 2983–2995.

Reiter, J. F., Verkade, H. and Stainier, D. Y. R. (2001). Bmp2b and Oep Promote Early Myocardial Differentiation through Their Regulation of gata5. *Developmental biology* **234**, 330–338.

Renaudin, A., Lehmann, M., Girault, J. and McKerracher, L. (2000). Organization of point contacts in neuronal growth cones. *Journal of neuroscience research* **55**, 458–471.

Resink, T. J., Philippova, M., Joshi, M. B., Kyriakakis, E. and Erne, P. (2009). Cadherins and cardiovascular disease. *Swiss Med Wkly* **139**, 122–134.

Riento, K. and Ridley, A. J. (2003). Rocks: multifunctional kinases in cell behaviour. *Nature Reviews Molecular Cell Biology* **4**, 446–456.

Rijsewijk, F., Schuermann, M., Wagenaar, E., Parren, P., Weigel, D. and Nusse, R. (1987). The Drosophila homology of the mouse mammary oncogene int-1 is identical to the segment polarity gene wingless. *Cell* **50**, 649–657.

Risebro, C. A. and Riley, P. R. (2006). Formation of the ventricles. *ScientificWorldJournal* **6**, 1862–1880.

Rohr, S., Otten, C. and Abdelilah-Seyfried, S. (2008). Asymmetric Involution of the Myocardial Field Drives Heart Tube Formation in Zebrafish. *Circulation Research* **102**, e12–e19.

Rossi, A., Kontarakis, Z., Gerri, C., Nolte, H., Hölper, S., Krüger, M. and Stainier, D. Y. R. (2015). Genetic compensation induced by deleterious mutations but not gene knockdowns. *Nature* **524**, 230–233.

Roszko, I., Sawada, A. and Solnica-Krezel, L. (2009). Regulation of convergence and extension movements during vertebrate gastrulation by the Wnt/PCP pathway. *Seminars in cell & developmental biology* **20**, 986–997.

Röper, K. (2014). Supracellular actomyosin assemblies during development. *BioArchitecture* **3**, 45–49.

Ruzicka, D. L. (1988). Sequential activation of alpha-actin genes during avian cardiogenesis: vascular smooth muscle alpha-actin gene transcripts mark the onset of cardiomyocyte differentiation. *The Journal of Cell Biology* **107**, 2575–2586.

Ryan, T., Shelton, M., Lambert, J. P., Malecova, B., Boisvenue, S., Ruel, M., Figeys, D., Puri, P. L. and Skerjanc, I. S. (2013). Myosin Phosphatase Modulates the Cardiac Cell Fate by Regulating the Subcellular Localization of Nkx2.5 in a Wnt/Rho-Associated Protein Kinase-Dependent Pathway. *Circulation Research* **112**, 257–266.

Rychter, Z. and Ostádal, B. (1971). Mechanism of the development of coronary arteries in chick embryo. *Folia morphologica* **19**, 113–124.

Saga, Y. (2000). Mesp1 Expression Is the Earliest Sign of Cardiovascular Development. *Trends in Cardiovascular Medicine* **10**, 345–352.

Sagar, Prols, F., Wiegreffe, C. and Scaal, M. (2015). Communication between distant epithelial cells by filopodia-like protrusions during embryonic development. *Development* **142**, 665–671.

Sakaguchi, T. (2006). The yolk syncytial layer regulates myocardial migration by influencing extracellular matrix assembly in zebrafish. *Development* **133**, 4063–4072.

Sander, J. D. and Joung, J. K. (2014). CRISPR-Cas systems for editing, regulating and targeting genomes. *Nat Biotechnol* **32**, 347–355.

Saneyoshi, T., Kume, S., Amasaki, Y. and Mikoshiba, K. (2002). The Wnt/calcium pathway activates NF-AT and promotes ventral cell fate in Xenopus embryos. *Nature* **417**, 295–299.

Sawyer, J. M., Harrell, J. R., Shemer, G., Sullivan-Brown, J., Roh-Johnson, M. and Goldstein, B. (2010). Apical constriction: A cell shape change that can drive morphogenesis. *Developmental biology* **341**, 5–19.

Scherz, P. J., Huisken, J., Sahai-Hernandez, P. and Stainier, D. Y. R. (2008). High-speed imaging of developing heart valves reveals interplay of morphogenesis and function. *Development* **135**, 1179–1187.

Schleiffarth, J. R., Person, A. D., Martinsen, B. J., Sukovich, D. J., Neumann, A., Baker, C. V. H., Lohr, J. L., Cornfield, D. N., Ekker, S. C. and Petryk, A. (2007). Wnt5a Is Required for Cardiac Outflow Tract Septation in Mice. *Pediatr Res* **61**, 386–391.

Schneider, V. A. (2001). Wnt antagonism initiates cardiogenesis in Xenopus laevis. *Genes & Development* **15**, 304–315.

Schoenebeck, J. J., Keegan, B. R. and Yelon, D. (2007). Vessel and Blood Specification Override Cardiac Potential in Anterior Mesoderm. *Developmental Cell* **13**, 254–267.

Scott, I. C., Masri, B., D'Amico, L. A., Jin, S.-W., Jungblut, B., Wehman, A. M., Baier, H., Audigier, Y. and Stainier, D. Y. R. (2007). The G Protein-Coupled Receptor Agtrl1b Regulates Early Development of Myocardial Progenitors. *Developmental Cell* **12**, 403–413.

Sedmera, D., Pexieder, T., Hu, N. and Clark, E. B. (1997). Developmental changes in the myocardial architecture of the chick. *The Anatomical record* **248**, 421–432.

Seguchi, O., Takashima, S., Yamazaki, S., Asakura, M., Asano, Y., Shintani, Y., Wakeno, M., Minamino, T., Kondo, H., Furukawa, H., et al. (2007). A cardiac myosin light chain kinase regulates sarcomere assembly in the vertebrate heart. *J. Clin. Invest.* **117**, 2812–2824.

Sehnert, A. J. and Stainier, D. Y. R. (2002). A window to the heart: can zebrafish mutants help us understand heart disease in humans? *Trends in Genetics* **18**, 491–494.

Selvaraj, A., Selvaraj, A., Prywes, R. and Prywes, R. (2004). Expression profiling of serum inducible genes identifies a subset of SRF target genes that are MKL dependent. *Nature* **496**, 494–497.

Sepich, D. S., Myers, D. C., Short, R., Topczewski, J., Marlow, F. and Solnica-Krezel, L. (2000). Role of the zebrafish trilobite locus in gastrulation movements of convergence and extension. *genesis* **27**, 159–173.

Serluca, F. C. (2008). Development of the proepicardial organ in the zebrafish. *Developmental biology* **315**, 18–27.

Shah, A. N., Davey, C. F., Whitebirch, A. C., Miller, A. C. and Moens, C. B. (2015). Rapid reverse genetic screening using CRISPR in zebrafish. *Nature Methods* **12**, 535–540.

Sharp, K. A. and Axelrod, J. D. (2016). Prickle isoforms control the direction of tissue polarity by microtubule independent and dependent mechanisms. *Biology Open* **5**, 229–236.

Sheldahl, L. C., Slusarski, D. C., Pandur, P., Miller, J. R., Kühl, M. and Moon, R. T.

(2003). Dishevelled activates Ca 2+flux, PKC, and CamKII in vertebrate embryos. *The Journal of Cell Biology* **161**, 769–777.

Shimizu, S., Yoshida, T., Wakamori, M., Ishii, M., Okada, T., Takahashi, M., Seto, M., Sakurada, K., Kiuchi, Y. and Mori, Y. (2006). Ca 2+-calmodulin-dependent myosin light chain kinase is essential for activation of TRPC5 channels expressed in HEK293 cells. *The Journal of Physiology* **570**, 219–235.

Shimojo, M. and Hersh, L. B. (2003). REST/NRSF-Interacting LIM Domain Protein, a Putative Nuclear Translocation Receptor. *Molecular and Cellular Biology* **23**, 9025–9031.

Shimojo, M. and Hersh, L. B. (2006). Characterization of the REST/NRSF-interacting LIM domain protein (RILP): localization and interaction with REST/NRSF. *J Neurochem* **96**, 1130–1138.

Shin, C. H., Liu, Z.-P., Passier, R., Zhang, C.-L., Wang, D.-Z., Harris, T. M., Yamagishi, H., Richardson, J. A., Childs, G. and Olson, E. N. (2002). Modulation of Cardiac Growth and Development by HOP, an Unusual Homeodomain Protein. *Cell* **110**, 725–735.

Shore, P. and Sharrocks, A. D. (1995). The MADS-box family of transcription factors. *European Journal of Biochemistry* **229**, 1–13.

Sienknecht, U. J. (2015). Current concepts of hair cell differentiation and planar cell polarity in inner ear sensory organs. *Cell and Tissue Research* **361**, 25–32.

Simoes, S. de M., Blankenship, J. T., Weitz, O., Farrell, D. L., Tamada, M., Fernandez-Gonzalez, R. and Zallen, J. A. (2010). Rho-Kinase Directs Bazooka/Par-3 Planar Polarity during Drosophila Axis Elongation. *Developmental Cell* **19**, 377–388.

Simoes, S. de M., Mainieri, A. and Zallen, J. A. (2014). Rho GTPase and Shroom direct planar polarized actomyosin contractility during convergent extension. *The Journal of Cell Biology* **204**, 575–589.

Sokol, S. Y. (2015). Spatial and temporal aspects of Wnt signaling and planar cell polarity during vertebrate embryonic development. *Seminars in cell & developmental biology* **42**, 78–85.

Solnica-Krezel, L. (2005). Conserved Patterns of Cell Movements during Vertebrate Gastrulation. *Current Biology* **15**, R213–R228.

Somlyo, A. P. and Somlyo, A. V. (2004). Signal transduction by G-proteins, Rho-kinase and protein phosphatase to smooth muscle and non-muscle myosin II. *The Journal of Physiology* **522**, 177–185.

Somogyi, K. and Rørth, P. (2004). Evidence for Tension-Based Regulation of Drosophila MAL and SRF during Invasive Cell Migration. *Developmental Cell* **7**, 85–93.

Sotiropoulos, A., Gineitis, D., Copeland, J. and Treisman, R. (1999). Signal-Regulated Activation of Serum Response Factor Is Mediated by Changes in Actin Dynamics. *Cell* **98**, 159–169.

Soufan, A. T., van den Berg, G., Ruijter, J. M., de Boer, P. A. J., van den Hoff, M. J. B. and Moorman, A. F. M. (2006). Regionalized sequence of myocardial cell growth and proliferation characterizes early chamber formation. *Circulation Research* **99**, 545–552.

Spéder, P., Petzoldt, A., Suzanne, M. and Noselli, S. (2007). Strategies to establish left/right asymmetry in vertebrates and invertebrates. *Current Opinion in Genetics & Development* **17**, 351–358.

Stainier, D. Y., Lee, R. K. and Fishman, M. C. (1993). Cardiovascular development in the zebrafish. I. Myocardial fate map and heart tube formation. *Development* **119**, 31–40.

Stanganello, E. and Scholpp, S. (2016). Role of cytonemes in Wnt transport. *Journal of Cell Science* **129**, 665–672.

Staudt, D. and Stainier, D. (2012). Uncovering the Molecular and Cellular Mechanisms of Heart Development Using the Zebrafish. *Annual Review of Genetics* **46**, 397–418.

Stepanova, O. V., Chadin, A. V., Masyutin, A. G., Kulikova, T. G., Poltavceva, R. A., Masenko, V. P. and Sukhikh, G. T. (2011). Myosin-activating protein kinases are possible regulators of nonmuscle myosin in developing human heart. *Bulletin of experimental biology and medicine* **152**, 198–201.

Straub, F.B. (1942). Actin. *Stud. Inst. Med. Chem. Univ. Szeged.* **II**: 3–15.

Strutt, D. I., Weber, U. and Mlodzik, M. (1997). The role of RhoA in tissue polarity and Frizzled signalling. *Nature* **387**, 292–295.

Sugi, Y. and Lough, J. (2005). Onset of expression and regional deposition of alpha-smooth and sarcomeric actin during avian heart development. *Developmental Dynamics* **193**, 116–124.

Sun, Q. (2005). Defining the mammalian CArGome. *Genome Research* **16**, 197–207.

Sun, Q., Chen, G., Streb, J. W., Long, X., Yang, Y., Stoeckert, C. J. and Miano, J. M. (2006). Defining the mammalian CArGome. *Genome Research* **16**, 197–207.

Sun, X., Meyers, E. N., Lewandoski, M. and Martin, G. R. (1999). Targeted disruption of Fgf8 causes failure of cell migration in the gastrulating mouse embryo. *Genes & Development* **13**, 1834–1846.

Swift, J., Ivanovska, I. L., Buxboim, A., Harada, T., Dingal, P. C. D. P., Pinter, J., Pajerowski, J. D., Spinler, K. R., Shin, J. W., Tewari, M., et al. (2013). Nuclear Lamin-A Scales with Tissue Stiffness and Enhances Matrix-Directed Differentiation. *Science* **341**, 1240104–1240104.

Tada, M. and Heisenberg, C. P. (2012). Convergent extension: using collective cell migration and cell intercalation to shape embryos. *Development* **139**, 3897–3904.

Tada, M. and Kai, M. (2009). Noncanonical Wnt/PCP Signaling During Vertebrate Gastrulation. *Zebrafish* **6**, 29–40.

Tada, M. and Smith, J. C. (2000). Xwnt11 is a target of Xenopus Brachyury: regulation of gastrulation movements via Dishevelled, but not through the canonical Wnt pathway. *Development* **127**, 2227–2238.

Tahinci, E. and Symes, K. (2003). Distinct functions of Rho and Rac are required for convergent extension during Xenopus gastrulation. *Developmental biology* **259**, 318–335.

Takashima, S. (2009). Phosphorylation of Myosin Regulatory Light Chain by Myosin Light Chain Kinase, and Muscle Contraction. *Circ J* **73**, 208–213.

Takeichi, M., Atsumi, T., Yoshida, C., Uno, K. and Okada, T. S. (1981). Selective adhesion of embryonal carcinoma cells and differentiated cells by Ca2+-dependent sites. *Developmental biology* **87**, 340–350.

Targoff, K. L., Colombo, S., George, V., Schell, T., Kim, S. H., Solnica-Krezel, L. and Yelon, D. (2013). Nkx genes are essential for maintenance of ventricular identity. *Development* **140**, 4203–4213.

Thisse, B., Heyer, V., Lux, A., Alunni, V., Degrave, A., Seiliez, I., Kirchner, J., Parkhill, J.-P. and Thisse, C. (2004). Spatial and Temporal Expression of the Zebrafish Genome by Large-Scale In Situ Hybridization Screening. *Methods in Cell Biology* **77**, 505–519.

Timmerman, L. A., Grego-Bessa, J., Raya, A., Bertrán, E., Pérez-Pomares, J. M., Díez, J., Aranda, S., Palomo, S., McCormick, F., Izpisúa-Belmonte, J. C., et al. (2003). Notch promotes epithelial-mesenchymal transition during cardiac development and oncogenic transformation. *Genes & Development* **18,** 99-115.

Totsukawa, G., Wu, Y., Sasaki, Y., Hartshorne, D. J., Yamakita, Y., Yamashiro, S. and Matsumura, F. (2004). Distinct roles of MLCK and ROCK in the regulation of membrane protrusions and focal adhesion dynamics during cell migration of fibroblasts. *The Journal of Cell Biology* **164**, 427–439.

Totsukawa, G., Yamakita, Y., Yamashiro, S., Hartshorne, D. J., Sasaki, Y. and Matsumura, F. (2000). Distinct Roles of Rock (Rho-Kinase) and Mlck in Spatial Regulation of Mlc Phosphorylation for Assembly of Stress Fibers and Focal Adhesions in 3t3 Fibroblasts. *The Journal of Cell Biology* **150**, 797–806.

Treisman, R. (1986). Identification of a protein-binding site that mediates transcriptional response of the c-fos gene to serum factors. *Cell* **46**, 567–574.

Treisman, R. (1994). Ternary complex factors: growth factor regulated transcriptional activators. *Current Opinion in Genetics & Development* **4**, 96–101.

Tu, C.-T., Yang, T.-C. and Tsai, H.-J. (2009). Nkx2.7 and Nkx2.5 Function Redundantly and Are Required for Cardiac Morphogenesis of Zebrafish Embryos. *PloS one* **4**, e4249.

Tufan, A. C., Daumer, K. M. and Tuan, R. S. (2002). Frizzled-7 and limb mesenchymal chondrogenesis: Effect of misexpression and involvement of N-cadherin. *Developmental Dynamics* **223**, 241–253.

Tzahor, E. (2007). Wnt/β-Catenin Signaling and Cardiogenesis: Timing Does Matter. *Developmental Cell* **13**, 10–13.

Ueno, S., Weidinger, G., Osugi, T., Kohn, A. D., Golob, J. L., Pabon, L., Reinecke, H., Moon, R. T. and Murry, C. E. (2007). Biphasic role for Wnt/beta-catenin signaling in cardiac specification in zebrafish and embryonic stem cells. *Proceedings of the National Academy of Sciences* **104**, 9685–9690.

Ulrich, F. and Heisenberg, C.-P. (2008). Probing E-Cadherin Endocytosis by Morpholino-Mediated Rab5 Knockdown in Zebrafish. *Methods in Molecular Biology* **440**, 371–387.

Ulrich, F., Krieg, M., Schötz, E.-M., Link, V., Castanon, I., Schnabel, V., Taubenberger, A., Mueller, D., Puech, P.-H. and Heisenberg, C.-P. (2005). Wnt11 Functions in Gastrulation by Controlling Cell Cohesion through Rab5c and E-Cadherin. *Developmental Cell* **9**, 555–564.

Unterseher, F., Hefele, J. A., Giehl, K., de Robertis, E. M., Wedlich, D. and Schambony, A. (2004). Paraxial protocadherin coordinates cell polarity during convergent extension via Rho A and JNK. *EMBO J* **23**, 3259–3269.

Usui, T., Shima, Y., Shimada, Y., Hirano, S., Burgess, R. W., Schwarz, T. L., Takeichi, M. and Uemura, T. (1999). Flamingo, a Seven-Pass Transmembrane Cadherin, Regulates Planar Cell Polarity under the Control of Frizzled. *Cell* **98**, 585–595.

van den Berg, G. and Moorman, A. F. M. (2009). Concepts of Cardiac Development in Retrospect. *Pediatric Cardiology* **30**, 580–587.

Vandekerckhove, J. and Weber, K. (1978). The amino acid sequence of Physarum actin. *Nature* **276**, 720–721.

Vanderploeg, J., Vazquez Paz, L. L., MacMullin, A. and Jacobs, J. R. (2012). Integrins are required for cardioblast polarisation in Drosophila. *BMC Dev Biol* **12**, 8.

Vartiainen, M. K., Guettler, S., Larijani, B. and Treisman, R. (2007). Nuclear Actin Regulates Dynamic Subcellular Localization and Activity of the SRF Cofactor MAL. *Science* **316**, 1749–1752.

Vicente-Manzanares, M., Ma, X., Adelstein, R. S. and Horwitz, A. R. (2009). Non-muscle myosin II takes centre stage in cell adhesion and migration. *Nature Reviews Molecular Cell Biology* **10**, 778–790.

Villasenor, A., Chong, D. C., Henkemeyer, M. and Cleaver, O. (2010). Epithelial dynamics of pancreatic branching morphogenesis. *Development* **137**, 4295–4305.

Voss, K., Stahl, S., Hogan, B. M., Reinders, J., Schleider, E., Schulte-Merker, S. and Felbor, U. (2009). Functional analyses of human and zebrafish 18-amino acid in-frame deletion pave the way for domain mapping of the cerebral cavernous malformation 3 protein. *Hum. Mutat.* **30**, 1003–1011.

Wadgaonkar R., Dudek S. M., Zaiman A. L., Linz-McGillem L., Verin A. D., Nurmukhambetova S., Romer L. H., Garcia JG. (2005). Intracellular interaction of myosin light chain kinase with macrophage migration inhibition factor (MIF) in endothelium. *J Cell Biochem* **95**, 849-858.

Walck-Shannon, E. and Hardin, J. (2013). Cell intercalation from top to bottom. *Nature Reviews Molecular Cell Biology* **15**, 34–48.

Waldo, K. L., Hutson, M. R., Ward, C. C., Zdanowicz, M., Stadt, H. A., Kumiski, D., Abu-Issa, R. and Kirby, M. L. (2005). Secondary heart field contributes myocardium and smooth muscle to the arterial pole of the developing heart. *Developmental biology* **281**, 78–90.

Wallingford, J. B. (2012). Planar Cell Polarity and the Developmental Control of Cell Behavior in Vertebrate Embryos. *Annual Review of Cell and Developmental Biology* **28**, 627–653.

Wallingford, J. B. and Habas, R. (2005). The developmental biology of Dishevelled: an enigmatic protein governingcell fate and cell polarity. *Development* **132**, 4421–4436.

Wallingford, J. B., Fraser, S. E. and Harland, R. M. (2002). Convergent Extension. *Developmental Cell* **2**, 695–706.

Wallingford, J. B., Rowning, B. A., Vogeli, K. M., Rothbächer, U., Fraser, S. E. and Harland, R. M. (2000). Dishevelled controls cell polarity during Xenopus gastrulation. *Nature* **405**, 81–85.

Walsh, E. C. and Stainier, D. Y. (2001). UDP-Glucose Dehydrogenase Required for Cardiac Valve Formation in Zebrafish. *Science* **293**, 1670–1673.

Wang, D., Zheng, W., Xie, Y., Gong, P., Zhao, F., Yuan, B., Ma, W., Cui, Y., Liu, W., Sun, Y., et al. (2014). Tissue-specific mechanical and geometrical control of cell viability and actin cytoskeleton alignment. *Scientific Reports* **4**, 6160.

Wang, D.-Z., Chang, P. S., Wang, Z., Sutherland, L., Richardson, J. A., Small, E., Krieg, P. A. and Olson, E. N. (2001). Activation of Cardiac Gene Expression by Myocardin, a Transcriptional Cofactor for Serum Response Factor. *Cell* **105**, 851–862.

Wang, H., Yang, H., Shivalila, C. S., Dawlaty, M. M., Cheng, A. W., Zhang, F. and Jaenisch, R. (2013). One-step generation of mice carrying mutations in multiple genes by CRISPR/Cas-mediated genome engineering. *Cell* **153**, 910–918.

Wang, Z., Wang, D.-Z., Hockemeyer, D., McAnally, J., Nordheim, A. and Olson, E. N. (2004). Myocardin and ternary complex factors compete for SRF to control smooth muscle gene expression. *Nature* **428**, 185–189.

Watanabe, Y., Miyagawa-Tomita, S., Vincent, S. D., Kelly, R. G., Moon, A. M. and Buckingham, M. E. (2010). Role of Mesodermal FGF8 and FGF10 Overlaps in the Development of the Arterial Pole of the Heart and Pharyngeal Arch Arteries. *Circulation Research* **106**, 495–503.

Watterson, D. M., Schavocky, J. P., Guo, L., Weiss, C., Chlenski, A., Shirinsky, V. P., Van Eldik, L. J. and Haiech, J. (1999). Analysis of the kinase-related protein gene found at human chromosome 3q21 in a multi-gene cluster: organization, expression, alternative splicing, and polymorphic marker. *Journal of Cellular Biochemistry* **75**, 481–491.

Weiford, B. C., Subbarao, V. D. and Mulhern, K. M. (2004). Noncompaction of the Ventricular Myocardium. *Circulation* **109**, 2965–2971.

Weis, W. I. and Nelson, W. J. (2006). Re-solving the Cadherin-Catenin-Actin Conundrum. *Journal of Biological Chemistry* **281**, 35593–35597.

Willert, K. and Nusse, R. (2012). Wnt Proteins. *Cold Spring Harbor Perspectives in Biology* **4**, a007864–a007864.

Winter, C. G., Wang, B., Ballew, A., Royou, A., Karess, R., Axelrod, J. D. and Luo, L. (2001). Drosophila Rho-Associated Kinase (Drok) Links Frizzled-Mediated Planar Cell Polarity Signaling to the Actin Cytoskeleton. *Cell* **105**, 81–91.

Wolff, T. and Rubin, G. M. (1998). Strabismus, a novel gene that regulates tissue polarity and cell fate decisions in Drosophila. *Development* **125**, 1149–1159.

Wong, L. L. and Adler, P. N. (1993). Tissue polarity genes of Drosophila regulate the subcellular location for prehair initiation in pupal wing cells. *The Journal of Cell Biology* **123**, 209–221.

Wu, G., Ge, J., Huang, X., Hua, Y. and Mu, D. (2011). Planar Cell Polarity Signaling Pathway in Congenital Heart Diseases. *Journal of Biomedicine and Biotechnology* **2011**, 1–8.

Yamashita, J. K., Takano, M., Hiraoka-Kanie, M., Shimazu, C., Peishi, Y., Yanagi, K., Nakano, A., Inoue, E., Kita, F. and Nishikawa, S.-I. (2005). Prospective identification of cardiac progenitors by a novel single cell-based cardiomyocyte induction. *The FASEB Journal* **19**, 1534–1536.

Yang, T., Bassuk, A. G. and Fritzsch, B. (2013). Prickle1 stunts limb growth through alteration of cell polarity and gene expression. *Developmental Dynamics* **242**, 1293–1306.

Yang, T., Bassuk, A. G., Stricker, S. and Fritzsch, B. (2014). Prickle1 is necessary for the caudal migration of murine facial branchiomotor neurons. *Cell and Tissue Research* **357**, 549–561.

Yap, A. S., Brieher, W. M. and Gumbiner, B. M. (1997). Molecular and functional analysis of cadherin-based adherens junctions. *Annual Review of Cell and Developmental Biology* **13**, 119–146.

Yates, L. L., Papakrivopoulou, J., Long, D. A., Goggolidou, P., Connolly, J. O., Woolf, A. S. and Dean, C. H. (2010a). The planar cell polarity gene Vangl2 is required for mammalian kidney-branching morphogenesis and glomerular maturation. *Human Molecular Genetics* **19**, 4663–4676.

Yates, L. L., Schnatwinkel, C., Murdoch, J. N., Bogani, D., Formstone, C. J., Townsend, S., Greenfield, A., Niswander, L. A. and Dean, C. H. (2010b). The PCP genes Celsr1 and Vangl2 are required for normal lung branching morphogenesis. *Human Molecular Genetics* **19**, 2251–2267.

Ybot-Gonzalez, P., Savery, D., Gerrelli, D., Signore, M., Mitchell, C. E., Faux, C. H., Greene, N. D. E. and Copp, A. J. (2007). Convergent extension, planar-cell-polarity signalling and initiation of mouse neural tube closure. *Development* **134**, 789–799.

Ye, J., Zhao, J., Hoffmann-Rohrer, U. and Grummt, I. (2008). Nuclear myosin I acts in concert with polymeric actin to drive RNA polymerase I transcription. *Genes & Development* **22**, 322–330.

Yelon, D., Horne, S. A. and Stainier, D. Y. R. (1999). Restricted Expression of Cardiac Myosin Genes Reveals Regulated Aspects of Heart Tube Assembly in Zebrafish. *Developmental biology* **214**, 23–37.

Yelon, D., Ticho, B., Halpern, M. E., Ruvinsky, I., Ho, R. K., Silver, L. M. and Stainier, D. Y. (2000). The bHLH transcription factor hand2 plays parallel roles in zebrafish heart and pectoral fin development. *Development* **127**, 2573–2582.

Yu, H., Ye, X., Guo, N. and Nathans, J. (2012). Frizzled 2 and frizzled 7 function redundantly in convergent extension and closure of the ventricular septum and palate: evidence for a network of interacting genes. *Development* **139**, 4383–4394.

Yu, J. C. and Fernandez-Gonzalez, R. (2016). Quantitative modelling of epithelial morphogenesis: integrating cell mechanics and molecular dynamics. *Seminars in cell & developmental biology* (in press).

Yusko, E. C. and Asbury, C. L. (2014). Force is a signal that cells cannot ignore. *Molecular Biology of the Cell* **25**, 3717–3725.

Zallen, J. A. (2007). Planar Polarity and Tissue Morphogenesis. *Cell* **129**, 1051–1063.

Zallen, J. A. and Blankenship, J. T. (2008). Multicellular dynamics during epithelial elongation. *Seminars in cell & developmental biology* **19**, 263–270.

Zallen, J. A. and Wieschaus, E. (2004). Patterned Gene Expression Directs Bipolar Planar Polarity in Drosophila. *Developmental Cell* **6**, 343–355.

Zhang, S. X., Garcia-Gras, E., Wycuff, D. R., Marriot, S. J., Kadeer, N., Yu, W., Olson, E. N., Garry, D. J., Parmacek, M. S. and Schwartz, R. J. (2005). Identification of Direct Serum-response Factor Gene Targets during Me2SO-induced P19 Cardiac Cell Differentiation. *Journal of Biological Chemistry* **280**, 19115–19126.

Zhang, X., Chai, J., Azhar, G., Sheridan, P., Borras, A. M., Furr, M. C., Khrapko, K., Lawitts, J., Misra, R. P. and Wei, J. Y. (2001). Early Postnatal Cardiac Changes and Premature Death in Transgenic Mice Overexpressing a Mutant Form of Serum Response Factor. *Journal of Biological Chemistry* **276**, 40033–40040.

Zhang, X., Zhu, J., Yang, G.-Y., Wang, Q.-J., Qian, L., Chen, Y.-M., Chen, F., Tao, Y., Hu, H.-S., Wang, T., et al. (2007). Dishevelled promotes axon differentiation by regulating atypical protein kinase C. *Nature cell biology* **9**, 743–754.

Zhou, W., Lin, L., Majumdar, A., Li, X., Zhang, X., Liu, W., Etheridge, L., Shi, Y., Martin, J., Van de Ven, W., et al. (2007). Modulation of morphogenesis by noncanonical Wnt signaling requires ATF/CREB family–mediated transcriptional activation of TGFβ2. *Nature Genetics* **39**, 1225–1234.

Zhou, Y., Cashman, T. J., Nevis, K. R., Obregon, P., Carney, S. A., Liu, Y., Gu, A., Mosimann, C., Sondalle, S., Peterson, R. E., et al. (2011). Latent TGF-β binding protein 3 identifies a second heart field in zebrafish. *Nature* **474**, 645–648.

Zhu, W., Shiojima, I., Ito, Y., Li, Z., Ikeda, H., Yoshida, M., Naito, A. T., Nishi, J.-I., Ueno, H., Umezawa, A., et al. (2008). IGFBP-4 is an inhibitor of canonical Wnt signalling required for cardiogenesis. *Nature* **454**, 345–349.

Znosko, W. A., Yu, S., Thomas, K., Molina, G. A., Li, C., Tsang, W., Dawid, I. B., Moon, A. M. and Tsang, M. (2010). Overlapping functions of Pea3 ETS transcription factors in FGF signaling during zebrafish development. *Developmental biology* **342**, 11–25.

7 Appendix

Abbreviations

µg	Microgram
µL	Microliter
µmol	Micromole
ALPM	Anterior lateral plate mesoderm
bp	Base pair(s)
BSA	Bovine serum albumin
cDNA	Complementary DNA
CE	Convergent extension
CHD	Congenital heart defect
Ct	Cycle threshold
DMEM	Dulbecco's modified eagle medium
DMSO	Dimethylsulfoxide
DNA	2-deoxyribonucleic acid
DNase	Deoxyribonuclease
dNTP	2'-deoxynucleoside 5'-triphosphate
dpf	Days post fertilization
EDTA	Ethylenediaminetetraacetic acid
FA	Formaldehyde
F-Actin	Filamentous Actin
FCS	Fetal calf serum
FHF	First heart field, primary heart field
fw	Forward
G-Actin	Globular Actin
h	Hour(s)
hpf	Hour(s) post fertilization
kDa	Kilo-Dalton
l	Liter
MHC	Myosin heavy chain
MI	Myocardial infarction
min	Minute

MLC	Myosin light chain
mRNA	Messenger RNA
NCBI	National centre for Biotechnology information
ng	Nanogram
OD	Optical density
PAM	Protospacer adjacent motif
PBS	Phosphate buffered saline
PCP	Planar cell polarity
PCR	Polymerase chain reaction
PFA	Paraformaldehyde
pMRLC	Phosphorylated Myosin Regulatory Light Chain
PTU	1-Phenyl-2-thiourea
qRT-PCR	Quantitative Real-Time-PCR
RNA	Ribonucleic acid
RNase	Ribonuclease
rpm	Revolutions per minute
RT	Room temperature
rv	Reverse
sec	Second
SHF	Second heart field
SRF	Serum response factor
TAE	Tris-acetate-EDTA
TE	Tris-EDTA
YSL	Yolk syncytial layer

List of Figures

List of Tables

Acknowledgements

Most importantly, I would like to thank Daniela Panáková for giving me the opportunity to work on this study in her lab and for providing me with her excellent supervision. I am grateful for all the enthusiastic discussions, the guidance and the incentive to grow as a researcher and person. It was a wonderful time – also because the Panáková Lab is a great team. Thanks to all of you!

I thank the members of my MDC committee, Harald Saumweber, Salim Seyfried and Francesca Spagnioli for the inspiring discussions and helpful suggestions. Special thanks goes to Salim Seyfried and Stefan Donat for fruitful discussions and providing the *slb* and *ppt* mutants. Along those lines, I want to thank Jan Huisken, Carl-Philipp. Heisenberg, Malgorzata Wiweger and Holger Gerhardt for providing me with fish lines and zebrafish insight.

Thanks to the MDC TransCard Research School, in which many insights on molecular mechanisms causing cardiovascular and metabolic diseases were offered.

Furthermore, I am very thankful to Prof. Dr. Christian Mosimann, Alexa Burger, Anastasia Felke and Christopher Hess, who helped me to improve the methods for the CRISPant technology within the Panáková lab.

Many thanks to Stephen Gilbert who wrote this great program to run the analysis on cardiomyocyte orientation within the ventricular chamber in such an incredibly short time. Also, I am very thankful to Zoltán Cseresnyés and the microscopy facility for their support in all aspects of microscopy data acquisition and cell shape analysis.

I am very grateful to Alexander Meyer for providing me with many very helpful tools during my studies and for fruitful and calming talks during the occasional cigarette break. Furthermore, I thank Jana Richter for her excellent assistance especially during the generation and identification of CRISPR-Cas9 mediated mutants.

Most importantly, I want to thank my family for their support and believe in me and my friends for giving me all the energy to ease the pain of setbacks and for providing me with distraction when it was needed. I am especially grateful to Anne and Tareck who guided me through difficult days in the lab and to David and Luisa who helped me calm down after several stressful periods throughout my PhD studies and the writing process.